STATIC AND DYNAMIC COMPRESSIBILITY OF SUFFIELD EXPERIMENTAL STATION SOILS

by

M. T. Davisson
T. R. Maynard
M. T. Davisson, Foundation Engineer
Champaign, Illnois

Contract AF 29(601)-6352

TECHNICAL REPORT NO. WL TR-64-118

Research and Technology Division
AIR FORCE WEAPONS LABORATORY
Air Force Systems Command
Kirtland Air Force Base
New Mexico

April 1965

WL TR-64-118

Research and Technology Division
AIR FORCE WEAPONS LABORATORY
Air Force Systems Command
Kirtland Air Force Base
New Mexico

CLEARINGHOUSE FOR FEDERAL SCIENTIFIC AND TECHNICAL INFORMATION, CFSTI
INPUT SECTION 410.11

LIMITATIONS IN REPRODUCTION QUALITY OF TECHNICAL ABSTRACT BULLETIN DOCUMENTS, DEFENSE DOCUMENTATION CENTER (DDC)

AD 611 497

☐ 1. AVAILABLE ONLY FOR REFERENCE USE AT DDC FIELD SERVICES. COPY IS NOT AVAILABLE FOR PUBLIC SALE.

☒ 2. AVAILABLE COPY WILL NOT PERMIT FULLY LEGIBLE REPRODUCTION. REPRODUCTION WILL BE MADE IF REQUESTED BY USERS OF DDC.

☒ A. COPY IS AVAILABLE FOR PUBLIC SALE.

☐ B. COPY IS NOT AVAILABLE FOR PUBLIC SALE.

☐ 3. LIMITED NUMBER OF COPIES CONTAINING COLOR OTHER THAN BLACK AND WHITE ARE AVAILABLE UNTIL STOCK IS EXHAUSTED. REPRODUCTIONS WILL BE MADE IN BLACK AND WHITE ONLY.

TSL-121-2 65

DATE PROCESSED: [illegible]

PROCESSOR: [illegible]

WL TR-64-118

STATIC AND DYNAMIC COMPRESSIBILITY OF SUFFIELD EXPERIMENTAL STATION SOILS

by

M. T. Davisson
T. R. Maynard
M. T. Davisson, Foundation Engineer
Champaign, Illnois
Contract AF 29(601)-6325

April 1965

FOREWORD

This work was performed under Contract AF 29(601)-6325 with M. T. Davisson, Foundation Engineer, Champaign, Illinois. The tests were performed with equipment belonging to the Soil Mechanics and Foundation Engineering Division of the Department of Civil Engineering, University of Illinois, Urbana, Illinois, and were arranged under Purchase Order No. AF (29-601)-64-3929 with the University of Illinois. The entire program was under the general direction of Mr. M. T. Davisson and immediate supervision of the testing was performed by Mr. T. R. Maynard; Messrs. Davisson and Maynard are the authors of this report. Major assistance was given to the authors by Messrs. E. E. Rice, K. G. Nolte, and H. H. Dalrymple. The authors wish to thank Mr. A. J. Hendron, Jr., for reviewing the draft of this report.

This research was funded by the Defense Atomic Support Agency under Project 5710, Subtask 13.144, Program Element 7.60.06.01.5. This program was originally discussed with Captain H. E. Auld, USAF, and was monitored in the early stages by Captain George Bulin, USAF. Lieutenant J. E. Seknicka, AFWL (WLDC), was the monitor during the later stages of the program. The equipment used to perform the tests was developed under Contract AF 29(601)-5535 with the Soil Mechanics and Foundation Engineering Division of the Department of Civil Engineering, University of Illinois.

The research reported herein covers the period from February to September 1964. This report was submitted to the Air Force Weapons Laboratory in March 1965.

This technical report has been reviewed and is approved.

JOHN E. SEKNICKA
Lt USAF
Project Officer

THOMAS J. LOWRY, JR.
Colonel USAF
Chief, Civil Engineering Branch

R. A. HOUSE
Colonel USAF
Chief, Development Division

ABSTRACT

Static and dynamic one-dimensional compression tests were performed on each of ten 5-inch undisturbed shelby tube soil samples taken from the site of Operation Snowball at the Suffield Experimental Station. The maximum stresses attained were generally in the 390 to 1,300 psi range. The results of the tests are presented in the form of plots of axial stress versus axial strain, constrained modulus versus axial stress, and radial stress versus axial stress. The dynamic modulus observed for the upper 13 feet of the soil profile has a minimum value of approximately 3,000 psi, and is approximately twice the static value. Between the depths of 13 feet and 23 feet, moduli values ranging from 18,000 to 24,000 psi are applicable at the 100 psi stress level. Below a depth of 23 feet, the estimated water level, the constrained modulus is considered equal to that of water--300,000 psi. An air-blast-induced ground motion prediction was made for a range of 250 feet from a 500-ton TNT explosion. A peak transient surface displacement of 4.6 inches was computed for a time of 39 milliseconds after arrival of the shock front at the ground surface. Because of differences between the laboratory and field loading histories, and the strain rate sensitivity of the soil, the computed displacement is probably from 50 to 100 percent of the actual displacement.

This page intentionally left blank.

CONTENTS

Section		Page
I	INTRODUCTION	1
	1. Object	1
	2. Scope	1
II	SOILS INVESTIGATED	2
	1. Site Conditions	2
	a. Location and Topography	2
	b. Geology	2
	2. Subsurface Investigation	2
	a. Field Data	2
	b. Laboratory	3
	c. Soil Profile	9
III	TEST APPARATUS	12
	1. Apparatus Requirements	12
	2. Confining Rings	14
	3 Sample Trimming Equipment	16
	4. Static Test Machine	18
	5. 10-kip Dynamic Machine	18
	6. Instrumentation	27
IV	TEST PROCEDURE	31
	1. Sample Preparation Procedure	31
	2. Static Test Procedure	32
	3. Dynamic Test Procedure	32
	4. Post-Test Procedure	33
	5. Data Reduction	33
	a. Static Tests	33
	b. Dynamic Tests	34
V	TEST RESULTS	36
	1. Static Test Results	36
	2. Dynamic Test Results	36
VI	INTERPRETATION OF TEST RESULTS	43
	1. General	43
	2. Stress-Strain Relationships	43
	3. Radial Stress-Axial Stress Relationships	45
	4. Constrained Modulus-Depth Relationships	46
	5. Ground Motion Predictions	48
	6. Cratering	52
VII	CONCLUSIONS	54
	REFERENCES	55

	Page
APPENDIXES	56
I BORING LOGS	56
II STATIC TEST RESULTS	73
III DYNAMIC TEST RESULTS	107
DISTRIBUTION	138

ILLUSTRATIONS

Figure		Page
1	BORING PLAN	4
2	GRADATION CURVES - N17	7
3	GRADATION CURVES - R	8
4	SOIL PROFILE	11
5	ONE-DIMENSIONAL TEST REQUIREMENTS	13
6	CONFINING RING DATA	15
7	SCHEMATIC OF RING CALIBRATOR	17
8	CONFINING RING ASSEMBLY	18
9	SAMPLE TRIMMING EQUIPMENT	18
10	SCHEMATIC OF STATIC TEST MACHINE SHOWING AXIAL STRAIN INSTRUMENTATION	20
11	STATIC TEST MACHINE	21
12	CONFINING RING ASSEMBLY IN STATIC TEST MACHINE	21
13	SCHEMATIC OF 10-KIP DYNAMIC MACHINE	22
14	INSTRUMENTATION FOR AXIAL STRAIN-DYNAMIC	24
15	10-KIP DYNAMIC MACHINE	25
16	CONFINING RING ASSEMBLY IN 10-KIP DYNAMIC MACHINE	25
17	TYPICAL FM MAGNETIC TAPE DATA RECORDING	26
18	INSTRUMENTATION OF CONFINING RINGS	28
19	INSTRUMENTATION OF LOAD CELL FOR 10-KIP DYNAMIC MACHINE	29
20	STRESS-STRAIN RELATIONSHIP IN ONE-DIMENSIONAL COMPRESSION	39
21	THE RELATIONSHIP BETWEEN CONSTRAINED MODULUS AND AXIAL STRESS	40
22	THE RELATIONSHIP BETWEEN RADIAL AND AXIAL STRESS IN ONE-DIMENSIONAL COMPRESSION	41
23	TIME-VERTICAL STRESS-DEPTH RELATIONSHIP	49
24	STRESS-STRAIN RELATIONSHIP IN ONE-DIMENSIONAL COMPRESSION, N17-4.3	74
25	STRESS-STRAIN RELATIONSHIP IN ONE-DIMENSIONAL COMPRESSION, N17-8.6	75
26	STRESS-STRAIN RELATIONSHIP IN ONE-DIMENSIONAL COMPRESSION, N17-9.4	76
27	STRESS-STRAIN RELATIONSHIP IN ONE-DIMENSIONAL COMPRESSION, N17-16.8	77
28	STRESS-STRAIN RELATIONSHIP IN ONE-DIMENSIONAL COMPRESSION, N17-21.3	78
29	STRESS-STRAIN RELATIONSHIP IN ONE-DIMENSIONAL COMPRESSION, N17-33.3	79
30	STRESS-STRAIN RELATIONSHIP IN ONE-DIMENSIONAL COMPRESSION, R-6.6	80
31	STRESS-STRAIN RELATIONSHIP IN ONE-DIMENSIONAL COMPRESSION, R-14.5	81
32	STRESS-STRAIN RELATIONSHIP IN ONE-DIMENSIONAL COMPRESSION, R-17.6	82
33	STRESS-STRAIN RELATIONSHIP IN ONE-DIMENSIONAL COMPRESSION, R-22.5	83
34	STRESS-STRAIN RELATIONSHIP IN ONE-DIMENSIONAL COMPRESSION, R-28.4	84
35	THE RELATIONSHIP BETWEEN CONSTRAINED MODULUS AND AXIAL STRESS, N17-4.3	85
36	THE RELATIONSHIP BETWEEN CONSTRAINED MODULUS AND AXIAL STRESS, N17-8.6	86

Page

37 THE RELATIONSHIP BETWEEN CONSTRAINED MODULUS AND AXIAL STRESS, N17-9.4 87
38 THE RELATIONSHIP BETWEEN CONSTRAINED MODULUS AND AXIAL STRESS, N17-16.8 88
39 THE RELATIONSHIP BETWEEN CONSTRAINED MODULUS AND AXIAL STRESS, N17-21.3 89
40 THE RELATIONSHIP BETWEEN CONSTRAINED MODULUS AND AXIAL STRESS, N17-33.3 90
41 THE RELATIONSHIP BETWEEN CONSTRAINED MODULUS AND AXIAL STRESS, R-6.6 91
42 THE RELATIONSHIP BETWEEN CONSTRAINED MODULUS AND AXIAL STRESS, R-14.5 92
43 THE RELATIONSHIP BETWEEN CONSTRAINED MODULUS AND AXIAL STRESS, R-17.6 93
44 THE RELATIONSHIP BETWEEN CONSTRAINED MODULUS AND AXIAL STRESS, R-22.5 94
45 THE RELATIONSHIP BETWEEN CONSTRAINED MODULUS AND AXIAL STRESS, R-28.4 95
46 THE RELATIONSHIP BETWEEN RADIAL AND AXIAL STRESS IN ONE-DIMENSIONAL COMPRESSION, N17-4.3 96
47 THE RELATIONSHIP BETWEEN RADIAL AND AXIAL STRESS IN ONE-DIMENSIONAL COMPRESSION, N17-8.6 97
48 THE RELATIONSHIP BETWEEN RADIAL AND AXIAL STRESS IN ONE-DIMENSIONAL COMPRESSION, N17-9.4 98
49 THE RELATIONSHIP BETWEEN RADIAL AND AXIAL STRESS IN ONE-DIMENSIONAL COMPRESSION, N17-16.8 99
50 THE RELATIONSHIP BETWEEN RADIAL AND AXIAL STRESS IN ONE-DIMENSIONAL COMPRESSION, N17-21.3 100
51 THE RELATIONSHIP BETWEEN RADIAL AND AXIAL STRESS IN ONE-DIMENSIONAL COMPRESSION, N17-33.3 101
52 THE RELATIONSHIP BETWEEN RADIAL AND AXIAL STRESS IN ONE-DIMENSIONAL COMPRESSION, R-6.6 102
53 THE RELATIONSHIP BETWEEN RADIAL AND AXIAL STRESS IN ONE-DIMENSIONAL COMPRESSION, R-14.5 103
54 THE RELATIONSHIP BETWEEN RADIAL AND AXIAL STRESS IN ONE-DIMENSIONAL COMPRESSION, R-17.6 104
55 THE RELATIONSHIP BETWEEN RADIAL AND AXIAL STRESS IN ONE-DIMENSIONAL COMPRESSION, R-22.5 105
56 THE RELATIONSHIP BETWEEN RADIAL AND AXIAL STRESS IN ONE-DIMENSIONAL COMPRESSION, R-28.4 106
57 STRESS-STRAIN RELATIONSHIP IN ONE-DIMENSIONAL COMPRESSION, N17-3.9 108
58 STRESS-STRAIN RELATIONSHIP IN ONE-DIMENSIONAL COMPRESSION, N17-9.0 109
59 STRESS-STRAIN RELATIONSHIP IN ONE-DIMENSIONAL COMPRESSION, N17-16.4 110
60 STRESS-STRAIN RELATIONSHIP IN ONE-DIMENSIONAL COMPRESSION, N17-20.9 111
61 STRESS-STRAIN RELATIONSHIP IN ONE-DIMENSIONAL COMPRESSION, N17-33.0 112
62 STRESS-STRAIN RELATIONSHIP IN ONE-DIMENSIONAL COMPRESSION, R-6.1 113

Page

63 STRESS-STRAIN RELATIONSHIP IN ONE-DIMENSIONAL COMPRESSION, R-14.0 114
64 STRESS-STRAIN RELATIONSHIP IN ONE-DIMENSIONAL COMPRESSION, R-17.2 115
65 STRESS-STRAIN RELATIONSHIP IN ONE DIMENSIONAL COMPRESSION, R-22.0 116
66 STRESS-STRAIN RELATIONSHIP IN ONE-DIMENSIONAL COMPRESSION, R-28.0 117
67 THE RELATIONSHIP BETWEEN CONSTRAINED MODULUS AND AXIAL STRESS, N17-3.9 118
68 THE RELATIONSHIP BETWEEN CONSTRAINED MODULUS AND AXIAL STRESS, N17-9.0 119
69 THE RELATIONSHIP BETWEEN CONSTRAINED MODULUS AND AXIAL STRESS, N17-16.4 120
70 THE RELATIONSHIP BETWEEN CONSTRAINED MODULUS AND AXIAL STRESS, N17-20.9 121
71 THE RELATIONSHIP BETWEEN CONSTRAINED MODULUS AND AXIAL STRESS, N17-33.0 122
72 THE RELATIONSHIP BETWEEN CONSTRAINED MODULUS AND AXIAL STRESS, R-6.1 123
73 THE RELATIONSHIP BETWEEN CONSTRAINED MODULUS AND AXIAL STRESS, R-14.0 124
74 THE RELATIONSHIP BETWEEN CONSTRAINED MODULUS AND AXIAL STRESS, R-17.2 125
75 THE RELATIONSHIP BETWEEN CONSTRAINED MODULUS AND AXIAL STRESS, R-22.0 126
76 THE RELATIONSHIP BETWEEN CONSTRAINED MODULUS AND AXIAL STRESS, R-28.0 127
77 THE RELATIONSHIP BETWEEN RADIAL AND AXIAL STRESS IN ONE-DIMENSIONAL COMPRESSION, N17-3.9 128
78 THE RELATIONSHIP BETWEEN RADIAL AND AXIAL STRESS IN ONE-DIMENSIONAL COMPRESSION, N17-9.0 129
79 THE RELATIONSHIP BETWEEN RADIAL AND AXIAL STRESS IN ONE-DIMENSIONAL COMPRESSION, N17-16.4 130
80 THE RELATIONSHIP BETWEEN RADIAL AND AXIAL STRESS IN ONE-DIMENSIONAL COMPRESSION, N17-20.9 131
81 THE RELATIONSHIP BETWEEN RADIAL AND AXIAL STRESS IN ONE-DIMENSIONAL COMPRESSION, N17-33.0 132
82 THE RELATIONSHIP BETWEEN RADIAL AND AXIAL STRESS IN ONE-DIMENSIONAL COMPRESSION, R-6.1 133
83 THE RELATIONSHIP BETWEEN RADIAL AND AXIAL STRESS IN ONE-DIMENSIONAL COMPRESSION, R-14.0 134
84 THE RELATIONSHIP BETWEEN RADIAL AND AXIAL STRESS IN ONE-DIMENSIONAL COMPRESSION, R-17.2 135
85 THE RELATIONSHIP BETWEEN RADIAL AND AXIAL STRESS IN ONE-DIMENSIONAL COMPRESSION, R-22.0 136
86 THE RELATIONSHIP BETWEEN RADIAL AND AXIAL STRESS IN ONE-DIMENSIONAL COMPRESSION, R-28.0 137

TABLES

Number		Page
I	SAMPLE INFORMATION - BORING N17	5
II	SAMPLE INFORMATION - BORING R	6
III	INITIAL SPECIMEN DATA	10
IV	SUMMARY OF STATIC TEST DATA - FIRST LOADING	37
V	SUMMARY OF DYNAMIC TEST DATA - FIRST LOADING . . .	42

NOTATION

<u>Symbol</u>

c	=	Seismic velocity
c_i	=	Velocity of initial stress
c_p	=	Velocity of peak stress
e	=	Void ratio
e_i	=	Initial void ratio
g	=	Acceleration of gravity
K_o	=	Coefficient of earth pressure at rest
LL	=	Liquid limit
M_c	=	Constrained modulus
PI	=	Plasticity index
PL	=	Plastic limit
q_u	=	Unconfined compression strength
S_r	=	Degree of saturation
S_{ri}	=	Initial degree of saturation
S_s	=	Specific gravity of soil solids
w	=	Water content, percent of dry weight
w_i	=	Initial water content
γ	=	Natural unit weight of soil
γ_d	=	Dry unit weight of soil
γ_{di}	=	Initial dry unit weight of soil
γ_i	=	Initial moist unit weight of soil
ϵ_a	=	Axial strain
ϵ_r	=	Radial strain

μ - Poisson's ratio

ρ = Mass density

σ_a = Axial normal stress

σ_r = Radial normal stress

SECTION I

INTRODUCTION

1. Object

The object of this study is to determine the static and dynamic one-dimensional stress-strain characteristics of typical soils from the Suffield Experimental Station in Alberta, Canada. The dynamic soil properties will be used in ground motion studies (Operation Snowball) involving air-blast loading in the zero to 1,000 psi pressure range

2. Scope

Ten 5-inch-diameter shelby tube samples were furnished by the Air Force for this study; five samples were taken from each of two borings. Both static-undrained and dynamic one-dimensional compression tests were performed on undisturbed specimens from each sample. The peak axial stress in the static tests varied from 80 psi to 5,000 psi, whereas in the dynamic tests the range was from approximately 390 psi to 1,300 psi. The results of the tests are presented in the form of plots of axial stress versus axial strain, constrained modulus versus axial stress, and radial stress versus axial stress. In addition, the natural water content, specific gravity, Atterberg Limits, and grain size distribution have been determined for each of the ten samples. A presentation is also made of the soil profile as determined from boring logs, the test apparatus and procedures, and the use of the test results in a ground-motion estimate.

SECTION II

SOILS INVESTIGATED

1. Site Conditions

a. Location and Topography - The location of the site is within the Suffield Experimental Station (SES) blast range at a location known as Watching Hill. The site is approximately 30 miles north of Medicine Hat, Alberta, Canada (ref. 1). Within the area of interest, the site is essentially level with a ground surface elevation of approximately 2167.0 ft.

b. Geology - A brief description of the geology of the site is available in reference 2 along with an estimate of the seismic velocities for the various layers. The site is in the southern end of the Ross Depression which, along with the areas to the south and west, has apparently been covered by a large lake. The soils to a depth of 200 ft are lacustrine deposits consisting of uniform beds of clay and silt with occasional sand lenses. However, glacio-fluvial processes and desiccation have altered the upper 30 ft, approximately. In reference 2 a seismic velocity of 2,200 fps has been assigned to the upper 30 ft, but indications are given that the upper 4 ft may have a velocity of 700 fps while the lower 26 ft has a velocity of 2,550 fps. From 30 ft to 200 ft, a velocity of 5,500 fps is indicated.

Bedrock at the site consists of Upper Cretaceous beds of the Foremost formation. These beds may be arenaceous shales and/or sandstones with many coal and carbonaceous beds. In many places the "Pale Beds" overlie the Foremost formation and consist of sandstone, shales and sandy shales. The seismic velocity for these beds has been estimated as 7,500 fps. At great depth, Mississippian limestone exists with a seismic velocity of approximately 20,000 fps.

2. Subsurface Investigation

a. Field Data - At least eight borings have been made at the site to depths varying from 22 ft to 83 ft. Boring A was made at ground zero for Operation Snowball

and the log of the boring was made available for this study by the U. S. Army Engineer Waterways Experiment Station (ref. 3). Using Boring A as the center of coordinates, Borings B, C, D, E, and F are located 15 ft left of a line N39°W at distances of 70 ft, 200 ft, 250 ft, 340 ft, and 560 ft, respectively, as shown in figure 1. Boring R (AFWL Hole No. 1) is located N38°W 250 ft, and Boring N17 is located N31°E 20 ft. The location of all borings and the logs for Borings N17 and R were obtained from the Air Force Weapons Laboratory (ref. 4). Reproductions of the field boring logs for Borings A, N17, and R are given in appendix I. The specific location of the water table was not available, but it is known to vary seasonally between depths of 15 ft and 30 ft, approximately.

Some recent information concerning the seismic velocity profile was obtained from reference 4. In the upper 23 ft the average velocity is 1,050 fps, whereas below 23 ft the velocity is between 5,100 fps and 5,500 fps; a possible interpretation of the data is that the water table is at a depth of 23 ft. There is some indication that the seismic velocity is less than 1,000 fps in the upper 9 ft of the soil profile.

Five samples from Boring N17 and five samples from Boring R, ranging in depth from 3 ft to 33 ft, were furnished for this study. The samples were taken with 5-inch-diameter shelby tubes and extruded immediately into 6-inch-diameter fibre-board containers (ref. 5). Wax was then used to fill the containers and seal the samples.

b. Laboratory Data - The ten samples received in the laboratory were subjected to routine identification and classification, and their unconfined compression strengths were determined with a pocket penetrometer. For Boring N17, the sample number, depth, description, Unified Classification, unconfined compression strength, water content, Atterberg Limits, specific gravity, and other tests performed are listed in table I; similar information is listed in table II for Boring R. The gradation curves for the samples from Borings N17 and R are presented in figures 2 and 3, respectively. The specific gravity for each sample was assigned on the basis of a visual inspection and comparison with determinations made for each of the ten specimens subjected to grain size analyses.

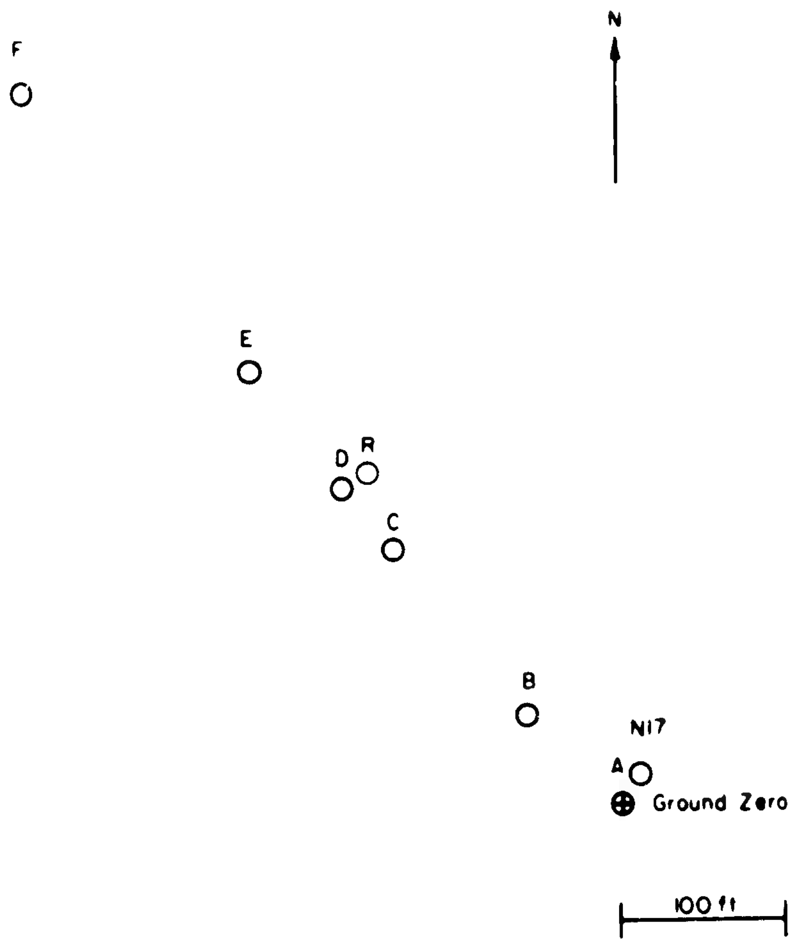

Figure 1. BORING PLAN

TABLE I

SAMPLE INFORMATION - BORING N17

SAMPLE NO.	DEPTH ft	DESCRIPTION	UNIFIED CLASSIF-ICATION	qu tsf	w %	LL %	PL %	Ss	OTHER TESTS
2	3.9	Brown very fissured silty clay, tr. of roots		3.75	10.2			2.82	Dynamic
	4.3	Brown fissured silty clay, tr. of roots and sand			13.9			2.82	Static
	4.6	Brown fissured silty clay, tr. of roots	CL			42.1	21.69	2.82	Grain size
5	8.6	Brown fissured clayey sandy silt, tr. of roots		4.5+	10.5			2.72	Static
	9.0	Brown fissured clayey sandy silt, tr. of roots		4.5+	11.1			2.72	Dynamic
	9.4	Brown fissured silty fine sand, tr. of roots			5.4			2.69	Static
	9.7	Brown fissured clayey sandy silt, tr. of roots	ML			27.5	23.9	2.72	Grain size
9	16.4	Brown fissured silty clay, tr. of sand		3.0	28.7			2.73	Dynamic
	16.8	Brown fissured silty clay			32.3			2.75	Static
	16.8	Brown fissured silty clay	CL			45.2	22.4	2.75	Grain size
11	20.9	Brown and Gray fissured silty clay, tr. of organic		2.8	33.6			2.75	Dynamic
	21.3	Brown and Gray fissured silty clay, tr. of organic			36.2			2.75	Static
	21.3	Brown and Gray fissured silty clay, tr. of organic	CL			48.7	24.3	2.75	Grain size
15	33.0	Gray fissured organic silty clay, tr. pebbles		0.8	22.6			2.73	Dynamic
	33.3	Gray fissured organic silty clay, tr. pebbles			19.4			2.73	Static
	33.3	Gray fissured organic silty clay, tr. pebbles	CL			44.5	17.7	2.73	Grain size

TABLE II

SAMPLE INFORMATION - BORING R

SAMPLE NO.	DEPTH ft	DESCRIPTION	UNIFIED CLASSIFICATION	qu tsf	w %	LL %	PL %	Ss	OTHER TESTS
4	6.1	Brown fissured silty clay, tr. of roots		4.4	15.1			2.78	Dynamic
	6.6	Brown fissured silty clay, tr. of sand and roots		3.0	18.7			2.76	Static
	7.0	Brown fissured silty clay, tr. of roots	CL		18.7	46.7	23.0	2.78	Grain size
12	14.0	Brown fissured silty clay, tr. of sand		3.0	13.3			2.75	Dynamic
	14.5	Brown fissured silty clay		2.5	23.9			2.76	Static
	14.9	Brown fissured silty clay	CL	3.5	22.1	42.6	23.1	2.76	Grain size
16	17.2	Brown fissured silty clay		2.0	31.5			2.76	Dynamic
	17.6	Brown fissured sandy silty clay		1.0	20.0			2.73	Static
	18.0	Brown fissured sandy silty clay	CL	2.3	12.6	31.2	22.3	2.73	Grain size
21	22.0	Brown fissured sandy clayey silt		1.0	29.8			2.72	Dynamic
	22.5	Brown fissured very fine sandy silt, tr. of clay		1.5	26.8			2.69	Static
	22.9	Brown fissured very fine sandy silt, tr. of clay	ML	1.4	24.4	NP	NP	2.69	Grain size
25	28.0	Gray fissured silty clay, tr. pebbles		0.25	34.8			2.73	Dynamic
	28.4	Gray fissured silty clay, tr. pebbles		0.4	31.9			2.73	Static
	28.7	Gray fissured silty clay, tr. pebbles	CL	0.5	33.2	38.7	23.1	2.73	Grain size

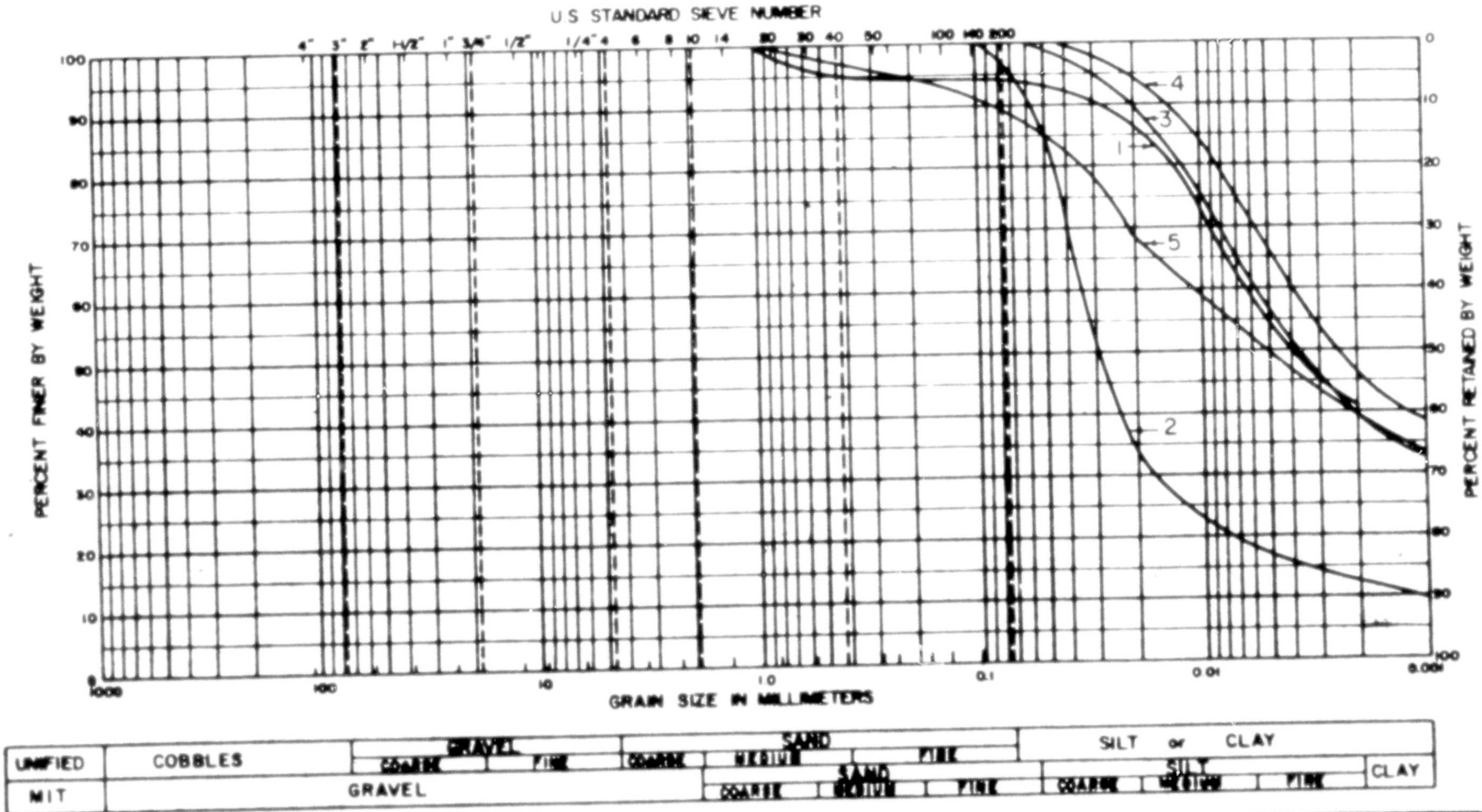

CURVE NO.	BORING NO.	SAMPLE NO.	DEPTH (Feet)	LL	PL	PI	UNIFIED CLASSIFICATION	
1	N17	2	4.6	42.1	21.7	20.4	Silty Clay, Tr. Sand	CL
2	"	5	9.7	27.5	23.9	3.6	Clayey Silt, Tr. Sand	ML
3	"	9	16.8	45.2	22.4	22.8	Silty Clay	CL
4	"	11	21.3	48.7	24.3	24.4	Silty Clay	CL
5	"	15	33.3	44.5	17.7	26.8	Sandy Silty Clay	CL

Figure 2. **GRADATION CURVES – N17**

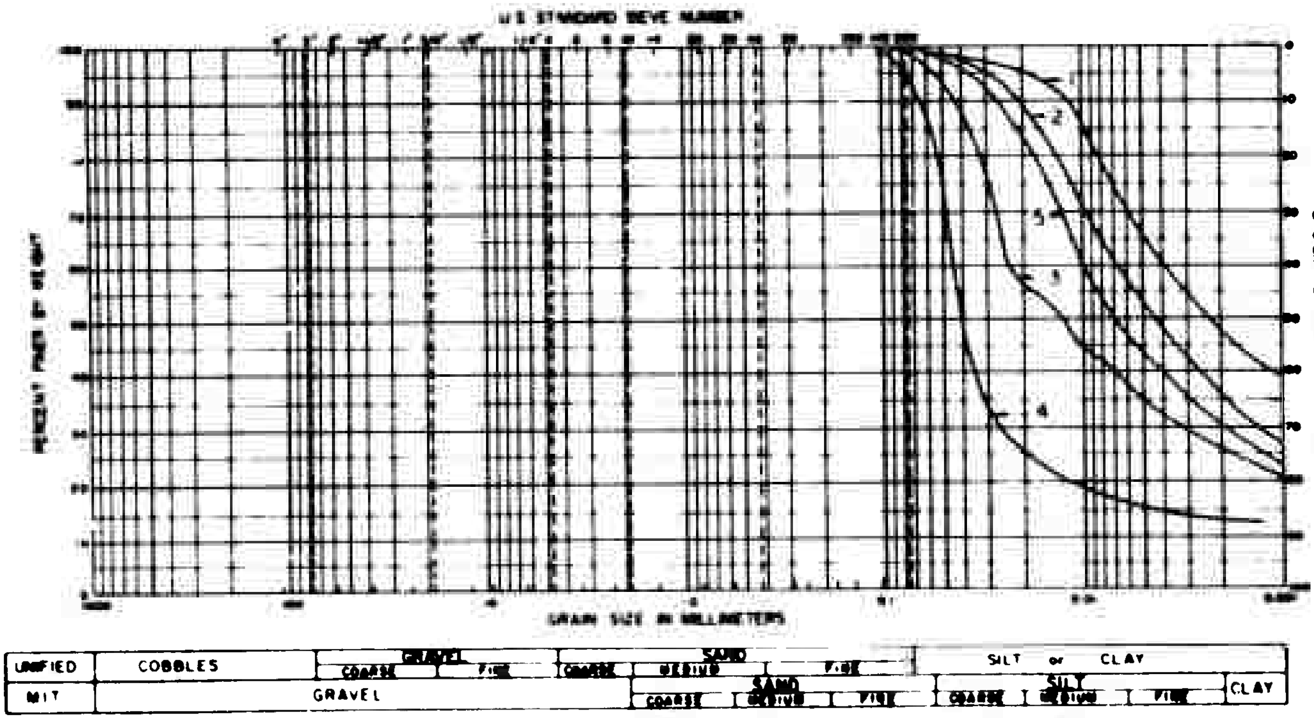

CURVE NO	BORING NO	SAMPLE NO	DEPTH (Feet)	LL	PL	PI	UNIFIED CLASSIFICATION	
1	R	4	7.0	46.7	23.0	23.7	Silty Clay	CL
2	"	12	14.9	42.6	23.1	19.5	Silty Clay	CL
3	"	16	18.0	31.2	22.3	8.9	Silty Clay	CL
4	"	21	22.9	NP	NP	NP	Clayey Silt, Tr Sand	ML
5	"	25	28.7	38.7	23.1	15.6	Silty Clay	CL

Figure 3. GRADATION CURVES – R

In denoting the actual test specimens, a designation involving both the boring number and the depth has been used. for example, sample N17-4.3 is from Boring N17 at a depth of 4.3 ft. The initial weight-volume data for each of the eleven static and ten dynamic test specimens are listed in table III. The eleventh static test was performed on sample N17-9.4 in the remolded state.

C. Soil Profile - On the basis of the boring logs in appendix I, the laboratory data in tables II and III, and the geological information in reference 2, the soil profile has been delineated as shown in figure 4. The upper layer, denoted as M1, is a brown sandy silt that is desiccated and fissured. the water content varies from 10 percent to 19 percent whereas the unconfined compression strength ranges from 3.7 tsf to values in excess of 4.5 tsf. The layer is approximately 13 ft thick.

Layer C2 is approximately 13 ft to 15 ft thick and consists of interbedded tan sandy silt and brown sandy clay. The water content varies from 20 percent to 35 percent, and the unconfined compression strength ranges from 1.4 tsf to 3.0 tsf.

Layer C3 is a blue-gray silty clay and varies from 0 to 12 ft in thickness. On one sample the water content was 33 percent and the unconfined strength 0.4 tsf.

Layer G4 consists of approximately 5 ft of coarse sand and gravel. Layer C5 is a gray silty clay presumably 170 ft thick. on sample N17-33.0 the water content was 21 percent and the unconfined strength 0.8 tsf.

It is possible that layer G4, in reality, consists of various separate lenses, and that layers C3 and C5 are continuous and the same.

The location of the ten samples furnished for this project are shown at their respective depths adjacent to the graphic logs on the soil profile, figure 4. The water content and the unconfined compression strength values are also shown on the profile. It should be noted that the soil profile is to scale vertically, but not horizontally. In constructing the soil profile a ground surface elevation of 2167.0 ft was assumed for all borings.

TABLE III

INITIAL SPECIMEN DATA

SAMPLE NO		DRY DENSITY	WATER CONTENT	DEGREE OF SATURATION	VOID RATIO	SPECIFIC GRAVITY
BORING NO - DEPTH	TEST*	γ_{di} - pcf	w_i - %	S_{ri} - %	e_i	Ss
N17 - 3.9	D	80.6	10.2	24.3	1.182	2.82
N17 - 4.3	S	86.3	13.9	37.8	1.038	2.82
N17 - 5.6	S	92.0	10.5	33.8	0.846	2.72
N17 - 9.0	D	86.9	11.1	31.7	0.953	2.72
N17 9.4	Rem S	88.2	5.4	16.1	0.902	2.69
N17 - 16.4	D	91.7	28.7	91.3	0.858	2.73
N17 - 16.8	S	89.7	32.3	97.3	0.913	2.75
N17 - 20.9	D	87.8	33.6	96.7	0.955	2.75
N17 - 21.3	S	84.3	36.2	96.2	1.035	2.75
N17 - 33.0	D	102.4	22.6	93.0	0.663	2.73
N17 - 33.3	S	104.3	19.4	83.7	0.633	2.73
R - 6.1	D	85.6	15.1	40.9	1.026	2.78
R - 6.6	S	83.8	18.7	48.9	1.055	2.76
R - 14.0	D	93.6	13.3	43.9	0.833	2.75
R - 14.5	S	84.8	23.9	64.0	1.031	2.76
R - 17.2	D	90.2	31.5	95.5	0.910	2.76
R - 17.6	S	91.0	20.0	62.6	0.872	2.73
R - 22.0	D	90.8	29.8	93.3	0.869	2.72
R - 22.5	S	86.3	26.8	76.3	0.945	2.69
R - 28.0	D	85.4	34.8	95.6	0.994	2.73
R - 28.4	S	86.8	31.9	90.4	0.963	2.73

* S = Static, D = Dynamic, Rem = Remolded

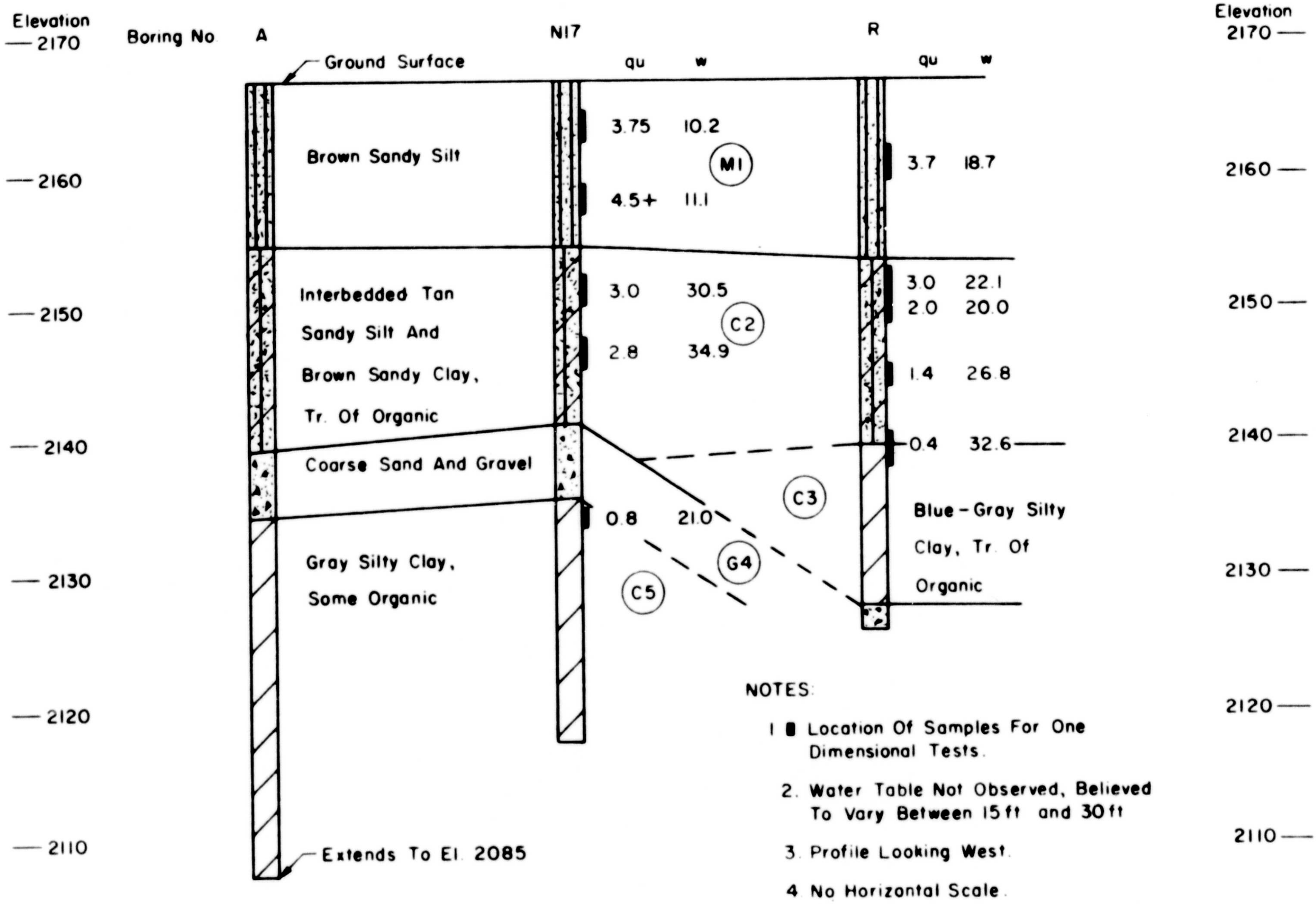

Figure 4. SOIL PROFILE

SECTION III

TEST APPARATUS

1. Apparatus Requirements

To perform dynamic one-dimensional compression tests, it is desirable to have a loading device capable of applying the full load in times as low as 5 milliseconds. Other desirable features are that the load be maintained for a controlled period of time and that the load be decayed rapidly. Consequently, the measuring equipment must be designed to respond to the high strain rates involved. For purposes of this study, the peak load capacity of the machine was required to be approximately 10 kips.

One-dimensional compression implies that no lateral strains are allowed to occur. Although this degree of lateral restraint is possible in static tests (reference 6), economical means are not available at present for controlling lateral strains in dynamic tests. Consequently, thick steel rings were used in this investigation to confine the soil specimens; the thickness of the ring was controlled to keep the radial strains to a minimum.

The problems and requirements of dynamic one-dimensional compression tests are illustrated schematically in figure 5. It is desirable to measure the axial stress, σ_a, the radial stress, σ_r, and the axial strain, ϵ_a, when the radial strain ϵ_r, is kept to a minimum. Further, simultaneous values of these measurements are desired, but such measurements are not feasible with the present state of the art of instrumenting soil tests. Therefore, indirect measurements are made that must be interpreted with considerable judgment to account for the influence of stress wave propagation on the time variation of the measured functions. For example, the peak axial stress wave passes through the SR-4 gage load cell before the soil specimen is stressed to this level. Furthermore, after the peak stress reaches the soil, there is a delay before the concomitant radial stress in the soil is indicated by the SR-4 gages on the periphery of the confining rings. In addition, inertia effects exist because of the mass of the

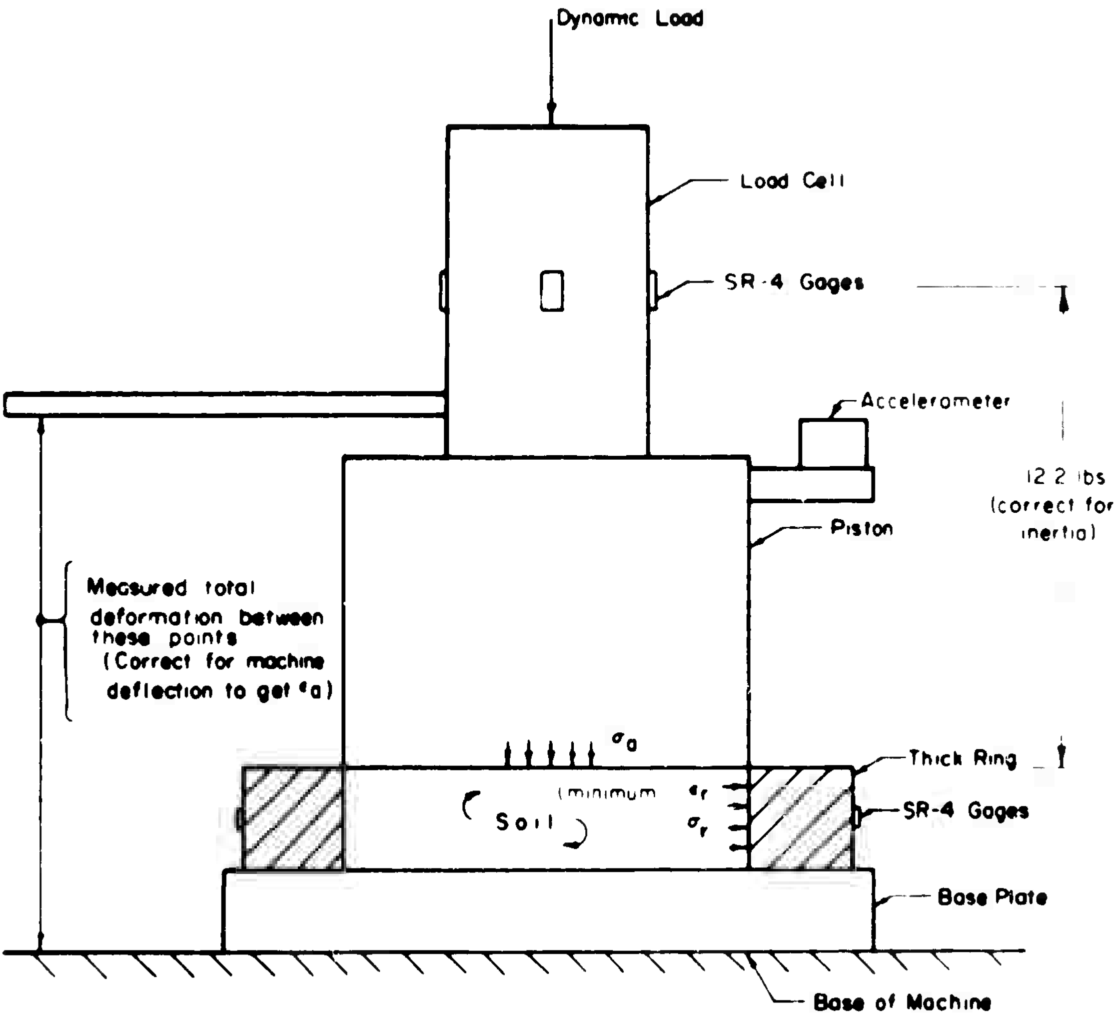

Figure 5. ONE-DIMENSIONAL TEST REQUIREMENTS

piston and load cell between the SR-4 gages on the load cell and the surface of the soil specimen; inertia effects also exist because of the mass of the ring between the soil perimeter and the SR-4 gages on the perimeter of the ring. Corrections may be made for these inertia effects providing the accelerations are known. It is possible to make a correction for the mass affecting the axial stress by measuring the acceleration of the piston, however, at present no practical means exists for measuring the radial accelerations. In previous studies (refs. 6 and 7) using similar equipment the corrections amounted to approximately 1 to 2 percent of the peak stresses and could be ignored, however, the inertia correction is a significant percentage of the peak stress attained in this study, and it must be accounted for.

Several other problems also exist even for static tests. The axial deflection is measured between two points remote from the soil specimen; therefore, the deflections of the equipment itself must be determined and subtracted from the recorded deflections. The usual problems of seating errors and ring wall friction are also present and must be minimized. The following section describes the details of the test apparatus along with the solutions, and compromises, to the foregoing problems.

2. Confining Rings

Thick steel rings 1.0 to 1.5 inches high with 4-inch inside diameters were used to confine the test specimens. To limit the amount of radial strain induced by an applied axial stress, the thickness of the ring in a radial direction was adjusted for the range of radial stresses that would be imposed. An attempt was made to limit the radial strains to the minimum value required to facilitate accurate recording by the use of SR-4 gages. A wall thickness of 0.1 inch was used for the 1,000-psi stress level, whereas the thickness ranged up to 0.5 inch for the static test carried to the 5,000-psi stress level. The dimensions of the rings, the pressure ranges in which they were used, the theoretical radial strain of the soil per psi of radial stress, and the output in microinches per psi of radial stress (as determined by calibration) are shown in figure 6.

Ring Number	Wall Thickness, inches	Ring Height, inches	Theoretical Strain, micro in/in psi	Recorded External Strain, micro in/in psi	Maximum Design Internal Pressure, psi
1	0.100	1.000	0.6460	1.333	1,000
2	0.100	1.000	0.6460	1.333	1,000
3	0.300	1.000	0.2460	0.429	2,500
4	0.300	1.000	0.2460	0.416	2,500
5	0.500	1.000	0.1620	0.240	5,000
6	0.500	1.000	0.1620	0.238	5,000
7	1.000	1.000	0.0965	0.105	10,000
8	1.000	1.000	0.0965	0.107	10,000
9	1.000	1.000	0.0965	0.110	10,000
10	0.100	1.500	0.6460	1.282	1,000
11	0.300	1.500	0.2460	0.420	2,500
12	0.500	1.500	0.1620	0.239	5,000

Figure 6. CONFINING RING DATA

Figure 7 is a schematic of the equipment that was used to calibrate the confining rings. The equipment consists essentially of a base and an upper cap having a chamber with a diameter equal to that of the inside diameter of the ring. The ring was inserted between the upper and lower parts and a clearance was maintained between them. The clearance was just sufficient for the ring to expand radially without inducing frictional forces against the upper and lower parts of the calibration device. A rubber diaphragm was used to contain the hydraulic fluid and prevent leakage between the clearances. Calibrations were carried out by inducing a pressure in the hydraulic fluid and recording this with a calibrated Bourdon gage. The output of the SR-4 gages was monitored with an SR-4 indicator; the calibrations were linear.

A photograph of the confining ring assembly is presented in figure 8. The confining ring is centered on the base plate with the aid of a lucite guide ring. In turn, the piston is centered on the soil specimen with the aid of a second lucite guide ring. Also shown in figure 8 are a split ring and an accelerometer. The split ring is mounted on the piston and furnishes a reaction for the dial indicators used to record axial deformation. The accelerometer is mounted on the cantilever bracket on the piston.

3. Sample Trimming Equipment

The important feature of the sample trimming equipment is the trimming ring. The trimming ring has a 4-inch inside diameter, equal to that of the confining rings, but the outside face is beveled to form a sharp cutting edge. The other face of the ring has a shoulder that fits the outside diameter of the 0.5-inch-thick confining rings. By using inserts, the shoulder can be made to fit the 0.3-inch and 0.1-inch-thick rings. When the confining ring and the trimming ring are pressed together, an integral unit is obtained that may be forced into a soil sample in a manner similar to the use of a thin-wall sampler in a field sampling operation.

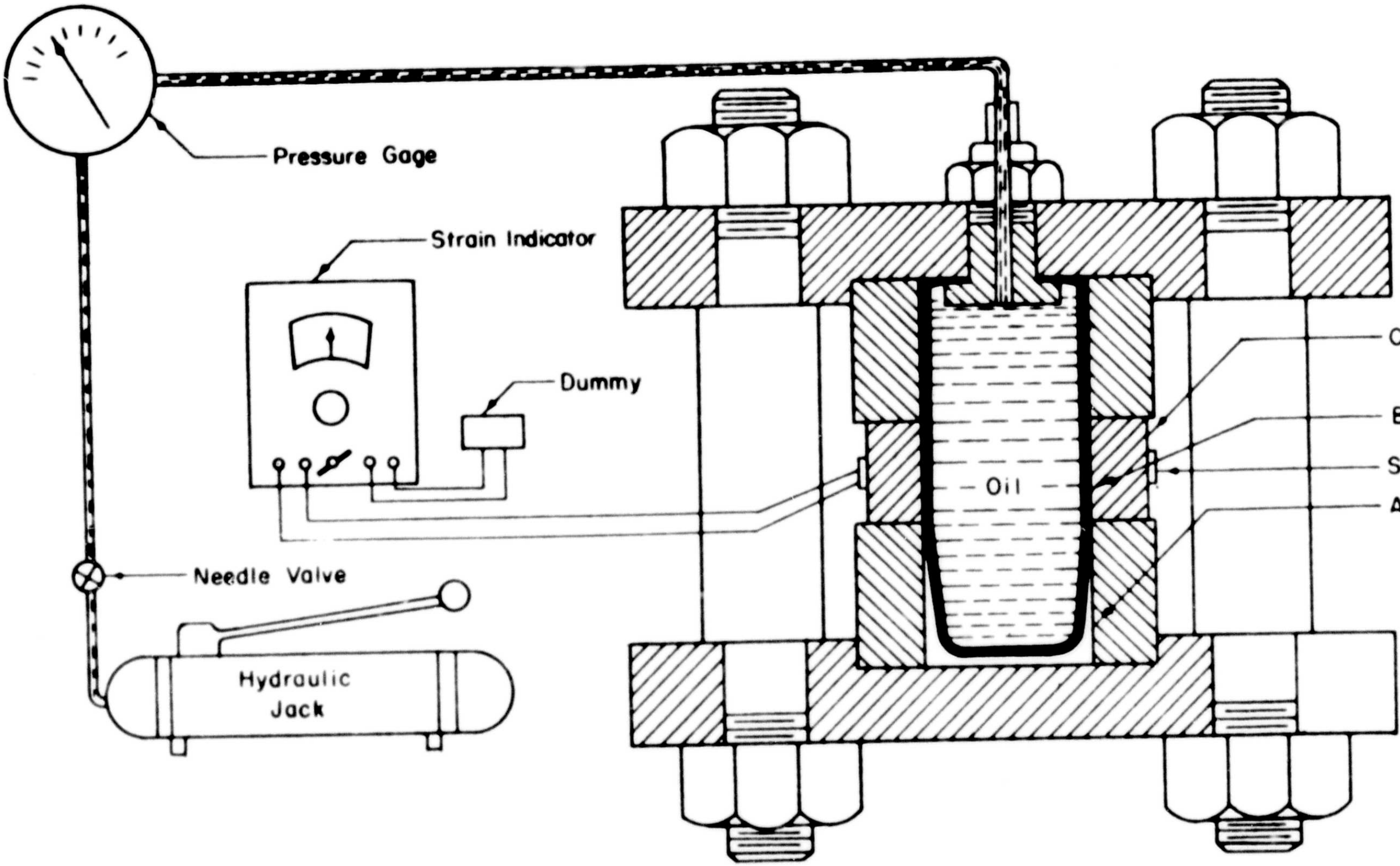

Figure 7. SCHEMATIC OF RING CALIBRATOR

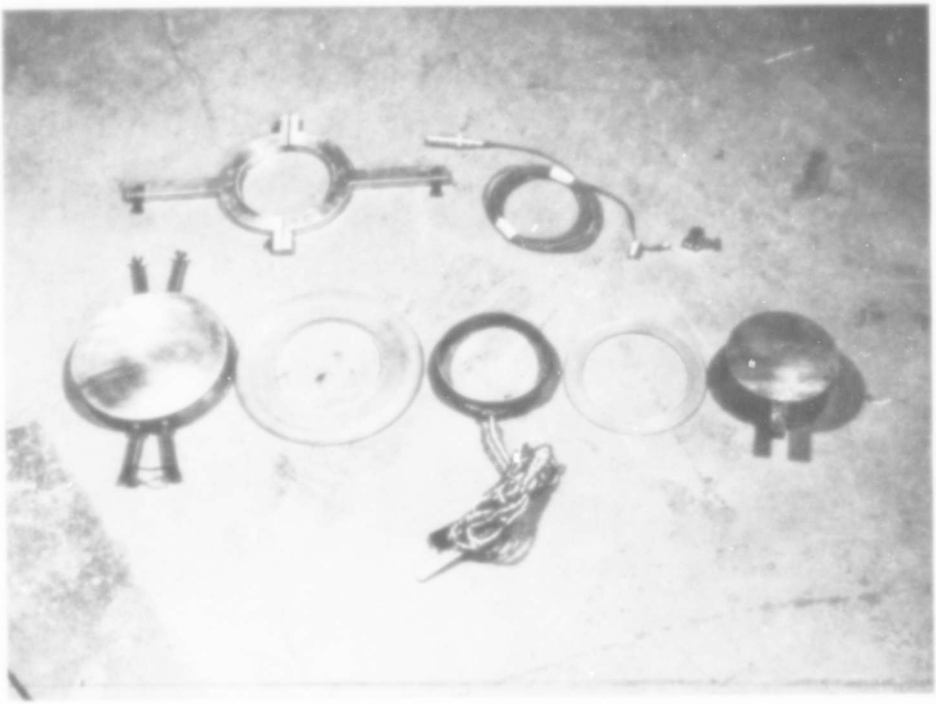

Figure 8. CONFINING RING ASSEMBLY

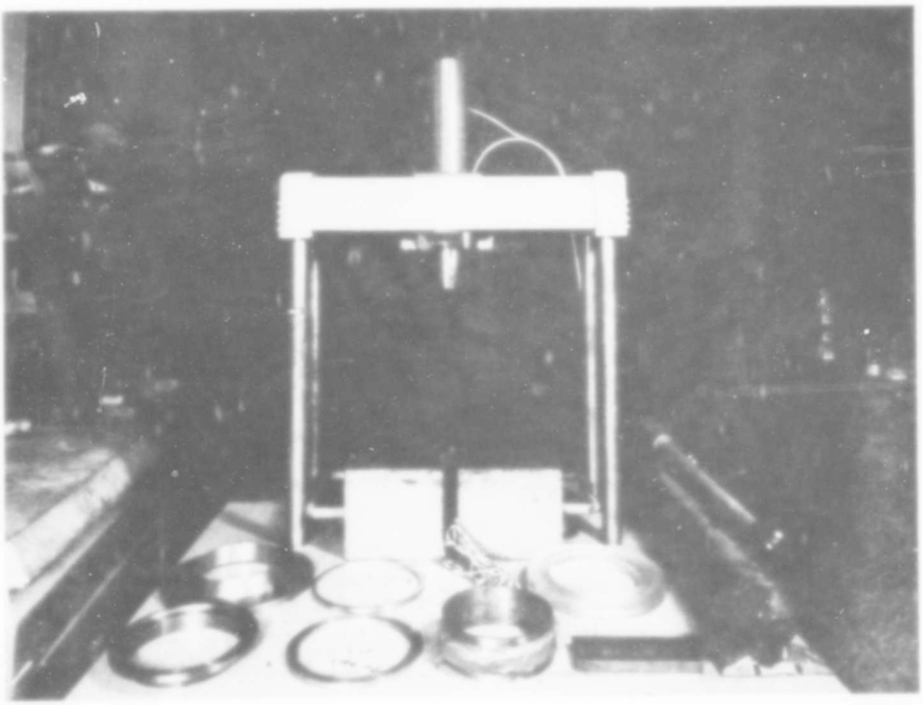

Figure 9. SAMPLE TRIMMING EQUIPMENT

A photograph of the sample trimming equipment is shown in figure 9, two beveled trimming rings are shown along with the inserts and a 1.5-inch-high confining ring. The hydraulic press is used to force the trimming ring into the soil sample.

4. Static Test Machine

A schematic of the apparatus used for the static one-dimensional tests is shown in figure 10. The loading device is a 300-kip universal Riehle hydraulic testing machine. The machine has six load ranges; the lowest range compatible with each test load was used to insure maximum accuracy in the axial load measurement. As indicated in figure 10, two dial indicators reading to 0.0001 inch per division were used to measure the axial strain. Circumferential strains on the exterior of the confining rings were recorded with an SR-4 indicator and converted to radial stresses in accordance with the calibrations described previously. A photograph of the static test machine is shown in figure 11; a close-up view of the confining ring assembly is shown in figure 12.

5. 10-kip Dynamic Machine

The main feature of the dynamic loader is the quick-opening valve that produces the dynamic load. The pneumatic valve will release gas from a reservoir (commercial nitrogen) at pressures up to 1,000 psi in times approaching 2 milliseconds. The details of the loader have been described previously in reference 8. Essentially, the pneumatic valve supplies a gas pressure which is collected on top of the main piston within an expansion chamber (fig. 13). The load applied on the main piston is carried through the dynamometer to the soil specimen.

The operation of the machine is initiated by raising the main piston to its upper position and closing the decay valve and main supply valve. A seating load is applied by slightly opening the main supply line valve and allowing 20 psi to build up in the expansion chamber; this produces sufficient load to overcome friction and induce a

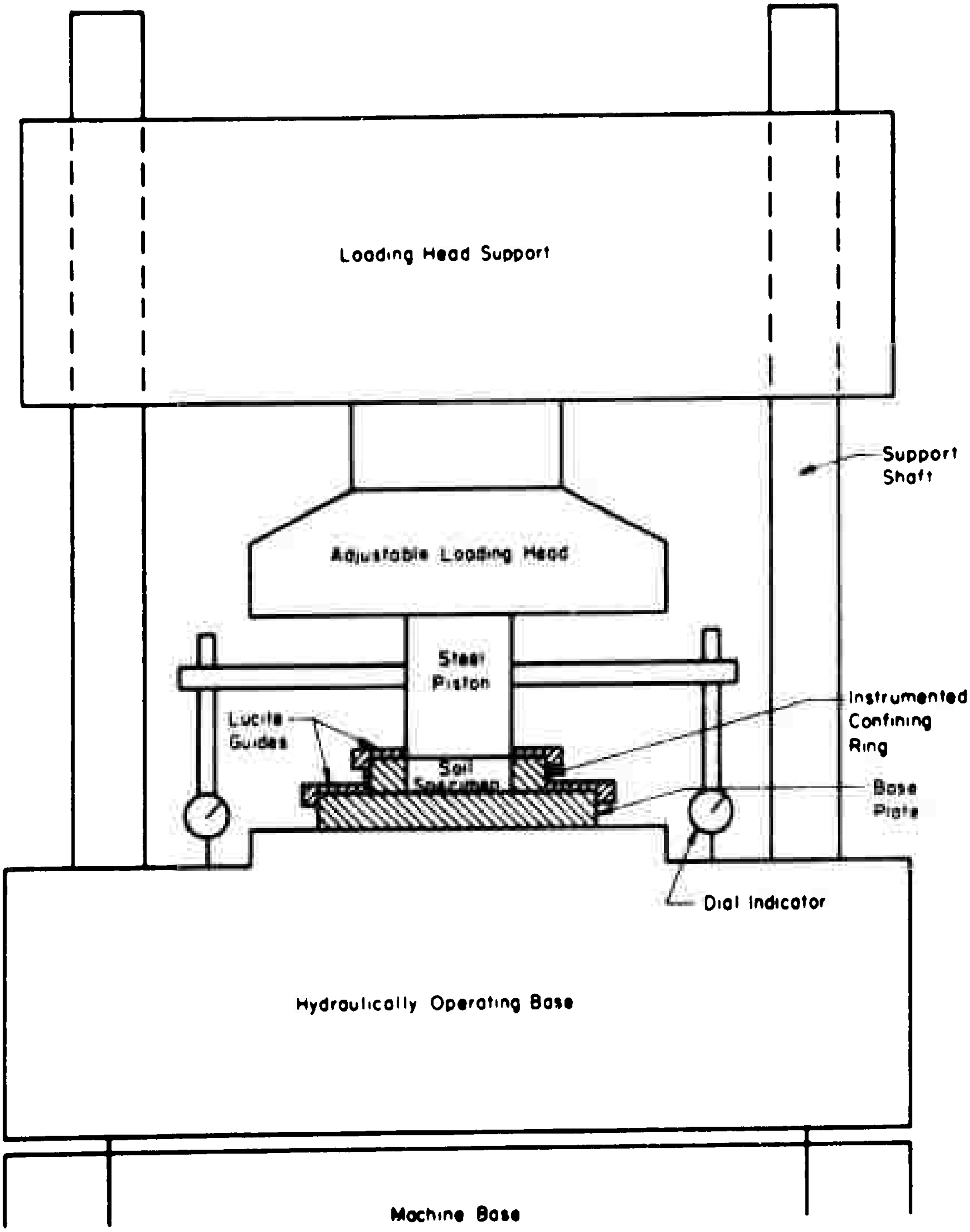

Figure 10. SCHEMATIC OF STATIC TEST MACHINE SHOWING AXIAL STRAIN INSTRUMENTATION

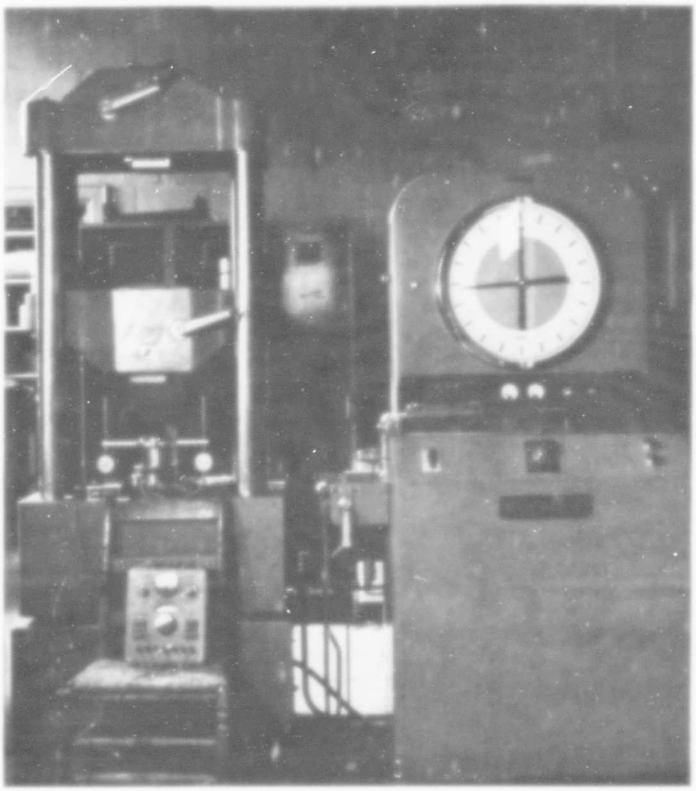

Figure 11. STATIC TEST MACHINE

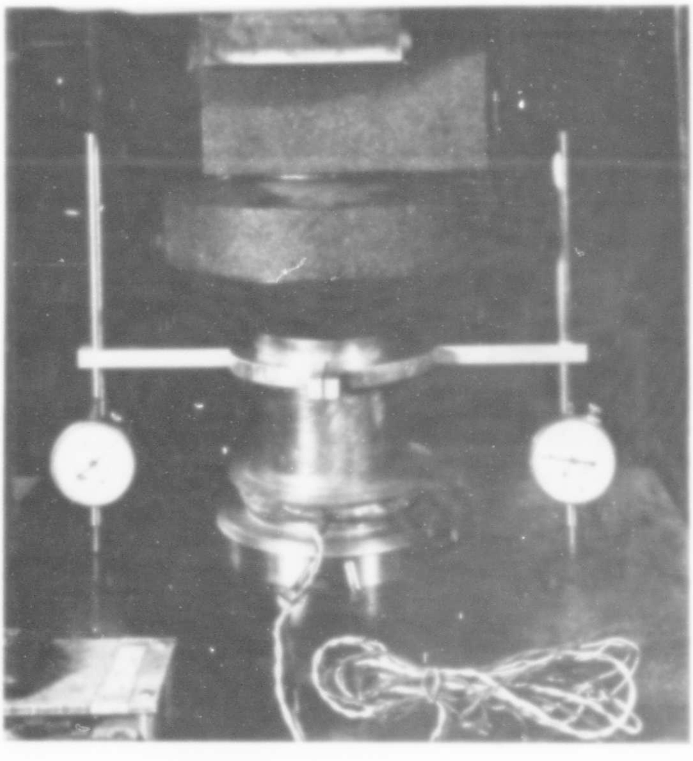

Figure 12. CONFINING RING ASSEMBLY IN STATIC TEST MACHINE

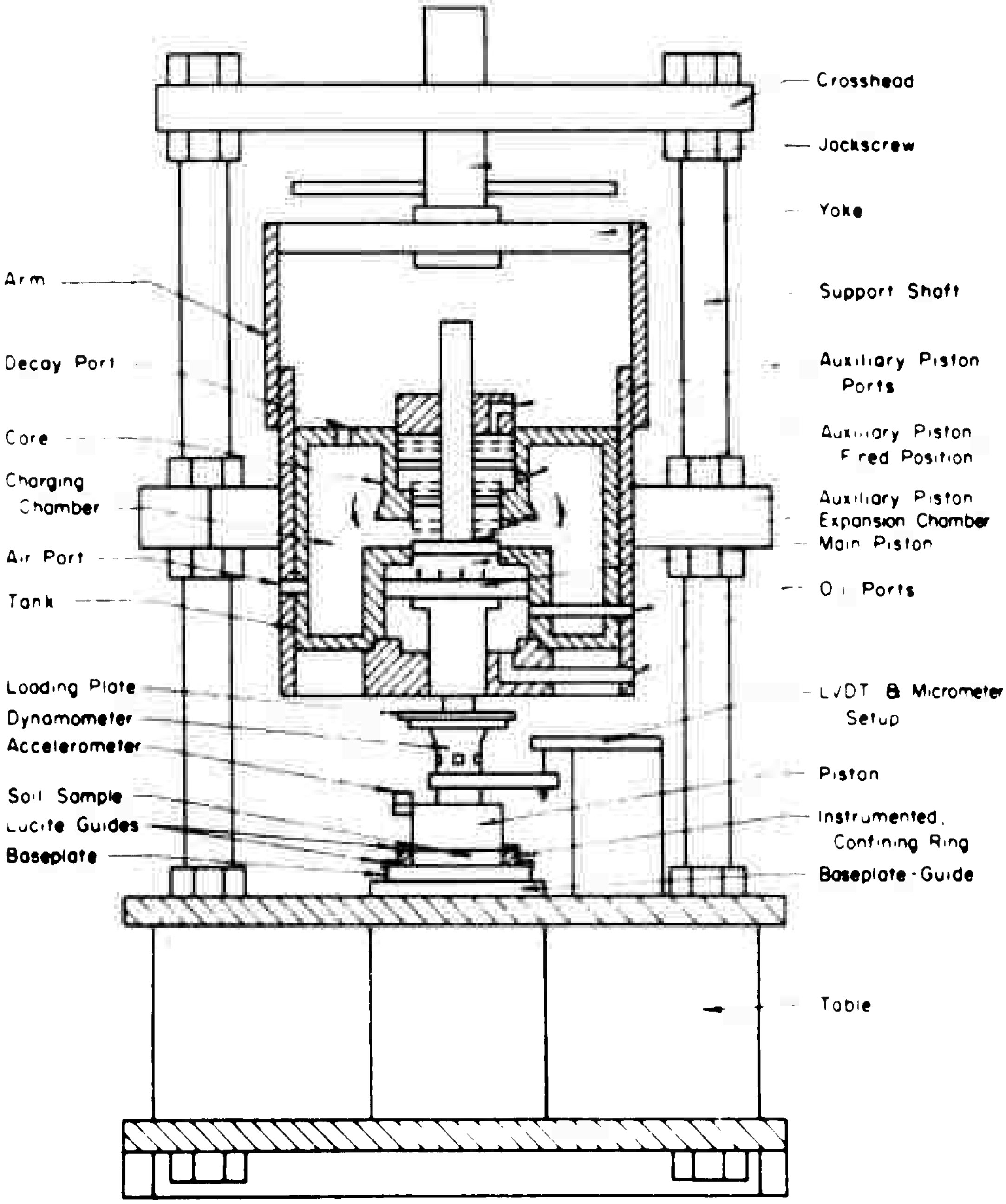

Figure 13. SCHEMATIC OF 10-KIP DYNAMIC MACHINE

stress of approximately 10 psi on the soil specimen. The auxiliary valve is then placed in the closed position, isolating the expansion chamber from the charging chamber, the charge pressure is then built up to the designated value (not exceeding 1,000 psi). The machine is now ready to be fired.

The auxiliary piston is held in the closed position by a mechanical stop. A solenoid-operated device trips the mechanical stop, thereby allowing the auxiliary piston to travel upward, opening the port from the charging chamber to the expansion chamber. This allows the gas to load the main piston, thereby producing the desired dynamic compressive loading on the soil specimen. The machine will maintain a load in equilibrium with the gas pressure in the expansion chamber until the decay valve is operated. The decay valve is operated in the same fashion as the auxiliary valve.

The confining ring assembly is shown schematically in the 10-kip Dynamic Machine in figure 14. A linear variable differential transformer (LVDT) was used to measure the axial deflection. A micrometer depth gage is attached to the LVDT core, and the assembly is cantilevered from the dynamometer. The LVDT transformer is attached to the platform of the machine. Two dial indicators reading to 0.001 inch per division are also mounted to the platform of the machine; these dials are used to record the axial deflection under the seating load. A photograph of the 10-kip Dynamic Machine is given in figure 15 and a close-up of the confining ring assembly is shown in figure 16.

A typical dynamic record obtained with the 10-kip Dynamic Machine is shown on figure 17. The record shown was originally recorded on an FM magnetic tape system and played back on an oscillograph employing a tape speed reduction factor of 16. Noise has been filtered out of the axial stress, axial deflection, and radial stress traces, but no filtering was employed on the accelerometer trace. An inspection was made of unfiltered traces to be sure that only noise produced by the electrical system itself was filtered out.

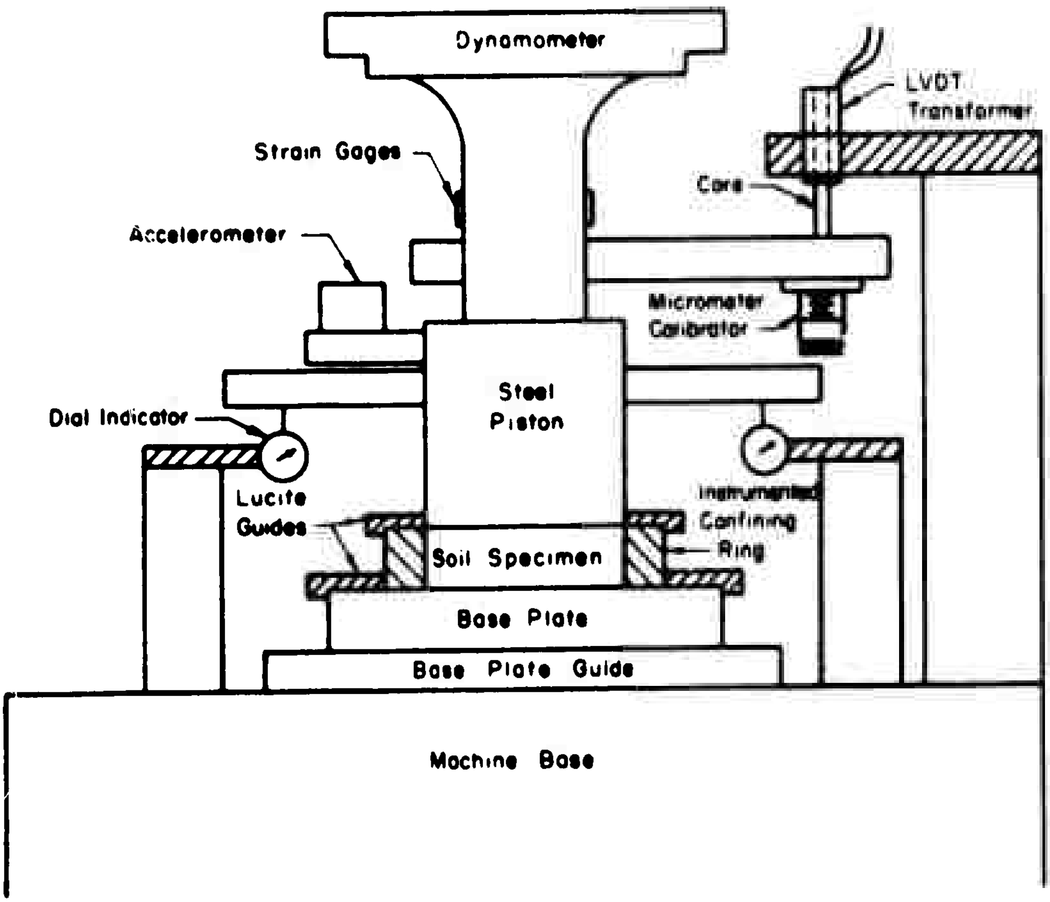

Figure 14. INSTRUMENTATION FOR AXIAL STRAIN-DYNAMIC

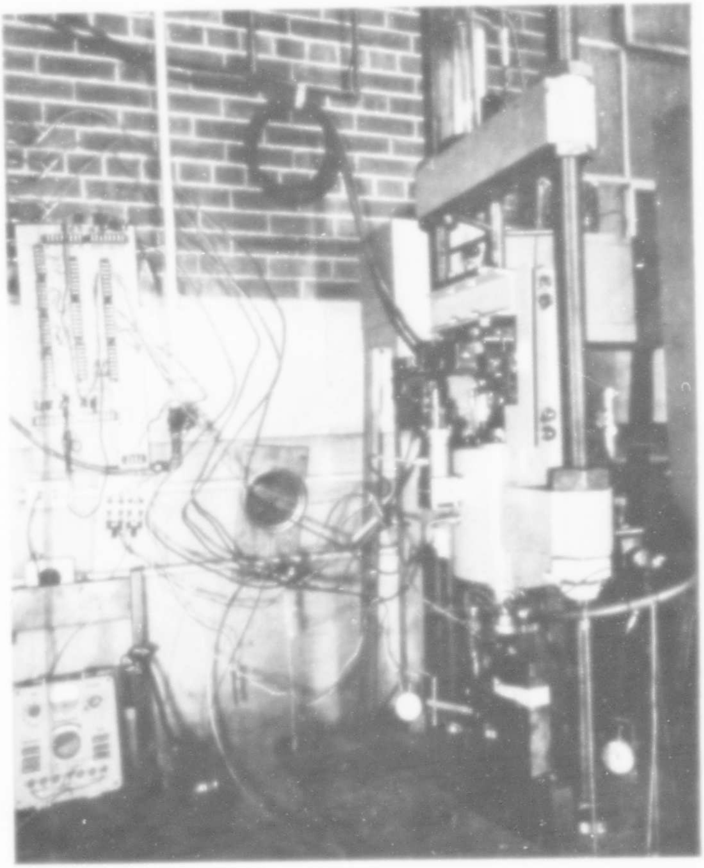

Figure 15. 10-KIP DYNAMIC MACHINE

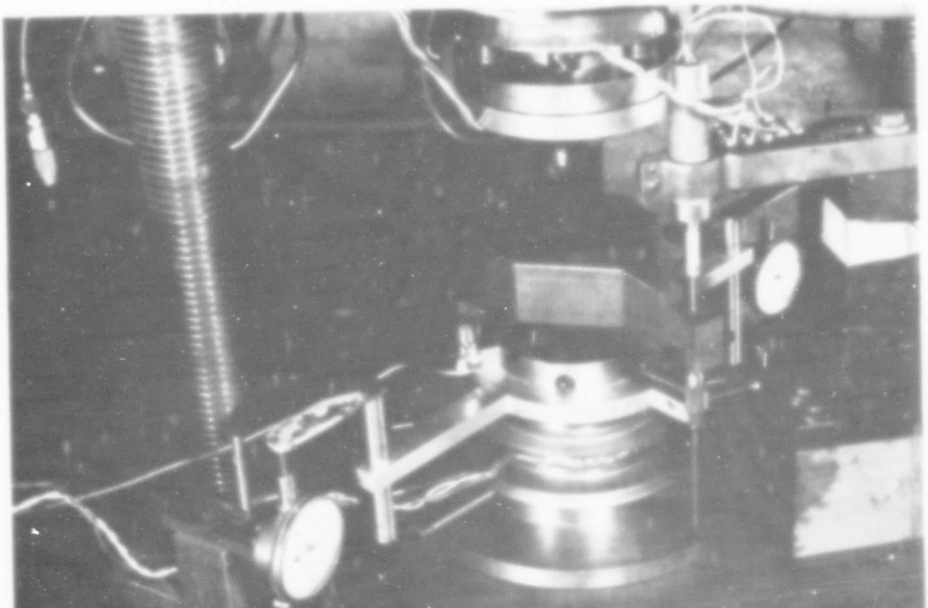

Figure 16. CONFINING RING ASSEMBLY IN 10-KIP DYNAMIC MACHINE

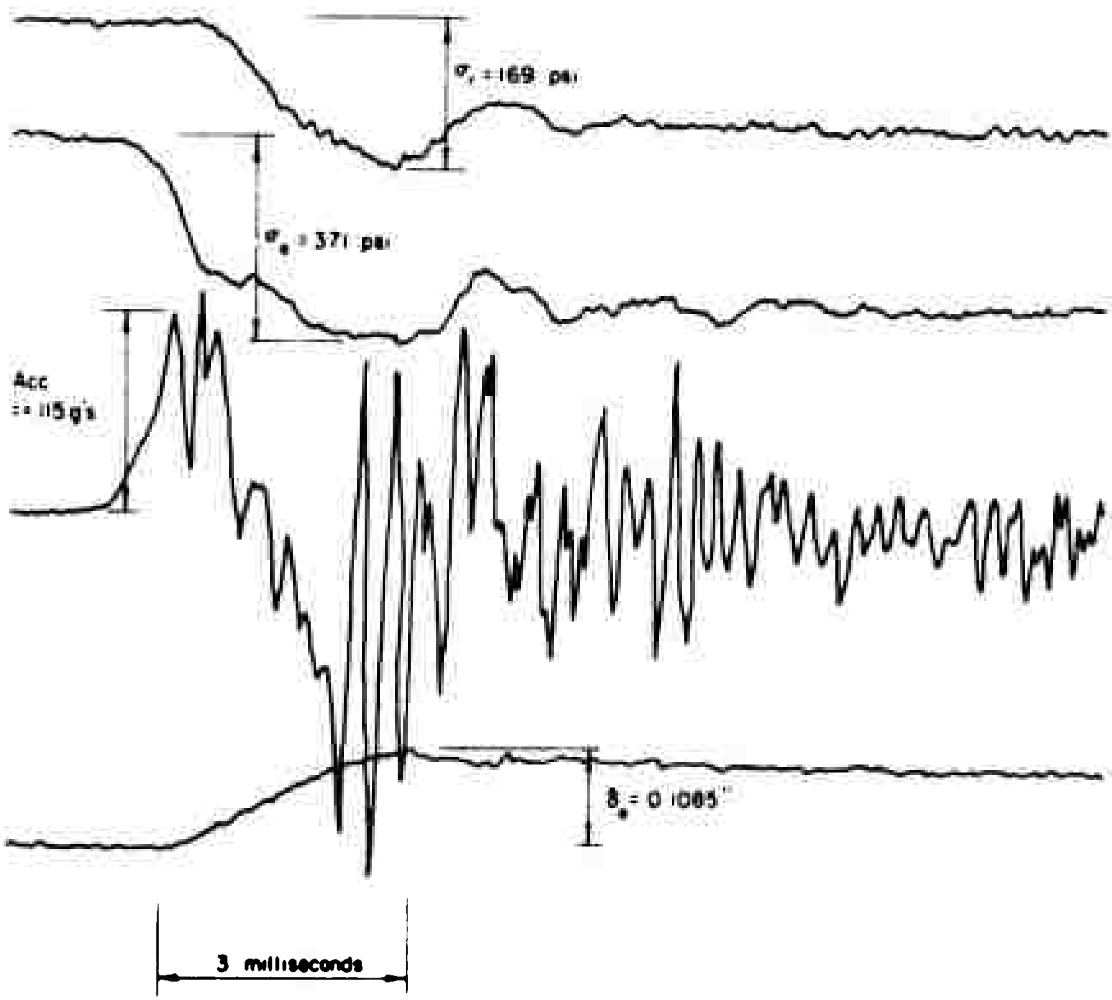

Dynamic Test on Sample N17-9.0, First Rise

Figure 17. TYPICAL FM MAGNETIC TAPE DATA RECORDING

6. Instrumentation

The confining ring and the load cell were instrumented with SR-4 gages connected in a standard four-arm bridge. The axial deformations were measured with an LVDT and the acceleration of the piston was measured with a piezoelectric accelerometer. These sensors were monitored with a CEC type 5-124 oscillograph and a Minneapolis Honeywell model 8100 FM magnetic tape recording system. The AC amplifiers used to drive the strain gage bridges and the LVDT were in a CEC type 1-127 20-kc 4-channel carrier system. The carrier system output was used to drive the galvanometers directly. A Kistler model 563 Charge Calibrator and model 566 Charge Amplifier were used, respectively, to calibrate and drive the accelerometer; the amplifier output was used directly to drive a galvanometer. All four amplifier output signals were fed through Dana model 2000 DC amplifiers to provide a signal for the FM tape system.

A CEC type 7-363 galvanometer with a 1000 cps response was used for the accelerometer; type 7-364 galvanometers with 500 cps response were used for the other three signals. A timing signal of 500 cps and a paper speed of 128 ips were used on the oscillograph. A timing signal of 10 kc and a tape speed of 30 inches per second were used on the FM tape.

Figure 18 is a schematic of the electrical hookup for the SR-4 gages on the confining ring. Four active gages were mounted on the periphery of the confining ring at 90-degree intervals. They record circumferential strains. Unstrained external dummy gages are used to complete the four-arm bridge.

Figure 19 is a schematic of the SR-4 gage hookup for the load cell used in the 10-kip Dynamic Machine. The hookup is a standard four-arm bridge. The table on figure 19 lists the various load cell capacities and the sensitivities in terms of stress on the soil specimen per microinch of output on the recorder as determined by static calibration in the static test machine. Load Cell No. 4 was used throughout this test program.

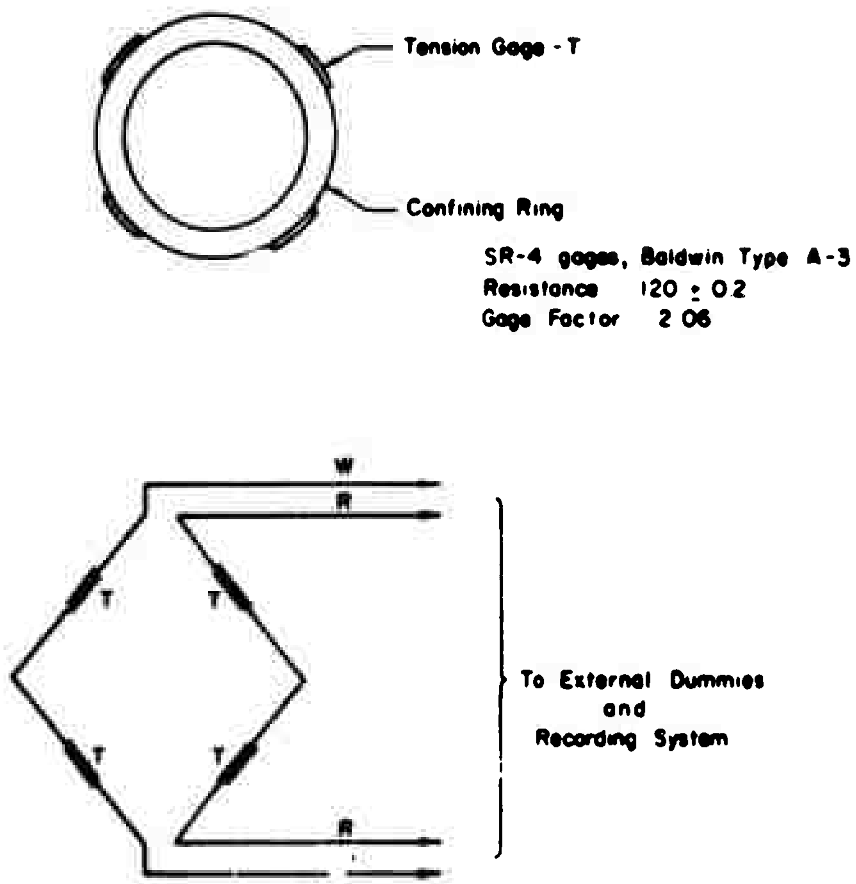

Figure 18. INSTRUMENTATION OF CONFINING RINGS

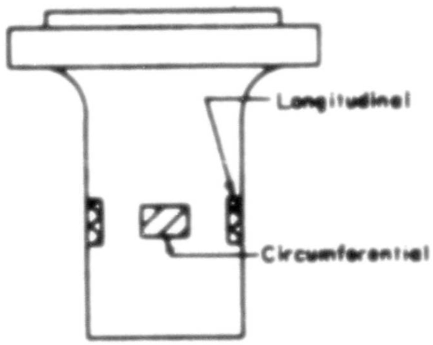

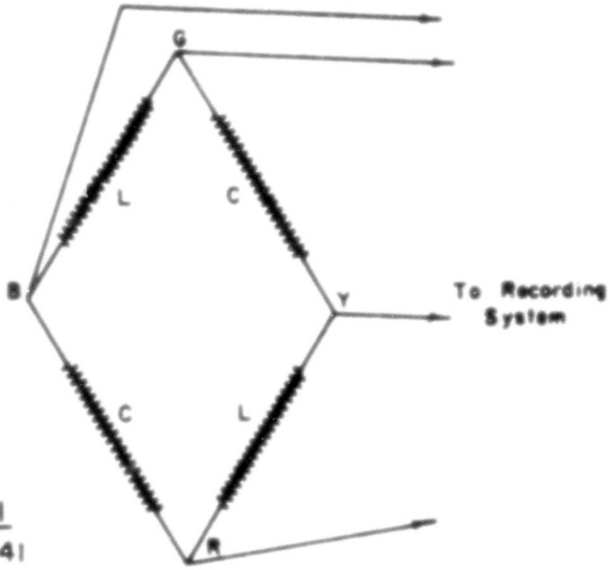

Material	Aluminum	Steel
Gage Type (Budd)	C12 - 141	C6 - 141
Resistance	120 ± 0.2	120 ± 0.2
Gage Factor	2.06	2.07

CELL NO.	MATERIAL	STRESS ON SPECIMEN, psi/micro in.	CAPACITY, kips
4	Aluminum 2024-T351	0.56	30
5	Steel, T-1	2.04	150
6	Steel, T-1	3.72	300

Figure 19. INSTRUMENTATION OF LOAD CELL FOR 10-KIP DYNAMIC MACHINE

A Schaevitz type 300SS-1 LVDT with a linear range of plus or minus 0.300 inch was used to measure the axial deflection. The LVDT core was attached to a micrometer depth gage to provide an accurate means of calibrating the core movement. An electrical null position was found before calibration of the LVDT; the core was then moved both up and down from the null position in predetermined increments as measured by the micrometer.

The accelerometer was an Endevco model 2252 with a Piezite Type II element. The working range was 0 to 500 g's. A calibration signal of 208 picocoulombs was specified for 100 g's of acceleration.

SECTION IV

TEST PROCEDURE

1. Sample Preparation Procedure

The preparation of each test specimen was initiated by cutting a 5-inch-long section from the lower end of the original shelby tube sample. Because sample disturbance is usually a minimum at the lower end of shelby tube samples, all test specimens were cut from as close to the bottom of the sample as feasible. Sample trimmings from the first test specimen cut from each shelby tube sample were set aside for specific gravity, Atterberg Limit, and grain size determinations. Water content samples were also taken from the shelby tube sections before and during the trimming process.

The trimming procedure involved placing the shelby tube section in the hydraulic press along with the sample trimming equipment described in section III.3. Excess soil was trimmed away with a knife as the trimming ring was forced into the sample. When the trimming ring had penetrated the soil a sufficient distance the trimming ring was carefully removed and the soil specimen was cut level with the height of the confining ring.

The tare weight of the confining ring is known along with its dimensions. Therefore, the weight of the ring and soil specimen furnishes sufficient data to calculate the initial density of the soil. With the specific gravity and water content data, complete weight-volume determinations can be made for the test specimen.

The final step is to place the confining ring on the base plate and to assemble the confining ring assembly. A height determination for the assembly is made in a dial comparator to an accuracy of 0.001 inch. Because the height of the assembly itself is known, the dial comparator reading furnishes a check on the initial height of the specimen.

2. Static Test Procedure

The confining ring assembly was placed in the static test machine as shown in figures 10 and 12. The dial indicators were set at zero under the load of the piston itself which corresponds to a stress of approximately 1 psi. The first applied load was a seating load of approximately 10 psi. Succeeding loads were applied in predetermined increments and held until the dial indicator and radial stress observations were made. A similar procedure was followed during unloading; however, at zero applied load the soil specimen was allowed to rebound for approximately 5 minutes, whereas the load increments required approximately 1 minute for completion. In general, the first loading was carried to a stress of 300 psi and the second loading to a stress of 1,000 psi.

3. Dynamic Test Procedure

The confining ring assembly was placed in the 10-kip Dynamic Machine as shown in figures 14 and 16. Zero readings were obtained for the dial indicators under the weight of the piston (1 psi). Calibration steps for the axial stress, radial stress, and acceleration were obtained on both the oscillograph and the FM tape by electric simulation. Then, a seating stress of approximately 10 psi was applied to the specimen statically and the axial deflection was observed on the dial indicators; the dial stems were freed from contact after the measurement. An SR-4 indicator was used to monitor the load cell during application of the seating load. At this point the LVDT was calibrated in steps over the range of axial deflection anticipated in the test. The first cycle of dynamic loading was then applied. A rise time of approximately 2 to 4 milliseconds was obtained; the dwell time was approximately 40 to 50 milliseconds and the decay time approximately 550 milliseconds.

Upon completion of the first dynamic load cycle the specimen was checked for extrusion and the residual deflection was recorded after the dial indicator stems were lowered into position. The residual axial load was approximately equal to the

seating load in all cases as recorded with an SR-4 indicator. An inspection was made of the oscillograph record to make sure that all systems behaved properly. Then, a second cycle of dynamic loading was applied to obtain the reload characteristics for those specimens that did not extrude under the first load cycle. The same check procedures were followed at the end of the second load cycle as were used at the end of the initial load cycle.

4. Post-Test Procedure

Upon removing the confining ring assembly from the test machine (either static or dynamic), the height was determined with the dial comparator. This reading was compared to the initial dial comparator reading and served as a check on the residual deflection. The confining ring and specimen were removed from the assembly and a careful inspection was made for extrusion before a final water content determination was made.

5. Data Reduction

a. Static Tests - The loads were predetermined to correspond to selected stresses; hence, no data reduction was necessary to obtain the axial stress. The average of the two dial indicator readings was used to obtain the axial deflection; machine deflections were subtracted as required according to a calibration. The net axial deflection was divided by the initial height of the specimen to obtain the corrected axial strain. The circumferential strains recorded with the SR-4 indicator were converted to radial stress according to the predetermined calibration factor.

Because of the large axial strains, on the order of 20 to 30 percent, a correction was applied to the measured radial strains in order to obtain radial stresses believed to be more representative of actual conditions. Because a thick ring is used as the radial strain sensing element, it is possible to have several pressure conditions on the inside of the ring that produce the same response in the strain gages on the

perimeter of the ring. For this reason, the confining ring is essentially a load measuring device. An attempt to correct the measured radial stresses has been made by dividing the load determined from a hydraulic calibration on the full height of the ring by the actual area of the specimen. This amounts to dividing the uncorrected radial stress by the quantity $1 - \epsilon_a$ to obtain the corrected radial stress.

The actual manipulation of the data was performed on an IBM 1620 digital computer. A program was written that requires the following input data: axial stress, axial deflection (uncorrected and unaveraged), circumferential strain from the SR-4 indicator, water content, specific gravity, diameter of specimen, height of specimen, weight of specimen, and acceleration of the piston. The acceleration is zero in the static tests, but provision was made in the program for acceleration so that the same program can be used for the dynamic tests also. The program processes the data and supplies the following output: axial stress, corrected axial strain, radial stress, corrected radial stress, void ratio, degree of saturation, dry density, tangent modulus, and secant modulus. The computer output is then ready for plotting.

b. Dynamic Tests - The FM tape recording was played back on the oscillograph to obtain a record like that shown in figure 17. Simultaneous determinations were made of the axial and radial stresses, the axial deflection, and the acceleration. Determinations were made at each peak or valley in the acceleration trace. The data obtained were fed into the computer program described in paragraph a above. The program corrects the axial stress for the inertia of the piston according to the acceleration data. The piston and the load cell between the SR-4 gages and the piston weigh 12.2 lb; the area of the soil specimen is 12.56 in^2. Therefore 1 g of acceleration is equivalent to slightly less than 1 psi of axial stress. Otherwise, the computer program supplies the same information supplied for the static tests.

Some doubt exists regarding the physical significance of the high frequency oscillations observed in the acceleration traces, such as the one shown in figure 17. It is possible that the oscillations are a function of the mounting of the accelerometer; however, the oscillations observed in the deflection trace may be used as an argument for the existence of the acceleration oscillations in the piston. The treatment of the test data described in the following section has the effect of using an acceleration trace that has been averaged through the oscillations.

SECTION V

TEST RESULTS

1. Static Test Results

The results obtained by using the digital computer data reduction program have been plotted in the form of axial stress versus corrected axial strain, constrained modulus versus axial stress, and corrected radial stress versus axial stress. The data points have not been shown on the plots because none of the points deviate from the curves. The axial stress versus axial strain plots for the 11 static tests are given in figures 24 to 34 in appendix II Similarly, the constrained modulus versus axial stress plots are given in figures 35 to 45 and the radial stress versus axial stress plots in figures 46 to 56. The boxes in the upper left corner of the Figures contain initial weight-volume data for the samples.

A summary of the static test data for the first load cycle is presented in table IV. For each test the initial degree of saturation and the seating stress and seating strain are given. At the maximum axial stress the corresponding values of axial strain and degree of saturation are given; in addition, the ratio of radial stress to axial stress (denoted as K_0) is given. The value of K_0 applicable to an arbitrary initial axial stress range is also given along with the limit of the axial stress range. A pseudo Poisson's ratio (μ) has been calculated assuming that elastic theory is applicable. The residual axial strain and the ratio of residual to maximum axial strain are also presented. A notation is made in table IV wherever extrusion occurred. Otherwise, the static test results may be interpreted in a straightforward manner.

2. Dynamic Test Results

The data obtained by using the digital computer program do not plot smoothly for the dynamic tests; therefore, some interpretation is required. The same types of plots have been made for the dynamic tests as were made for the static tests. The manner in which the plots were made is described in the following paragraphs.

TABLE IV

SUMMARY OF STATIC TEST DATA - FIRST LOADING

SAMPLE NO.	INITIAL VALUE	SEATING VALUES		INITIAL PEAK				INITIAL VALUE	POISSON'S RATIO	RESIDUAL STRAIN	RATIO OF RESIDUAL STRAIN TO MAX. STRAIN
(Boring No - Depth)	S_r - %	σ_a - psi	ϵ_a - in/in	σ_a - psi	ϵ_a - in/in	S_r - %	K_o	K_o/Limit σ_a - psi	$u = K_o/1 + K_o$	ϵ_a - in/in	ϵ_a resid. / ϵ_a max.
N17 - 4.3	37.8	11.1	0.0046	300	0.106	47.5	0.42	0.25/100	0.20	0.084	0.793
N17 - 8.6	33.8	9.6	0.0026	299	0.103	43.5	0.50	0.28/ 50	0.22	0.083	0.799
N17 - 9.4	16.1	23.9	0.0065	300	0.057	18.3	0.44	0.44/300	0.31	0.046	0.806
*N17 -16.8	97.3	10.0	0.0021	600	0.068	113.4	0.95	0.95/600	0.49	0.078	0.872
*N17 -21.3	96.2	10.0	0.0043	108	0.055	107.9	0.90	0.90/108	0.47	0.055	1.000
*N17 -33.3	83.7	10.0	0.0109	5000	0.027	90.0	1.00	1.00/5000	0.50	0.034	1.260
R - 6.6	48.9	9.6	0.0067	299	0.198	79.5	0.80	0.65/100	0.44	0.177	0.894
R -14.5	64.0	9.6	0.0080	299	0.147	90.0	0.75	0.80/100	0.37	0.116	0.788
R -17.6	62.6	9.6	0.0026	299	0.057	71.3	0.40	0.25/100	0.29	0.043	0.754
R -22.5	76.3	9.6	0.0080	299	0.091	93.9	0.47	0.47/299	0.32	0.074	0.813
*R -28.4	90.4	9.6	0.0019	80	0.018	93.9	1.00	1.00/ 80	0.50	0.018	1.000

* - Extrusion

The axial stress versus axial strain relationship for sample R-6.1 is presented in figure 20. Straight lines connecting the data points have been drawn to indicate the basic data through which the stress-strain curve was drawn. It was assumed that, in general, the data points oscillate about the desired curve. Also, more weight was given to data points where the acceleration was negligible. Once the stress-strain curve has been obtained, the constrained secant modulus can be determined as a function of the axial stress, as shown in figure 21.

The data points for the corrected radial stress versus axial stress plot have been connected with straight lines as shown in figure 22. Again, more weight was given to data points where the acceleration was negligible. Because of radial inertia in the confining ring, the strain gages indicated a lower radial stress than actually exists, especially near the beginning of the test. These factors, plus judgment based on previous experience, have been considered in arriving at the radial stress-axial stress relationship.

The stress-strain curves for the ten dynamic tests are presented in figures 57 to 66 in appendix III. Similarly, the constrained modulus-axial stress plots are presented in figures 67 to 76, and the radial stress-axial stress plots in figures 77 to 86. A summary of the dynamic test data for the first load cycle is presented in table V. The same information is given for the dynamic tests as was given for the static tests in table IV, with the exception that Poisson's ratio was deleted. Additional information is given concerning the time required for the load to reach its maximum value (rise time), the time interval that the steady state load was held (dwell time), and the time required to release the load (decay time).

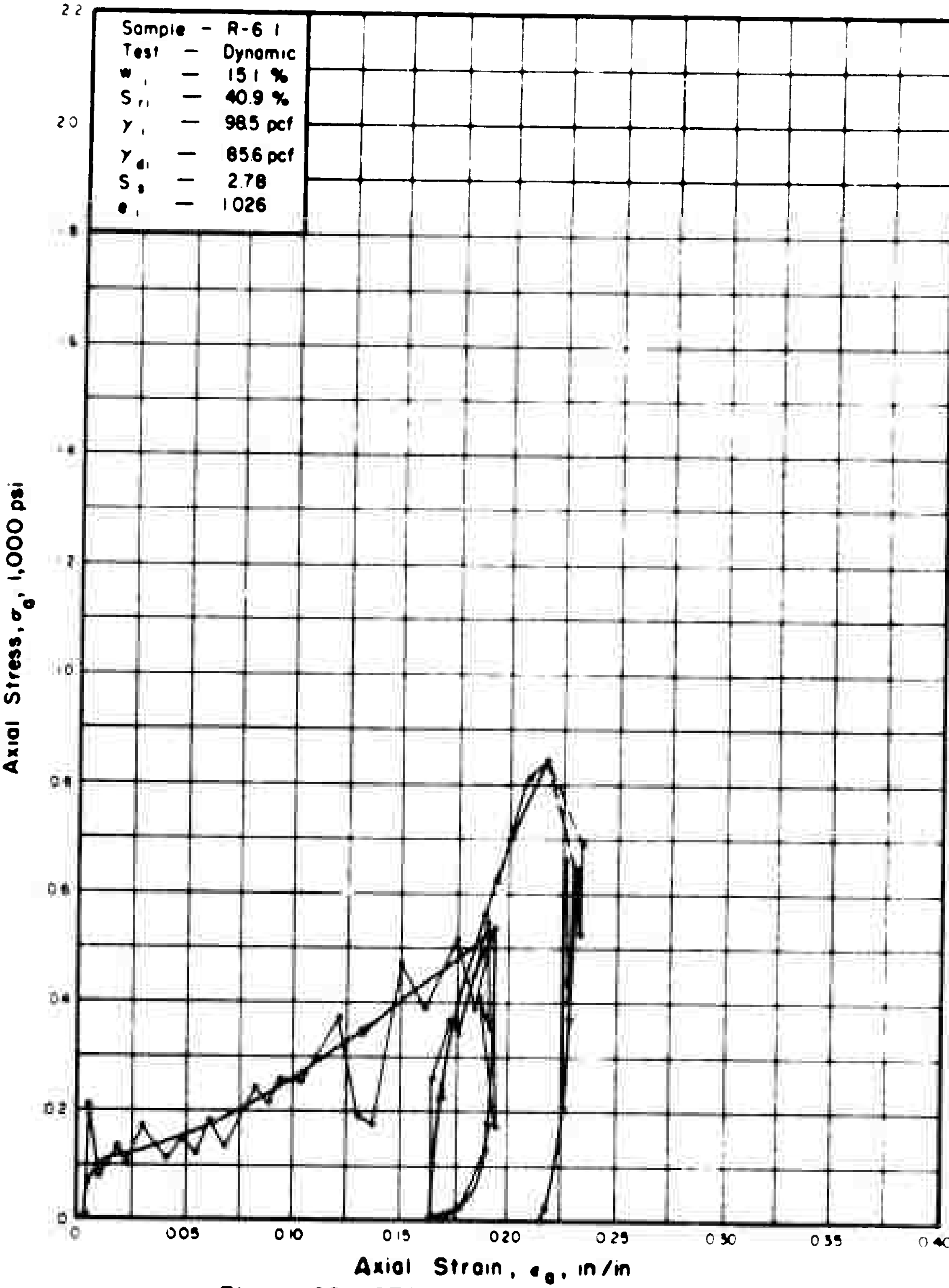

Figure 20. STRESS-STRAIN RELATIONSHIP IN ONE-DIMENSIONAL COMPRESSION

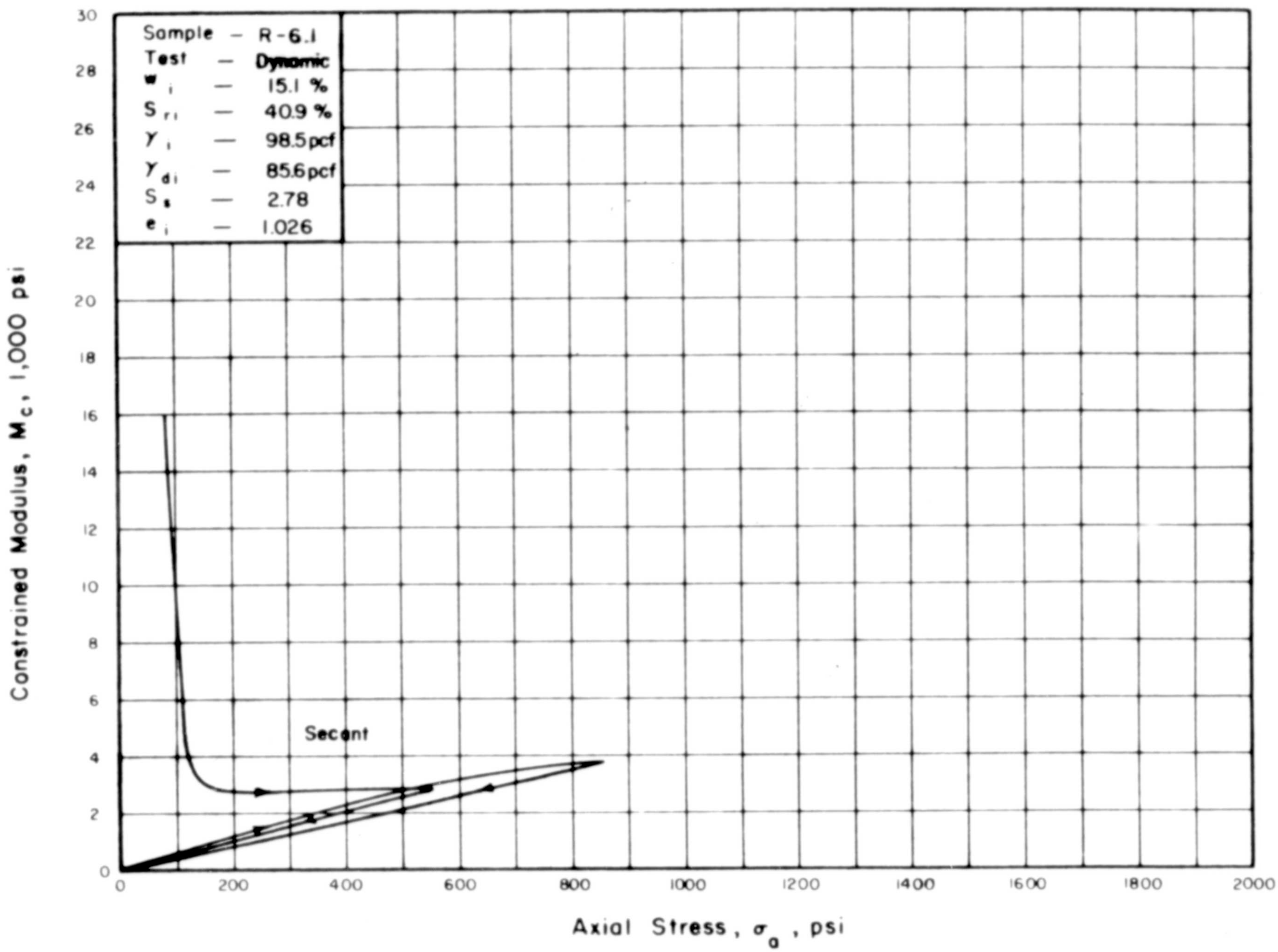

Figure 21. THE RELATIONSHIP BETWEEN CONSTRAINED MODULUS AND AXIAL STRESS

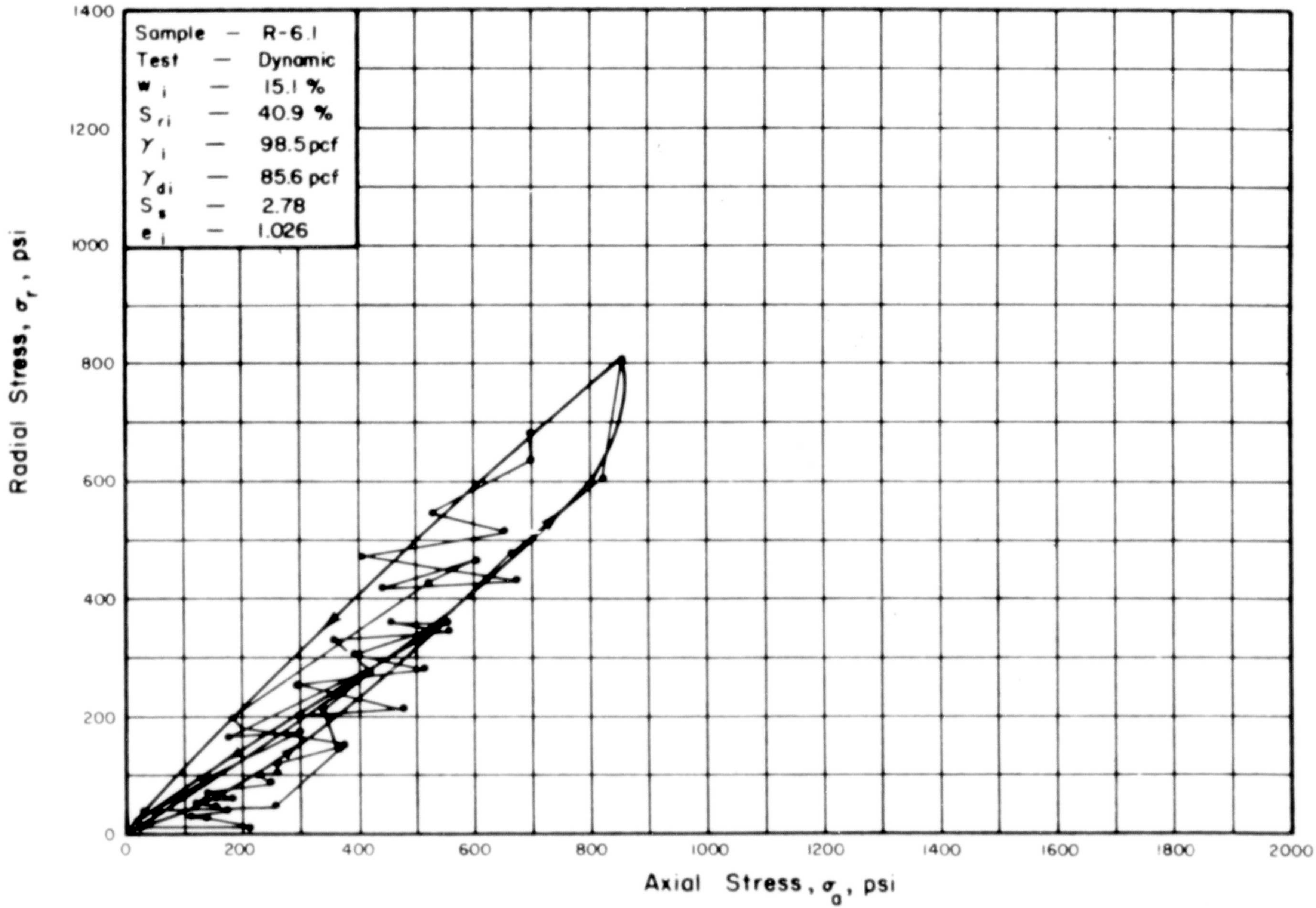

Figure 22. THE RELATIONSHIP BETWEEN RADIAL AND AXIAL STRESS IN ONE-DIMENSIONAL COMPRESSION

TABLE V

SUMMARY OF DYNAMIC TEST DATA - FIRST LOADING

SAMPLE NO	INITIAL VALUE	SEATING VALUES		TIME, milliseconds			INITIAL PEAK				INITIAL VALUE	STEADY STATE		RESIDUAL STRAIN	RATIO OF RESIDUAL STRAIN TO MAX. STRAIN
(Boring No - Depth)	S_r - %	σ_a - psi	ϵ_a - in/in	RISE	DWELL	DECAY	σ_a - psi	ϵ_a - in/in	S_r - %	K_o	K_o/Limit σ_a - psi	σ_a - psi	ϵ_a - in/in	ϵ_a - in/in	ϵ_a resid. / ϵ_a max.
N17 - 3.9	24.3	11.4	0.0098	4.1	44.4	551.5	410	0.152	33.8	0.40	0.30/200	232	0.147	0.138	0.908
N17 - 9.0	31.7	11.9	0.0053	3.2	41.8	555.0	550	0.094	39.2	0.34	0.20/250	274	0.090	0.084	0.894
[a]N17 - 16.4	91.3	14.4	0.0080	2.2	47.3	550.5	774	0.025	96.3	0.83	0.65/400	292	0.025	0.018	0.720
N17 - 20.9	96.7	14.9	0.0092	2.2	45.6	552.2	971	0.043	106.0	0.60	0.38/400	274	0.036	0.020	0.465
[a]N17 - 33.0	93.0	14.4	0.0056	1.5	46.1	552.4	728	0.013	96.1	0.71	0.75/400	291	0.012	0.010	0.770
R - 6.1	40.9	10.9	0.0054	4.4	46.4	549.2	550	0.192	65.8	0.63	0.46/220	274	0.189	0.164	0.854
R - 14.0	43.9	10.9	0.0023	4.1	54.6	541.3	597	0.164	68.6	0.66	0.37/270	270	0.154	0.126	0.768
R - 17.2	95.5	15.4	0.0062	2.2	48.2	549.6	481	0.012	98.0	0.84	0.35/200	274	0.012	0.011	0.917
[a]R - 22.0	93.3	13.4	0.0067	1.8	47.6	550.6	804	0.017	96.8	0.50	0.38/530	282	0.018	0.016	0.942
[b]R - 28.0	95.6	10.4	0.0312	2.3	47.4	550.3	392	0.035	101.9	0.72	0.80/100	Ext	Ext	Ext	Ext

a - Slight extrusion

b - Extrusion at seating pressure

BLANK PAGE

SECTION VI

INTERPRETATION OF TEST RESULTS

1. General

In interpreting the data, it is recognized that the constrained modulus is the most important quantity under consideration. The constrained modulus is required as input data in the procedures presently used to predict ground motions resulting from a nuclear blast. In the following discussion the factors influencing the magnitude of the constrained modulus, such as sampling and testing procedures and the position of the water table, will be considered in developing the constrained modulus versus depth relationship for the site of Operation Snowball at the Suffield Experiment Station.

2. Stress-Strain Relationships

The dynamic stress-strain properties of major interest are those for layer M1, generally the upper 13 ft of the soil profile described on figure 4. The stress-strain curve of figure 20 is typical of this layer. Initially, the curve is quite steep (high modulus), but at a stress level on the order of 100 to 150 psi the curve "breaks" and the soil becomes quite compressible. However, there is a tendency for the modulus to increase progressively as the stress level increases. During unloading the curve is quite steep until the stress level decreases below the 100 to 150 psi zone whereupon the majority of the rebound takes place. According to the data in table V, the residual strain varies from 77 to 91 percent of the maximum strain and averages 85 percent. A very high modulus is observed during the initial part of the second load cycle. When the stress level reaches the maximum stress obtained during the first load cycle, there is a break in the curve and the modulus decreases somewhat. The unloading behavior is similar to that observed during the first load cycle.

The foregoing discussion of dynamic test results applies to samples N17-3.9, N17-9.0, R-6.1, and R-14.0, whose initial degrees of saturation varied betwe n 24 and 44 percent. An entirely different behavior was observed for the remaining six dynamic tests, whose initial degrees of saturation exceeded 91 percent. The stress-strain curves were generally steep and extrusion occurred in four of the six tests; it is probable that extrusion occurred on Sample N17-20.9 also. Because of extrusion the moduli obtained from these tests are too low. It is probable that these soils are saturated in situ and that the bulk modulus of water (300,000 psi) would be a reasonable estimate of the constrained modulus.

A comparison between the static and dynamic test results is of interest, but consideration must be given to the rapid changes in gradation that occur in the vertical direction; therefore, although the static and dynamic test specimens are within 5 inches of each other vertically, they may consist of soils of different gradation. Samples N17-9.0 and N17-9.4 are an example of this occurrence. The four undisturbed static test results applicable to layer M1 exhibit the same general pattern observed for the dynamic tests except that the initial stiffness and the sharp "break" in the curve are not present. Otherwise, for a given stress the strains are approximately twice those observed in the dynamic tests. Therefore, the constrained secant modulus in the dynamic tests is approximately twice that observed for the static tests. This behavior is in accordance with that observed for similar soils from the Nevada Test Site (ref. 7). However, layer M1 is not as strong nor as highly cemented as the Nevada soils; therefore, the observed moduli are lower. Extrusion was observed in four of the remaining tests, but they confirm the conclusion that the soil will behave in situ as a saturated soil. The initial degrees of saturation for samples R-17.6 and R-22.5 were lower than those for the corresponding dynamic tests; extrusion was not observed in these tests.

3. Radial Stress-Axial Stress Relationships

At any given axial stress level, the ratio of radial stress to axial stress is denoted as K_o; this ratio is based on total stresses, not effective stresses. The subscript zero in the symbol K_o usually signifies that no radial strains are involved; however, limited amounts of radial strain did occur for the tests discussed herein.

In general, the value of K_o is closely related to the degree of saturation. Saturated soils have a K_o value of unity because the stresses are primarily carried by the fluid phase. In dry soils, the values generally range between 0.2 and 0.6. For degrees of saturation up to approximately 80 percent, the value of K_o corresponds nearly to that of a dry soil. For degrees of saturation exceeding approximately 80 percent, an increment of radial stress very nearly equals the applied increment of axial stress, and K_o approaches a value of unity. Because the degree of saturation depends on the axial strain, the value of K_o can vary continuously throughout the test.

For the four samples representative of layer M1, the dynamic tests indicate K_o values varying between 0.20 and 0.46. The corresponding static tests indicate higher values, varying between 0.25 and 0.65. Similarly, at the peak axial stress in the first load cycle, the dynamic K_o values vary from 0.34 to 0.66, whereas the static values vary from 0.42 to 0.80. Because the static strains were higher than the dynamic strains, the degrees of saturation were higher and, correspondingly, the values of K_o. For the remaining six samples, the degrees of saturation were generally high and the K_o values were nearly unity, or approached unity as the strain was increased.

In situ, K_o may be considered as unity under dynamic conditions for soils below the water table. For soils above the water table having high degrees of saturation, by capillarity or otherwise, the value of K_o will be nearly unity. Where the water table fluctuates, as it does at the Suffield Experimental Station, the values of K_o (and the constrained modulus) will depend on the applied stress and the degree of

saturation existing at the time a field test takes place. Therefore, a detailed knowledge of the soil profile and considerable judgment are required to delineate the K_0 versus depth relationship applicable to a given field test.

During the unloading cycle the values of K_0 often exceed unity. This occurs because increments of axial stress tend to relieve themselves at a higher rate than do the radial stresses. Similar behavior has been observed for other soils as described in references 6, 7 and 8.

4. Constrained Modulus-Depth Relationships

For making predictions of ground motions due to air blast, the constrained secant modulus is the soil property of interest. Although the constrained tangent modulus is also of interest, it is extremely sensitive to errors in measurement. For the dynamic tests described herein, the determination of the tangent modulus was not possible; only the secant modulus will be discussed.

The values of constrained modulus for soils are related to the degree of saturation in a manner similar to the relationship between K_0 and the degree of saturation. For saturated soils the constrained modulus should be at least equal to the bulk modulus of water, namely, 300,000 psi. Furthermore, saturated soils should exhibit nearly elastic behavior, both statically and dynamically, if only one-dimensional compression is involved. For dry granular soils (ref. 6), the constrained modulus is essentially zero at zero axial stress, but increases nearly in proportion to the axial stress as the axial stress is increased. The modulus decreases, however, when the axial stress level is sufficient to induce crushing of the soil grains; this generally occurs only at stress levels exceeding 2,000 psi. There are indications that only very small strain rate effects exist in the stress-strain properties of granular soils, and that the dynamic and static behaviors are approximately equal. Moist granular soils will probably exhibit the same behavior as dry granular soils.

An important intermediate zone exists between dry soils (and moist granular soils) and saturated soils. Partially saturated cohesive soils exhibit significantly higher moduli in dynamic tests than in static tests. At the Nevada Test Site (ref. 7) a factor of approximately 2 was observed; the same factor was observed for the tests from layer M1. The explanation for this behavior is probably that the air and water in the soil voids do not have time to adjust geometrically to the applied strains as the soil skeleton is stressed. This causes a transient pore pressure which has a variable magnitude from void to void. Part of the observed soil stiffness is, therefore, due to the high bulk modulus of the water in the soil voids. In the static tests, sufficient time was available for partial air drainage and at least partial redistribution of the pore water in the voids; therefore, the observed moduli were lower than those from the dynamic tests.

A constrained modulus - axial stress relationship typical of those for partially saturated cohesive soils, such as layer M1, is presented in figure 21. At very low stress levels a relatively high modulus is observed corresponding to that which would be obtained from seismic or vibration tests. As the stress level is increased, the modulus decreases rapidly corresponding to a breaking down of cementation and a decrease in air voids. At a stress level of approximately 100 to 200 psi the modulus begins to increase nearly in proportion to the increase in axial stress. For unloading, and any further loading cycles, the modulus is essentially proportional to the axial stress, as shown in figure 21. Therefore, the constrained modulus is a function of the degree of saturation, the stress history, the applied stress, and the strain rate; various values may be used according to the stress levels and strain rates involved in the problem under consideration.

It is not possible to delineate the modulus-depth relationship in a fully definitive manner; only general statements can be made. For that part of the soil profile wherein the water table fluctuates, the constrained modulus will depend on

the degree of saturation of the soil at the time of the field experiment. For soils below the permanent water table the constrained modulus should exceed 300,000 psi. In layer M1, the modulus will depend on the factors described in the previous paragraph. Other factors, such as sample disturbance must also be considered. The samples furnished for this study suffered disturbance when they were extruded from the shelby tube in the field; this would tend to cause the moduli observed in the tests to be too low. This effect was balanced somewhat by the sample trimming procedure that was utilized plus the reconsolidation that occurred under the seating load. Clearly, defining modulus-depth relationships requires an intimate knowledge of the soil profile and considerable judgment, in addition to the test results. In the following section a ground motion prediction will be made to illustrate the factors to be considered in selecting the constrained modulus at various depths.

5. Ground Motion Predictions

To illustrate the use of the test data, an air-blast-induced ground motion prediction will be made for the location of Boring R under the following assumed conditions: 500-ton high-explosive detonation at ground zero (Boring A, figure 4); 200-psi peak air pressure at Boring R, 250 ft from ground zero. The surface air pressure-time relationship for Boring R has been scaled on a cube-root basis from the measurements given in reference 9 for a similar 100-ton high-explosive detonation. In figure 23 time has been plotted vertically upwards and pressure horizontally, whereas depth has been plotted vertically downward. The peak pressure-depth relationship has been computed by the attenuation procedure given in reference 10; this relationship has been plotted in figure 23 along with the surface air pressure-time relationship. It is recognized that the vertical stress attenuates with depth because of energy absorption, but the attenuation has been computed by a procedure based on spatial dispersion. This procedure was used because it gives results in agreement with measurements at the Nevada Test Site; it was assumed that the

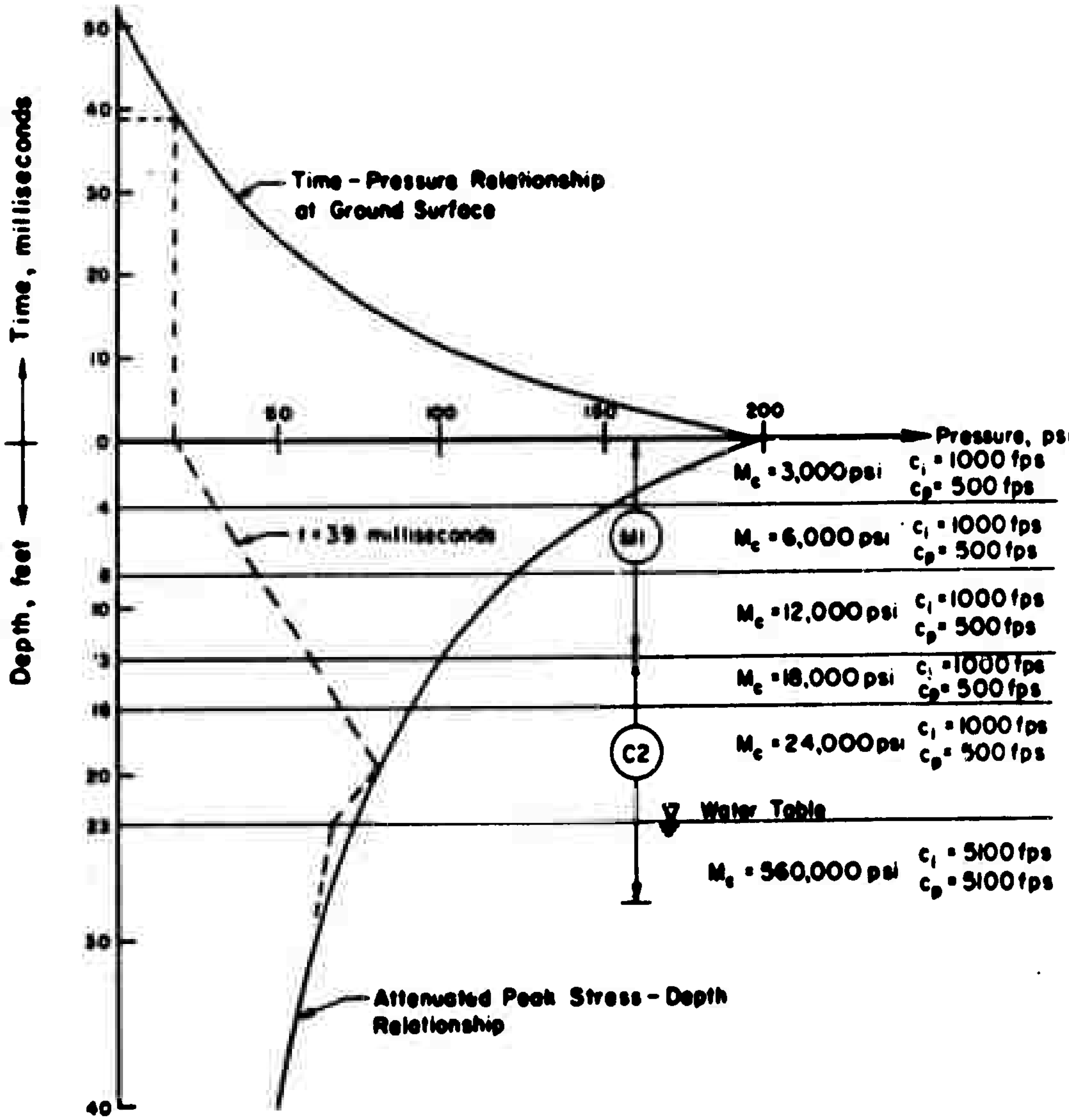

Figure 23. TIME - VERTICAL STRESS - DEPTH RELATIONSHIP

same procedure will work at Suffield due to the similarity of layer M1 to the soils at the Nevada Test Site.

Only layers M1 and C2 of the soil profile in figure 4 are pertinent to this discussion; because the water table occurs in layer C2, all deeper soil layers have a constrained modulus of 300,000 psi, or higher, and only negligible ground motions can be attributed to them. Layer M1 has been divided into three zones because the stress reduces from 200 psi at the top to 100 psi at the bottom, and the moduli must be selected to be compatible with the stress level. Layer C2 has also been divided into three zones; the top of the lower zone is at a depth of 23 ft where the water table has been assumed on the basis of seismic data (ref. 4). The upper two zones in layer C2 have been defined on the basis of the test data. The test data from both borings have been considered in arriving at the moduli values for each zone shown in figure 23, but more weight was generally given to the results from Boring R.

The seismic data from reference 4 have been considered in choosing the initial stress velocity of 1,000 fps and the peak stress velocity of 500 fps for the upper 23 ft of the soil profile. The moduli used in figure 23 were selected independently from the initial and peak stress velocities; therefore, they may not be fully compatible with the relationship $M_c = \rho c^2$. Below 23 ft, the seismic velocity of 5100 fps has been used throughout along with the constrained modulus corresponding to this velocity. By trial and error it was found that the peak transient surface displacement would occur 39 milliseconds after arrival of the blast front at Boring R. The assumed wave shape is shown by the dashed line on figure 23. The ground motions were computed in the following manner:

1. Select a time after arrival of the blast front at the point of interest.
2. Using the peak stress velocities, compute the depth of the transient peak stress.

3. Using the initial stress velocities, compute the depth of the stress pulse front.

4. Assume a straight-line stress-depth relationship between (a) the peak stress and the stress pulse front and (b) the peak stress and the stress at the ground surface corresponding to the time selected in step 1 above.

5. Compute the transient deformation of each zone using moduli values consistent with the stress level and loading history (loading or unloading)

6. Add the deformations of each zone to get the transient surface displacements.

7. Repeat steps 1 through 6 above for several values of time to determine the time at which the peak transient surface displacement occurs.

Considering the shape of the stress-strain curve in figure 20, it is clear that very little strain rebound occurs until the stress reaches a very low value. Therefore, if deformations are computed as though the peak stress-depth curve existed as a load, regardless of time, they would be an upper bound to the peak transient displacement. Furthermore, because of the very high residual strains, the upper bound should be very close to the magnitude of the peak transient displacement. For the upper 23 ft an upper bound displacement of 4.9 inches was computed. If displacements are considered below 23 ft, approximately 0.1 inch should be added to the 4.9 inches.

Using the stress pulse assumed at 39 milliseconds, a peak transient displacement of 4.6 inches is computed. A rebound of 10 percent was assumed after the peak in the upper 4 ft, but all other zones were considered to be compressed at their peak strain. By taking the residual strains as 80 percent of the maximum strains in the upper 16 ft, and as 20 percent between 16 ft and 23 ft, the residual strain is computed to be 3.8 inches. No residual strains are considered below the water table.

If consideration is given to how closely the dynamic tests duplicate field conditions, a very important conclusion can be drawn, namely, that the ground motions computed on the basis of the dynamic tests are probably too low. In a dynamic test, the peak stress occurs for less than 1 millisecond before reducing to the steady state value; the steady state stress is on the order of one-third to one-half of the peak stress. In the field, stresses in excess of 80 percent of the peak stress exist for several milliseconds. Considering that the soils in layer M1 are strain rate sensitive, it is probable that more motion occurs in layer M1 during a field experiment than would be predicted on the basis of the test results presented herein. Because the static moduli for layer M1 are approximately 50 percent of the dynamic moduli, the actual ground motions should not exceed twice the computed motions.

6. Cratering

An elementary consideration of the shear strength characteristics of the soil profile leads to the conclusion that cratering will conform to one of two possible modes. If a reasonably uniform detonation is obtained under the 35-ft-diameter hemisphere of TNT used for Operation Snowball, a condition of one-dimensional compression may exist in the region of the hemisphere. However, at the edges, a very high stress difference will exist and will spread radially (air blast). In the first mode, cratering will be controlled by the weakest layer, namely, layer C2 which probably cannot sustain rapidly imposed stress differences exceeding 100 psi. This dynamic strength was arrived at by considering the unconfined compression strength and adding 50 percent to account for the increased strength of cohesive soils under dynamic loading. Layer G4 is a very strong layer of sand and gravel existing at depths of 26 to 28 ft which, according to the first cratering mode, will be the lower extent of the crater. The crater would extend radially outward from the edges of the hemisphere.

If the imposed stress differences are sufficient to overcome the strength of layer G4, then the properties of layer C5 would become dominant. Layer C5 is relatively weak, having an unconfined compression strength of 0.8 tsf, but it probably increases in strength with depth. In the second cratering mode, the bottom of the crater would be in layer C5.

SECTION VII

CONCLUSIONS

The dynamic moduli for the upper 13 ft of the soil profile are approximately twice the static values. the general behavior is similar to that observed for the soils at the Nevada Test Site. The constrained secant modulus is relatively high at low stress levels, but decreases markedly to a minimum in the 100 to 200 psi stress range. Thereafter the modulus increases nearly linearly with increasing stress. The minimum values of the moduli are approximately 3,000 psi.

Between the depths of 13 ft and 23 ft, the moduli-values increase somewhat because of the higher degrees of saturation; moduli-values ranging from 18,000 to 24,000 psi are applicable at the 100 psi stress level. Below the water table (at 23 ft) the constrained modulus is equal to that of water, namely, 300,000 psi.

At a range of 250 ft from ground zero at Operation Snowball, the peak transient surface displacement was computed to be approximately 4.6 inches based on the commonly used prediction procedure and the test data presented herein. Approximately 90 percent of the displacement takes place in the upper 13 ft of the soil profile. Because the upper 13 ft of the soil profile is strain rate sensitive, and because the peak stresses in the dynamic tests occur within smaller time intervals than the peak stresses in the field, the test results lead to an underestimate of the strains that would occur in situ; therefore, the ground motion prediction of 4.6 inches is lower than the actual observed value. However, the actual motion cannot exceed twice the predicted value.

In making ground motion predictions at the Suffield Experimental Station, consideration must be given to the strain rate sensitivity of the moduli for the upper 13 ft of the soil profile. Furthermore, the fact that the constrained modulus is a function of the applied stress must be accounted for

REFERENCES

1. "Operation Snowball," Technical and Administrative Information for Operation Snowball, United States Participation with Canada and Great Britain in a Nuclear Weapons Effects 500-ton High Explosive Experimental Program.

2. Jones, G. H. S., (1963), Strong Motion Seismic Effects of the Suffield Explosions, Suffield Report No. 208, Suffield Experimental Station, Ralston, Alberta.

3. Brown, F. R., (1964), Letter to M. T. Davisson, 15 April 1964.

4. Seknicka, J. E., (1964), Personal communication, 5 August 1964 and 22 October 1964.

5. Hvorslev, M. J., (1949), Subsurface Exploration and Sampling of Soils for Civil Engineering Purposes, Report, Waterways Experiment Station, Vicksburg

6. Hendron, A. J., Jr., (1963) The Behavior of Sand in One-Dimensional Compression, Ph.D. Thesis, University of Illinois, Urbana

7. Hendron, A. J., Jr., and Davisson, M. T., (1963), Static and Dynamic Behavior of a Playa Silt in One-Dimensional Compression, Technical Documentary Report No. RTD TDR-63-3078, Air Force Weapons Laboratory, Kirtland Air Force Base, New Mexico, September.

8. Kane, H., Davisson, M. T., Olson, R. E. and Sinnamon, G. K., (1963), A Study of the Dynamic Soil-Structure Interaction Characteristics of Soil, Technical Documentary Report No. RTD TDR-63-3116, Air Force Weapons Laboratory, Kirtland Air Force Base, New Mexico, December

9. Kingery, C. N., Keefer, J. H., and Day, J. D., (1962), Surface Air Blast Measurements from a 100-ton TNT Detonation, Memorandum Report No. 1410, Ballistic Research Laboratories, Aberdeen Proving Ground, Maryland, June.

10. Newmark, N. M. and Haltiwanger, J. D., (1962) Principles and Practices for Design of Hardened Structures, Technical Documentary Report No. AFSWC-TDR-62-138, Air Force Special Weapons Center, Kirtland Air Force Base, New Mexico, December.

APPENDIX I

BORING LOGS

BORING LOG

FIELD DATA

Project 500 TON SES SHOT – A — Location AT GZ

Drill Rig W-17473 — Inspector ALM & AOB — Operator AOB — Surface Elev ______

HOLE ADVANCED W/ 7 1/2" HINGED EARTH AUGER. — Natural Ground Elev 2167.70

SAMPLE NUMBER	DATE TAKEN 1963	STRATUM		DRIVE		SAMPLE		TYPE OF SAMPLER	CONT	HYD PRESS	CLASSIFICATION AND REMARKS
		FROM	TO	FROM	TO	FROM	TO				
1	16 NOV.	0.0		0.0	0.5	0.0	1.2	5" SHELBY TUBE		100	TAN SILT W/ GRASS ROOTS.
1A				0.5	1.0	1.2	1.3		JAR	400	" " " " "
2				1.0	1.5	1.3	2.4		TUBE	440	" " " " "
				1.5	2.0					480	
2A			2.5	2.0	2.5	2.4	2.5		JAR	500	" " " " "
3	11 NOV.	2.5		2.5	3.0	2.5	3.6	5" S.T.	TUBE	75	TAN SILT.
3A				3.0	3.5	3.6	3.7		JAR	100	" "
4				3.5	4.0	3.7	4.7		TUBE	450	" "
4A				4.0	4.5	4.7	4.8		JAR	450	" "
			5.0	4.5	5.0					500	
5		5.0		4.9	5.4	5.0	6.3	5" S.T.	T	75	BROWNISH TAN SILT.
5A				5.4	5.9	6.3	6.4		J	250	" " "
				5.9	6.4					525	
6				6.3	6.8	6.4	7.7	5" S.T.	T	150	" " "
6A				6.8	7.3	7.7	7.8		J	450	" " "
	11 NOV.			7.3	7.8					550	
		7.8	7.9	7.8	8.3			5" SHELBY TUBE		100	BROWNISH TAN SILTY SAND.

BORING LOG

FIELD DATA

Project 500 TON SLS SHOT - A Location AT GZ

Drill Rig W-17473 Inspector ALM & AOB Operator AOB Surface Elev

HOLE ADVANCED W/ TRI-HINGED EARTH AUGER Natural Ground Elev 2187.1

SAMPLE NUMBER	DATE TAKEN 1963	STRATUM FROM	STRATUM TO	DRIVE FROM	DRIVE TO	SAMPLE FROM	SAMPLE TO	TYPE OF SAMPLER	CONT	HYD PRESS	CLASSIFICATION AND REMARKS
7	11 NOV	7 9		8 3	8 8	7 9	9 0		TUBE	500	BROWNISH TAN SILT
7A			9 2	8 8	9 2	9 0	9 2		JAR	545	" " "
8		9 2		9 2	9 7	9 2	10 6	5" ST	T	100	TAN SANDY SILT
8A				9.1	10.2	10.6	10.7		J	375	" " "
				10.2	10.7					560	
9A				10 6	11 1	10 7	10.9	5" ST	J		" " "
9			11.4	11.1	11 6	10.9	11.5		T		" " "
9B		11 4	12 1	11.6	12 1	11.5	12.0		J		TAN SAND, LOOSE + DRY
10		12 1	12 9	12.1	12 6	12 0	12 9		T		TAN SANDY SILT
10A		12 9	13 0	12.6	13.0	12.9	13 0		J		TAN SILTY SAND
		13 0		12 9	13 4			5" S.T		50	
11				13.4	13 9	13 0	14.0		T	150	TAN SILTY SAND & BROWN SILTY
11A				13 9	14 4	14 0	14 4		J	275	CLAY IN ALTERNATING LAYERS
12				14 4	14 9	14 4	15 4		T	350	DO
	11 NOV			14. 9	15.4					425	
13				15 5	15 8	15 4	16 6	5" SHELBY TUBE	TUBE	125	TAN SILTY SAND W/ LENSES OF
13A				15 8	16 3	16 6	17.4		JAR	240	BROWN SILTY CLAY
				16 3	16 8					320	
			17 4	16 8	17 3					380	

BORING LOG

FIELD DATA

Project 500 TON SES SHOT - A Location AT GZ

Drill Rig W-17475 Inspector ALM & AOB Operator AOB Surface Elev

HOLE ADVANCED W/ 1½ HINGED EARTH AUGER Natural Ground Elev 2161.70

SAMPLE NUMBER	DATE TAKEN 1963	STRATUM		DRIVE		SAMPLE		TYPE OF SAMPLER	CON'T	HYD PRESS	CLASSIFICATION AND REMARKS
		FROM	TO	FROM	TO	FROM	TO				
13B	11 NOV	17 4		17 3	17 7	17 4	17.7		JAR	400	TAN & GRAY CLAY W/VERTICAL SAND
											LENSES
14				17 6	18 1	17 7	18 7	5" S T	T	75	GRAYISH TAN CLAY W/ SILTY SAND
											LENSES
14A				18 1	18 6	18 7	18.8		J	200	" " " " "
15				18 6	19 1	18.8	19 8		T	250	" " " " "
15A				19 1	19.6	19 8	19 9		J	250	" " " " "
			20 0	19 6	20 0					250	
16		20 0		19 9	20 4	20 0	21 0	5" S T	T	25	BROWN SILTY CLAY W/ SILTY SAND
											LENSES
16A				20 4	20 9	21.0	21 1		J	75	SILTY SAND
16B				20 9	21.4	21 1	21 2		J	120	SILTY CLAY
17				21 4	21 9	21 2	22 0		T	180	BROWN SILTY CLAY W/SILTY SAND
											LENSES
17A			22 4	21 9	22 4	22 0	22 2		J	180	" " "
18		22 4		22 4	22 9	22 5	23 5	5" SHELBY TUBE	TUBE	50	BROWN SILTY CLAY W/ SANDY
											SILT LENSES
18A				22 9	23 4	23 5	23 6		JAR	140	" " " " "
19				23 4	23 9	23 6	24 6		TUBE	180	"

BORING LOG

FIELD DATA

Project 500 TON SES SHOT - A Location AT GZ

Drill Rig W-17473 Inspector ALM & AOB Operator AOB Surface Elev

Natural Ground Elev 2167.70

SAMPLE NUMBER	DATE TAKEN 1963	STRATUM FROM	STRATUM TO	DRIVE FROM	DRIVE TO	SAMPLE FROM	SAMPLE TO	TYPE OF SAMPLER	CONT	HYD PRESS	CLASSIFICATION AND REMARKS
19A	11NOV			239	244	246	248		JAR	180	BROWN SILTY CLAY w/ SANDY SILT
											LENSES
				244	249					200	
20				249	254	250	260	5" S T	T	25	" " " " "
20A				254	259	260	261		J	75	" " " " "
21				259	264	261	272		T	120	" " " " "
21A				264	269	272	274		J	180	" " " " "
	11NOV		274	269	274					180	
	12NOV	274		274	279			5" S T. *		40	
22A				279	284	28.0	285		JAR	60	COARSE SAND & GRAVEL
			292	284	28.9					120	
22B		292	295	289	294	292	295		JAR	180	SANDY SILT
22C		295		294	299	295	299		JAR	225	COARSE SAND & GRAVEL
				299	309			5 1/2" FISHTAIL BIT			" " "
				309	314			5" SHELBY TUBE		0	" " "
											.

* CUTTING EDGE OF TUBE BENT DURING DRIVE

NOTE HOLE ADVANCED TO 25 FT W/ 7 1/2 HINGED EARTH AUGER. WATER CAME UP IN HOLE AFTER SAMPLING DRIVE TO 274 FT HOLE ADVANCED W/ 5 1/2" BAFFLED FISHTAIL BIT USING MOGCOGEL & WATER AS DRILLING FLUID BELOW

BORING LOG

FIELD DATA

Project 500 TON SES SHOT - A Location AT GZ

Drill Rig W-17473 Inspector ALM & AOB Operator A.O. BROWN Surface Elev

HOLE ADVANCED W/ 5½" FISHTAIL BIT USING MAGCOGEL & WATER AS DRILLING FLUID. Natural Ground Elev 2167.70

SAMPLE NUMBER	DATE TAKEN 1965	STRATUM		DRIVE		SAMPLE		TYPE OF SAMPLER	CONT	HYD PRESS	CLASSIFICATION AND REMARKS
		FROM	TO	FROM	TO	FROM	TO				
	12 NOV			31.4	31.9			*		20	
				31.9	32.4					60	
				32.4	32.9					280	
			33.0	32.9	33.4					250	
		33.0		33.0	33.5			5' ST		40	
23				33.5	34.0	33.6	35.2		TUBE	60	GRAY SILTY CLAY W/TRACE GRAVEL
23A				34.0	34.5	35.2	35.4		JAR	100	″ ″ ″ ″ ″
				34.5	35.0					160	
				35.0	35.4					220	
				35.4	35.9			5' ST		20	
24				35.9	36.4	35.9	37.8		TUBE	60	″ ″ ″ ″ ″
24A				36.4	36.9	37.8	37.9		JAR	120	″ ″ ″ ″ ″
				36.9	37.4					200	
				37.4	37.9					240	
25				37.7	38.2			5' SHELBY TUBE	TUBE	4[illegible]	″ ″ ″
25A				3[illegible]	38.7				JAR	6[illegible]	″ ″
26				38.7	39.[illegible]				TUBE	160	″ ″ ″ ″ ″
[illegible]A				39.2	39.7				JAR	210	″ ″ ″ ″ ″

* BOTTOM OF SAMPLER TUBE BENT DURING DRIVE - NO SAMPLE RECOVERY

BORING LOG

FIELD DATA

Project 500 TON SES SHOT - A Location AT GZ

Drill Rig W-17475 Inspector ALM & AOB Operator A.O. BROWN Surface Elev

HOLE ADVANCED W/ 5½" FISHTAIL BIT USING MAGCOGEL & WATER AS DRILLING FLUID Natural Ground Elev 2167.70

SAMPLE NUMBER	DATE TAKEN 1963	STRATUM FROM	STRATUM TO	DRIVE FROM	DRIVE TO	SAMPLE FROM	SAMPLE TO	TYPE OF SAMPLER	CONT	HYD PRESS	CLASSIFICATION AND REMARKS
	12 NOV			39 7	40.2					220	
27				40 0	40.0			5" SHELBY TUBE	T	20	GRAY SILTY CLAY W/ TRACE GRAVEL
27A				40 5	41.0				J	40	" " " " "
28				41.0	41.5				T	120	" " " " "
28 A				41 5	42 0				J	200	" " " " "
				42 0	42 5					220	
	13 NOV			41 8	42 3			5" S T		50	
29				42 3	42 8	42 7	44 1		T	150	" " " " "
29A				42 8	43 3	44 1	44 2		J	200	" " " " "
				43 3	43 8					250	
				43 8	44 3					300	
30				44 1	44 6	44 4	45 3	5" SHELBY TUBE	TUBE	40	" " " "
30A				44 6	45 1	45 3	45 4		JAR	100	" " " " "
31				45 1	45 6	45 4	46 4		TUBE	200	" " " " "
31A				45 6	46 1	46 4	46 5		JAR	300	" " " " "
				46 1	46 6					300	
32				46 5	47 0	46 6	47 7	5" S T	T	20	" " " " "
32 A				47 0	47 5	47 7	47 8		J	60	" " " " "

NOTE SET 40 FT OF 6" PIPE AS CASING AFTER SAMPLING TO 42 5 FT DEPTH

BORING LOG

FIELD DATA

Project 500 TON SES SHOT - A Location AT GZ

Drill Rig W-17473 Inspector ALM & AOB Operator A O BROWN Surface Elev ——

HOLE ADVANCED W/ 5½" FISHTAIL BIT USING MAGCOGEL & WATER AS DRILLING FLUID Natural Ground Elev 2161 70

SAMPLE NUMBER	DATE TAKEN 1963	STRATUM		DRIVE		SAMPLE		TYPE OF SAMPLER	CONT	HYD PRESS	CLASSIFICATION AND REMARKS
		FROM	TO	FROM	TO	FROM	TO				
33	13 NOV			475	480	478	488		T	100	GRAY SILTY CLAY w/ TRACE GRAVEL
33A				480	485	488	489		J	240	″ ″ ″ ″ ″
				485	490					240	
34				490	495	492	502	5" S T	T	40	″ ″ ″ ″ ″
34A				495	500	502	503		J	60	″ ″ ″ ″ ″
35				500	505	503	510		T	120	″ ″ ″ ″ ″
35A				505	510	513	514		J	240	″ ″ ″ ″ ″
				510	515					260	
36				513	518	517	525	5" SHELBY TUBE	TUBE	20	GRAY SILTY CLAY w/ SANDY SILT +
											TR GRAVEL
36A			526	518	523	525	526		JAR	60	″ ″ ″ ″ ″
37		526		523	528	526	536		TUBE	120	GRAY SILT CLAY W/ TRACE GRAVEL
37A				528	533	536	537		JAR	220	″ ″ ″ ″ ″
				533	538					300	
38				536	541	538	549	5" S T	T	60	″ ″ ″ ″ ″
38A				541	546	549	550		J	120	″ ″ ″ ″ ″
39				546	551	550	560		T	200	″ ″ ″ ″ ″
39A				551	556	560	561		J	220	″ ″ ″ ″ ″
				556	561					210	

BORING LOG

FIELD DATA

Project 500 TON SES SHOT - A Location AT GZ

Drill Rig W-17473 Inspector ALM & AQB Operator A Q BROWN Surface Elev

HOLE ADVANCED W/ 5½" FISHTAIL BIT USING MAGCOGEL & WATER AS DRILLING FLUID Natural Ground Elev 2167.70

SAMPLE NUMBER	DATE TAKEN 1965	STRATUM FROM	STRATUM TO	DRIVE FROM	DRIVE TO	SAMPLE FROM	SAMPLE TO	TYPE OF SAMPLER	CONT	HYD PRESS	CLASSIFICATION AND REMARKS
40	13 NOV			559	564	561	571	5 ST	T	20	GRAY SILTY CLAY W/ TRACE GRAVEL
40A				564	569	571	572		J	40	
41				569	574	572	582		T	120	" " " "
41A				574	579	582	585		J	240	" " " " "
				579	584						
				581	586			5" ST		60	
42				586	591	585	601		TUBE	210	GRAY SILTY SANDY CLAY W TR
											GRAVEL
42A				591	596	601	605		JAR	280	
				596	601					280	
			604	601	606					300	
*		604	680					5½ FISHTAIL BIT			GRAY MED SAND
										NOTE	SET 70 FT OF 4 FLUSH JOINT CSG.
*		680	830					3½ FISHTAIL BIT			GRAY SANDY CLAY W/ TR GRAVEL
					BOTTOM OF HOLE 820 FT						
*	NO SAMPLES TAKEN - SEE LOG + SAMPLES BORING N-18 & BORING S18										
	HOLE BACKFILLED WITH SAND COLUMN MIX AND CASING PULLED AS SAND COLUMN MIX INSTALLED										

BORING LOG

FIELD DATA

Project 500 TON SES SHOT - N17 Location 20 FT N 31° E OF GZ

Drill Rig W-17473 Inspector ALM + AOB Operator AOB Surface Elev

Natural Ground Elev 2167.87

SAMPLE NUMBER	DATE TAKEN 1963	STRATUM FROM	STRATUM TO	DRIVE FROM	DRIVE TO	SAMPLE FROM	SAMPLE TO	TYPE OF SAMPLER	CONT	HYD PRESS	CLASSIFICATION AND REMARKS
1	12 DEC	00		00	05	02	24	5" SHELBY TUBE		80	TAN SILT
				05	10			"		100	
				10	15			"		120	
				15	20			"		200	
				20	25			"		360	
				23	28			5" SHELBY TUBE		50	" "
2				28	33	25	48	"	TUBE	80	"
				33	38			"		180	
				38	43			"		240	
				43	48			"		350	
				47	52			5" SHELBY TUBE		60	" "
3				52	57	48	63		TUBE	280	
				57	62					540	
				62	63					540	
				62	67			5" SHELBY TUBE		80	
4				67	72	63	79		TUBE	280	
				72	77					480	
				77	79					540	
			80								

BORING LOG

FIELD DATA

Project 500 TON SES SHOT - N17 Location 20 FT N31° E OF GZ

Drill Rig W - 17473 Inspector ALM + AOB Operator AOB Surface Elev

Natural Ground Elev 2167.87

SAMPLE NUMBER	DATE TAKEN 1963	STRATUM		DRIVE		SAMPLE		TYPE OF SAMPLER	CONT	HYD PRESS	CLASSIFICATION AND REMARKS
		FROM	TO	FROM	TO	FROM	TO				
	12-12	8.0		7.8	8.3			5" SHELBY TUBE		80	
5				8.3	8.8	7.9	9.9	"		150	BROWN SANDY SILT
				8.8	9.3			"		500	
				9.3	9.9			"		540	
				9.9	10.4			5" SHELBY TUBE		40	
6			10.9	10.4	10.9	10.0	10.9	"	TUBE	60	" " "
6A		10.9	11.4	10.9	11.4	10.9	11.4	"	JAR	140	FINE SAND W/ TR LIGNITE - DRY
7		11.4	12.2	11.4	11.9	11.4	12.2	"	TUBE	300	BROWN SANDY SILT
		12.2	12.4	11.9	12.3	–	–	"		440	FINE SAND
		12.4		12.3	12.8			5" SHELBY TUBE		50	
8				12.8	13.3	12.5	14.7		TUBE	50	BROWN SILTY CLAY W/ SANDY
				13.3	13.8					100	SILT LENSES
				13.8	14.3					120	BREAK IN SPLE AT 12.9, 13.8, & 14.4
				14.3	14.8					280	FT DEPTH
				14.6	15.1			5" SHELBY TUBE		50	BROWN SILTY CLAY W/SOME SANDY
9				15.1	15.6	14.9	17.0		TUBE	50	SILT LENSES & SAND LENSES
				15.6	16.1					80	BREAK IN SPLE AT 16.6.
			16.0	16.1	16.6					100	
	12-12	16.0		16.6	17.1					200	BROWN SILTY CLAY W/SAND LENSES

BORING LOG

FIELD DATA

Project 500 TON SES SHOT - N17 Location 20 F I N 31°E OF GZ

Drill Rig W - 17473 Inspector ALM & AOB Operator AOB Surface Elev

Natural Ground Elev 2167.87

SAMPLE NUMBER	DATE TAKEN 1963	STRATUM FROM	STRATUM TO	DRIVE FROM	DRIVE TO	SAMPLE FROM	SAMPLE TO	TYPE OF SAMPLER	CONT	HYD PRESS	CLASSIFICATION AND REMARKS
	12 DEC	16.0		17.0	17.5			5" SHELBY TUBE		50	
10				17.5	18.0	17.3	19.4	"	TUBE	50	BROWN SILTY CLAY w/ SAND
				18.0	18.5			"		50	LENSES - DAMP
				18.5	19.0			"		60	
				19.0	19.5			"		80	
	13 DEC			19.4	19.9			5" SHELBY TUBE		50	DO
11				19.9	20.4	19.6	21.9	"		50	DO
				20.4	20.9			"		60	
				20.7	21.4			"		100	
				21.4	21.9			"		240	
				21.9	22.4			5" SHELBY TUBE		40	
12				22.4	22.9	22.1	24.4	"	TUBE	50	DO
				22.9	23.4			"		60	
				23.4	23.9			"		100	
				23.9	24.4			"		180	
				24.4	24.9			5" SHELBY TUBE		40	BROWN SILTY CLAY W/ SAND
13			25.3	24.9	25.4	24.4	25.3	"	TUBE	60	LENSES
				25.4	25.9					60	
13A		25.3		25.9	26.4	25.3	25.6		JAR	180	SAND & GRAVEL w/ CLAY LENSES

BORING LOG

FIELD DATA

Project 500 TON SES SHOT - N17 Location 20 FT N 31° E OF GZ

Drill Rig W-17473 Inspector ALM & AOB Operator AOB Surface Elev

Natural Ground Elev 2167.B1

SAMPLE NUMBER	DATE TAKEN 1963	STRATUM FROM	STRATUM TO	DRIVE FROM	DRIVE TO	SAMPLE FROM	SAMPLE TO	TYPE OF SAMPLER	CONT.	HYD. PRESS.	CLASSIFICATION AND REMARKS
	13 DEC			26.4	26.9					300	(WATER BEARING. WATER TEMP 43°F)
			29.5								
14 A		29.5		26.9	31.5	30.5	–	8" AUGER *	JAR		GRAY SILTY CLAY
				31.4	31.9			5" SHELBY TUBE		50	
15				31.9	32.4	32.1	33.8	"	TUBE	50	" " "
				32.4	32.9			"		100	
				32.9	33.4			"		150	
				33.4	33.9			"		250	
				36.1	36.6			5" SHELBY TUBE		50	GRAY SILTY CLAY W/ TR. GRAVEL
16				36.6	37.1	36.8	38.5	"	TUBE	50	
				37.1	37.6			"		60	
				37.6	38.1			"		80	
				38.1	38.6			"		150	
				38.6	41.7	–	–	8" FLIGHT AUGER *			" " "
	14 DEC			41.7	42.2			5" SHELBY TUBE		40	
17				42.2	42.7	42.2	44.1	"	TUBE	50	" " "

*ADDED 50 GAL. DRILLING MUD-MOBCOGEL & WATER AND ADVANCED HOLE W/ 8" FLIGHT AUGER WITH DRILLING MUD IN HOLE AFTER 26.9 FT DEPTH.

BORING LOG

FIELD DATA

Project 500 TON SES SHOT – N17 Location 20 FT N 31° E OF GZ

Drill Rig W-17473 Inspector ALM & AOB Operator AOB Surface Elev

Natural Ground Elev 2167.87

SAMPLE NUMBER	DATE TAKEN 1963	STRATUM FROM	STRATUM TO	DRIVE FROM	DRIVE TO	SAMPLE FROM	SAMPLE TO	TYPE OF SAMPLER	CONT	HYD PRESS	CLASSIFICATION AND REMARKS
	14 DEC			427	432			5" SHELBY TUBE		60	
				432	437			"		90	
				437	442			"		130	
				442	470			8 FLIGHT AUGER			GRAY SILTY CLAY W/ TR GRAVEL
				470	475			5" SHELBY TUBE		50	
18				475	480	476	494	"	TUBE	50	" " "
				480	485			"		60	
				485	49.0			"		80	
	14 DEC			490	495			"		150	

BOTTOM OF HOLE 495 FT

AFTER COMPLETING HOLE TO 495 FT

SET 414 FT OF 6" PIPE AND LEFT HOLE OPEN AS PER RC WGLD, SES

BORING LOG

FIELD DATA

Project 3.7 SNOWBALL - R Location SUFFIELD EXP STA

Drill Rig CONTRACTOR Inspector R. O. C. Operator BILL AKERSTROM Surface Elev

Natural Ground Elev

SAMPLE NUMBER	DATE TAKEN 1964	STRATUM		DRIVE		SAMPLE		TYPE OF SAMPLER	CONT	HYD PRESS	CLASSIFICATION AND REMARKS
		FROM	TO	FROM	TO	FROM	TO				
1	6-2	00		AUGER		20	22	6" AUGER JAR			GRAY SILT FIRM
2			25	25		25	48	5" ST			BROWN SILT FIRM
3		25			5.0	48	50	JAR ST			" " "
4	6-3			50		50	74	5" ST			" " " MOIST @ 53
5					75	74	75	JAR ST			" " "
6				75		75	99	5" ST			" " "
7					100	99	100	JAR ST			" " "
8			112	100		100	120	5" ST			BROWN CLAYEY SILT FIRM
											FINE SAND FROM 112 - 117
9		112	117		121	120	121	JAR ST			" " "
10		117		121		121	135	5" ST			" "
11						135	137	JAR ST			NOTE SAMPLE LOSS AT BOTTOM
12			137			137	142	5" ST			BROWNISH SILTY CLAY W/SAND
13		137			143	142	143	JAR ST			LENSES
14				143		144	164	5" ST			" " " "
15					165	164	165	JAR ST			" "
16			165	165		165	181	5" ST			BROWN SILTY CLAY W/TR SAND
											LENSES
17		165			182	181	182	JAR ST			

BORING LOG

FIELD DATA

Project 3.7 SNOWBALL - R　　　Location SUFFIELD EXP STA

Drill Rig CONTRACTOR　　Inspector R D C.　　Operator BILL AKERSTROM　　Surface Elev

Natural Ground Elev

SAMPLE NUMBER	DATE TAKEN 1964	STRATUM		DRIVE		SAMPLE		TYPE OF SAMPLER	CONT	HYD PRESS	CLASSIFICATION AND REMARKS
		FROM	TO	FROM	TO	FROM	TO				
18	6-3		185	182		186	205	5 ST			BROWN SILTY CLAY PLASTIC
19		185			207	205	207	JAR ST			
20			210	207	21.6	210	216	JAR			BROWN SILTY CLAY TR FINE SAND
21		210		216	241	216	230	5' ST			BROWNISH SILTY W/ SAND LENSE
22		210			241	230	241	JAR			FINE SILTY SAND
23			230	24		24[illegible]	265	5' ST			[illegible]H SAND AT TOP OF SAMPLE
24		2[illegible]	265		266	265	266	JAR ST			BROWN SILTY CLAY PLASTIC
25		265		266		266	288	5' ST			" "
26					291	288	291	JAR ST			W SAND LENSES AT TOP OF S
27			298	29[illegible]		291	314	5' ST			BLUISH CLAY PLASTIC FIRM
28		298			316	314	316	JAR ST			" " " "
29				316	341	316	335	5' ST			" " " MED
											(WATER ON TOP OF SAMPLE)
30					34[illegible]	[illegible]	[illegible]	JAR ST			
31	6-4			342		342	350	5 ST			BLUISH SILTY CLAY
											WATER AFTER SETTING OVERNIGHT
[illegible]					[illegible]	[illegible]	351	JAR [illegible]			292 FROM GZ
[illegible]	6-5		[illegible]	35[illegible]	365	360	365	JAR [illegible]			2 SOFT SANDY SILT ON TOP OF
		36[illegible]									[illegible]AMPLE [illegible]OARSE [illegible]AN[illegible] & GRAVEL

BORING LOG

FIELD DATA

Project 3.7 SNOWBALL - R Location SUFFIELD EXP STA

Drill Rig CONTRACTOR Inspector R O C Operator BILL AKERSTROM Surface Elev

Natural Ground Elev

SAMPLE NUMBER	DATE TAKEN 1964	STRATUM		DRIVE		SAMPLE		TYPE OF SAMPLER	CONT	HYD PRESS	CLASSIFICATION AND REMARKS
		FROM	TO	FROM	TO	FROM	TO				
34	6-5			36 5	38 0	37 5	38 0	6" AUGER JAR SA			BLUISH CLAY w/ COARSE SAND &
											GRAVEL
35			39 0	38.0	39.5	39 0	39 5	" " "			" " " "
36	6-5			39 5	41 5	41 0	41 5	" " "			BROWNISH COARSE SAND w/ TR
											CLAY LENSES

APPENDIX II

STATIC TEST RESULTS

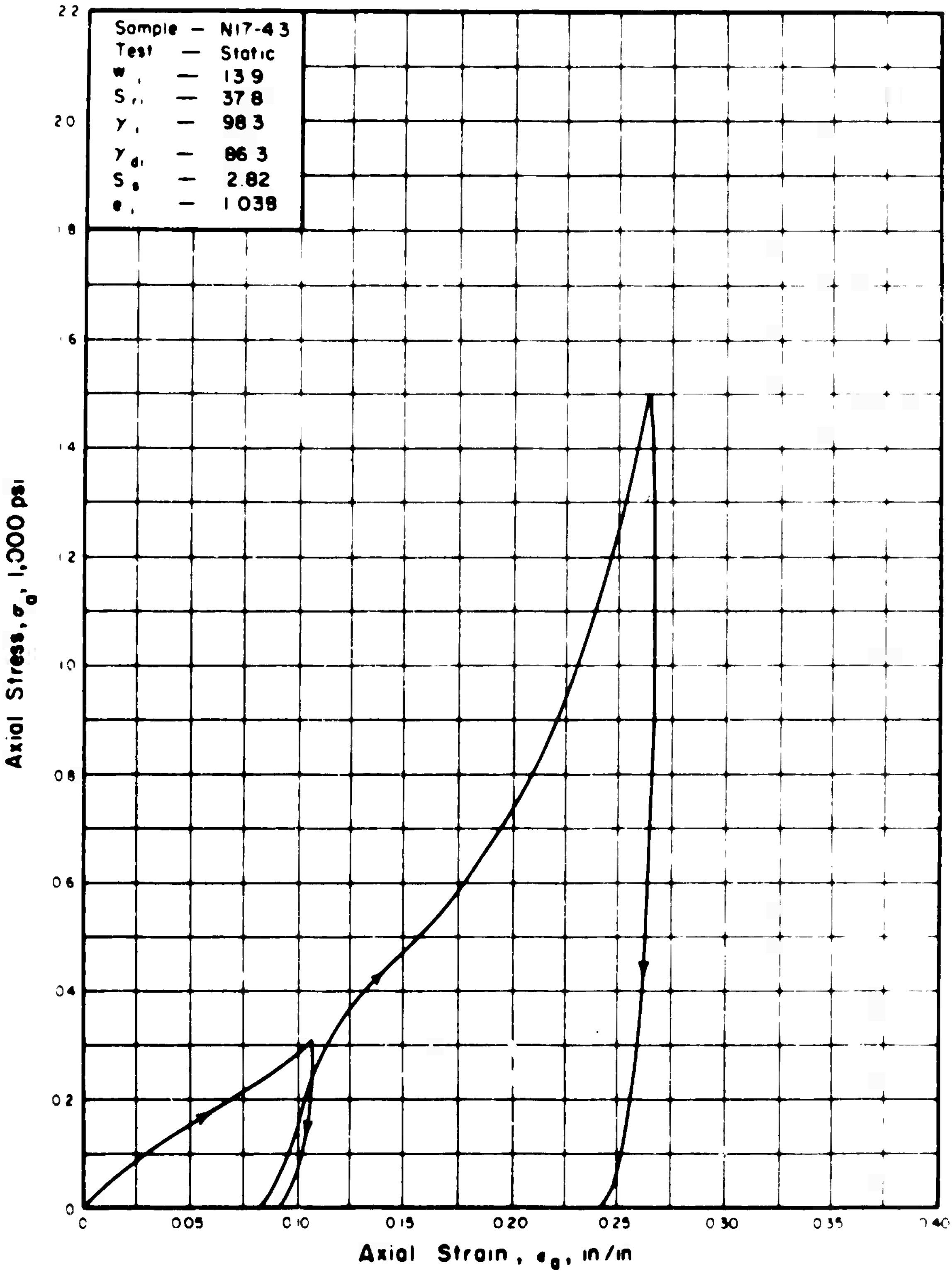

Figure 24. STRESS-STRAIN RELATIONSHIP IN ONE-DIMENSIONAL COMPRESSION.

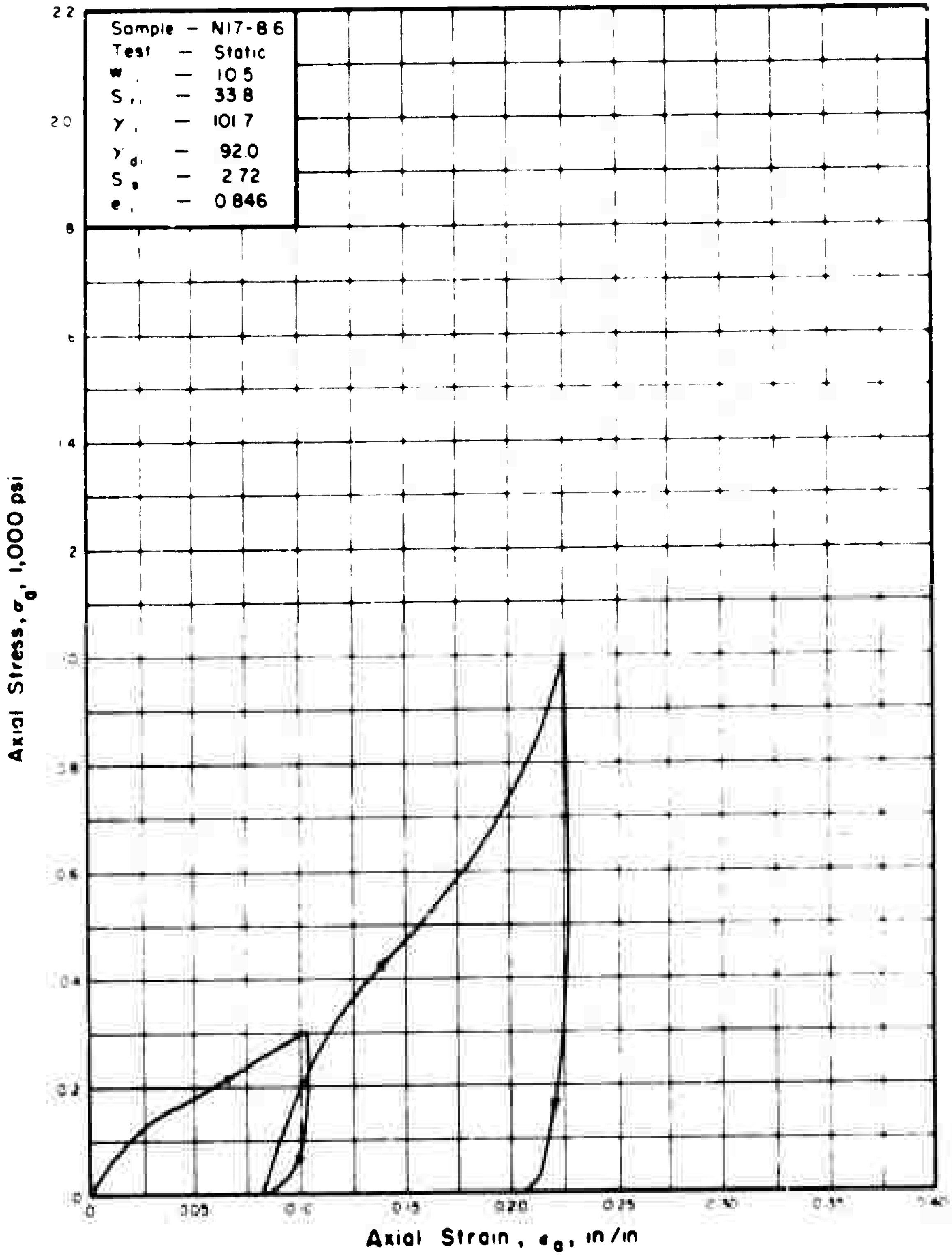

Figure 25. STRESS-STRAIN RELATIONSHIP IN ONE-DIMENSIONAL COMPRESSION.

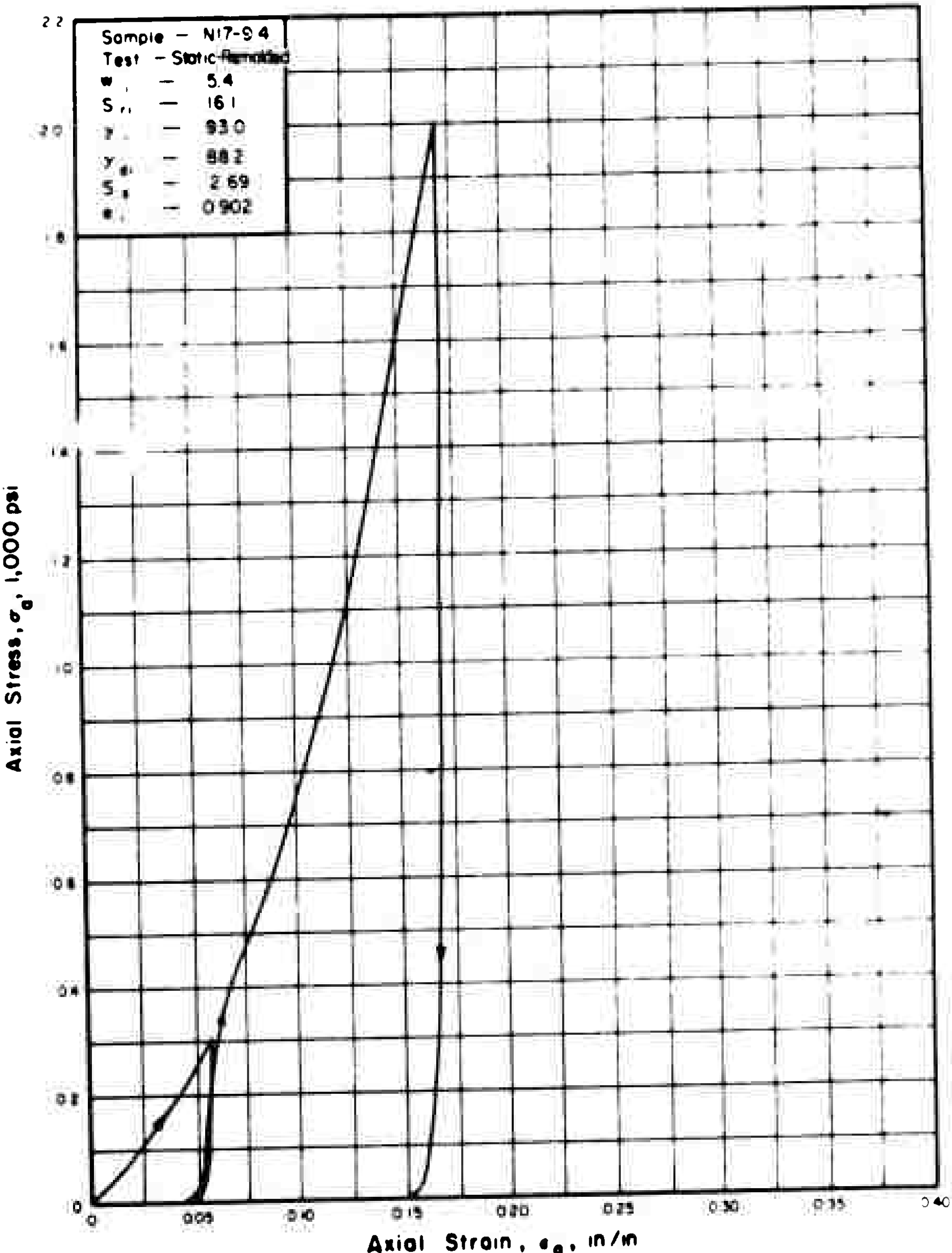

Figure 26. STRESS-STRAIN RELATIONSHIP IN ONE-DIMENSIONAL COMPRESSION.

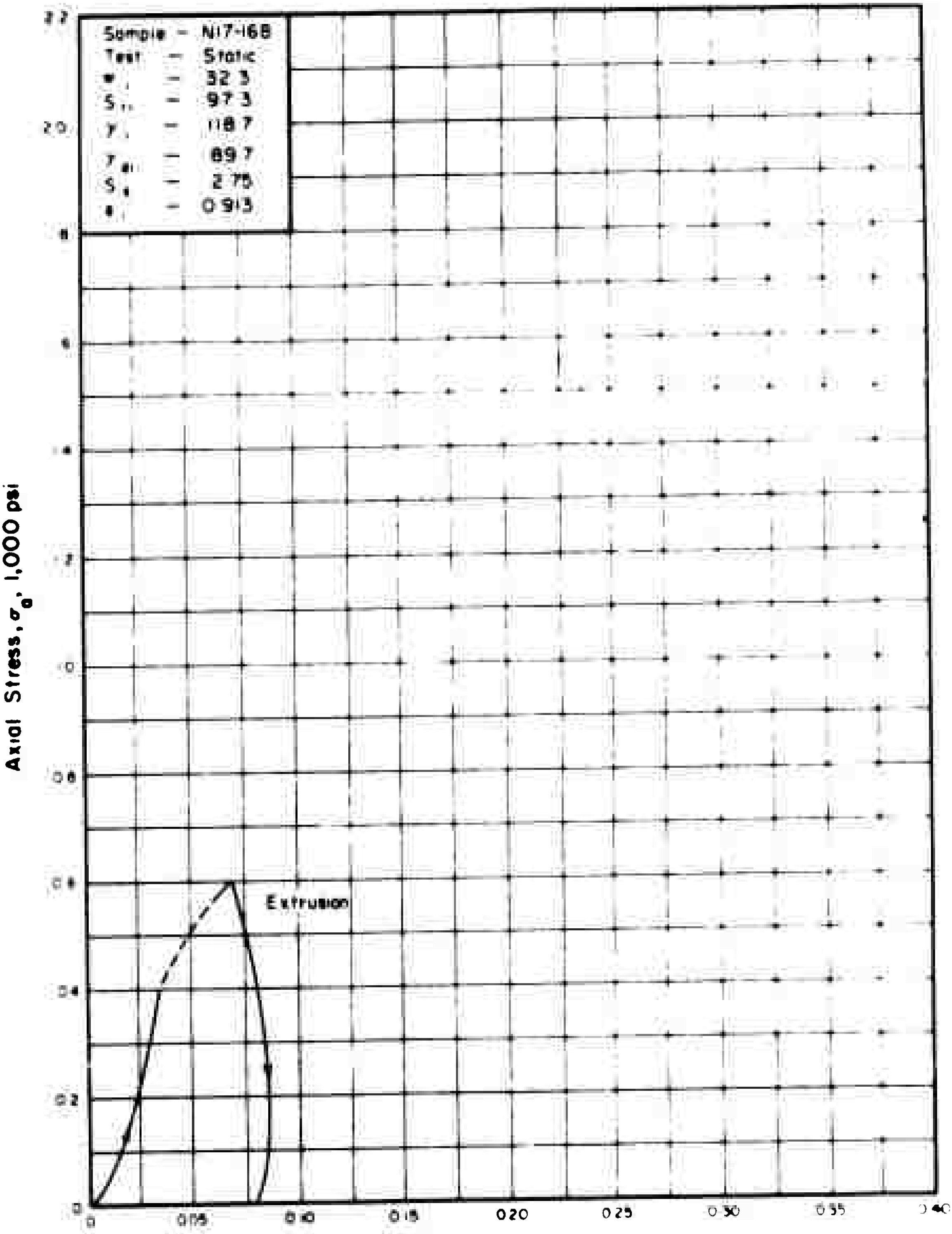

Figure 27. STRESS-STRAIN RELATIONSHIP IN ONE-DIMENSIONAL COMPRESSION.

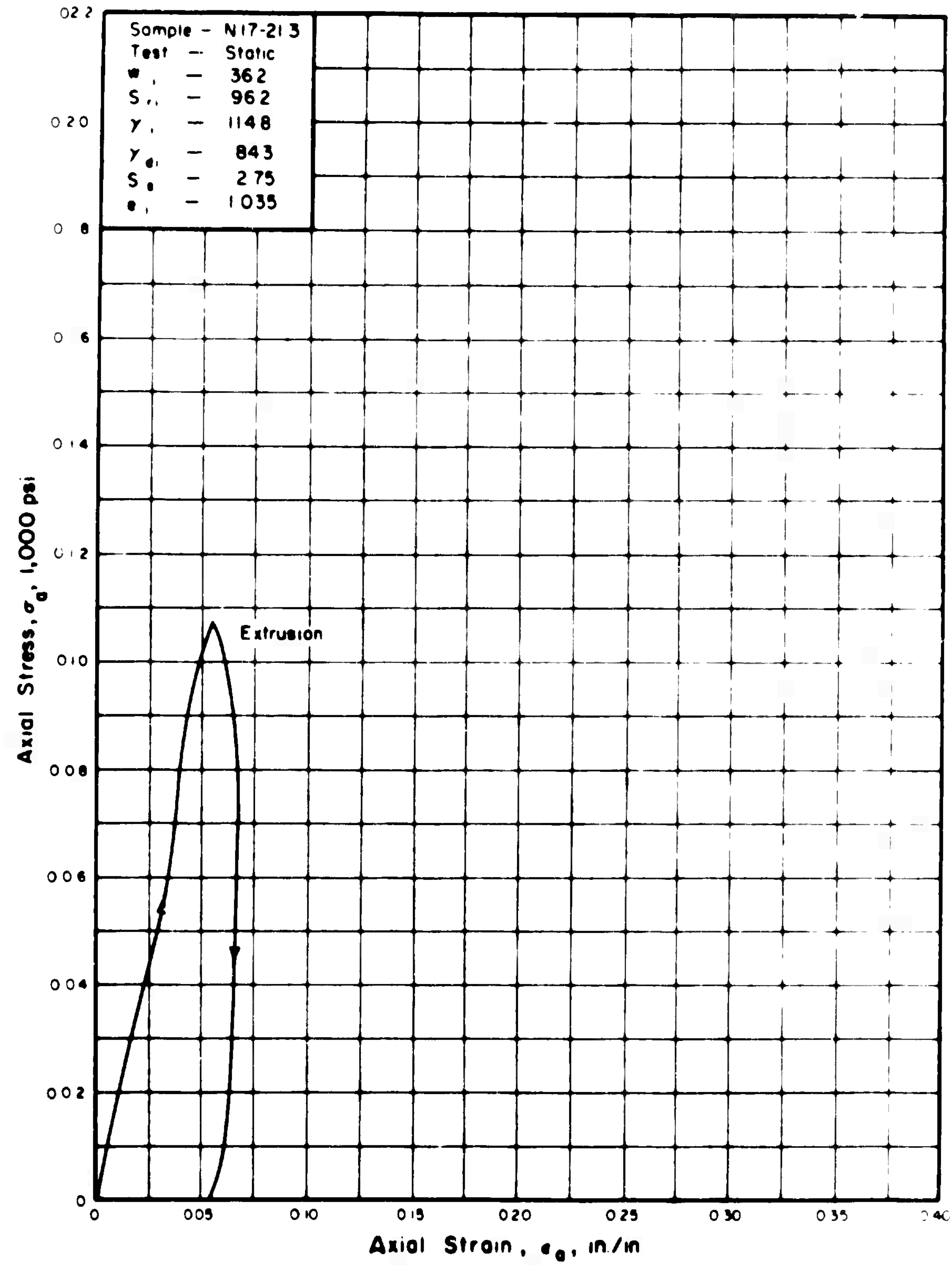

Figure 28. STRESS-STRAIN RELATIONSHIP IN ONE-DIMENSIONAL COMPRESSION.

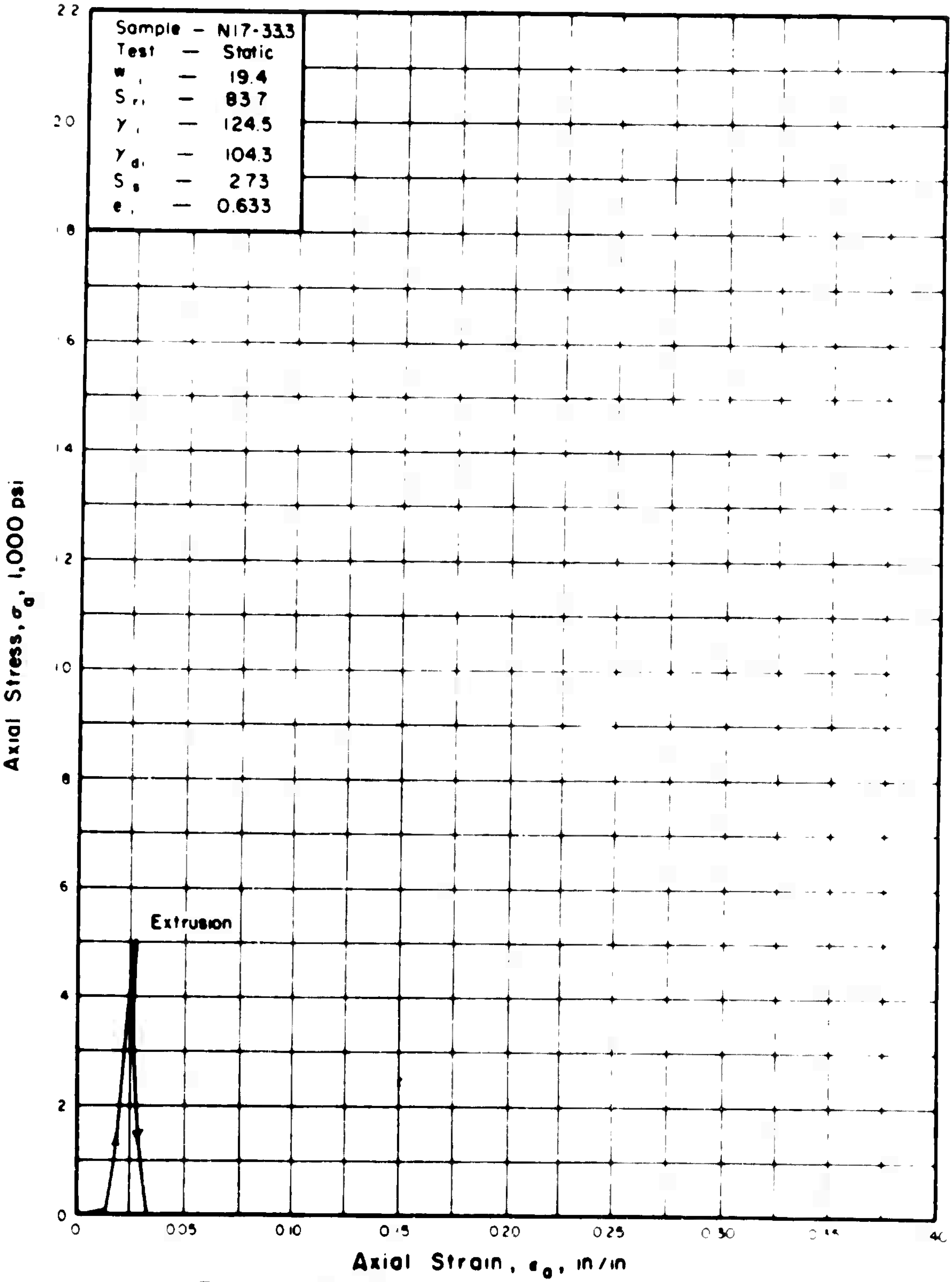

Figure 29. STRESS-STRAIN RELATIONSHIP IN ONE-DIMENSIONAL COMPRESSION.

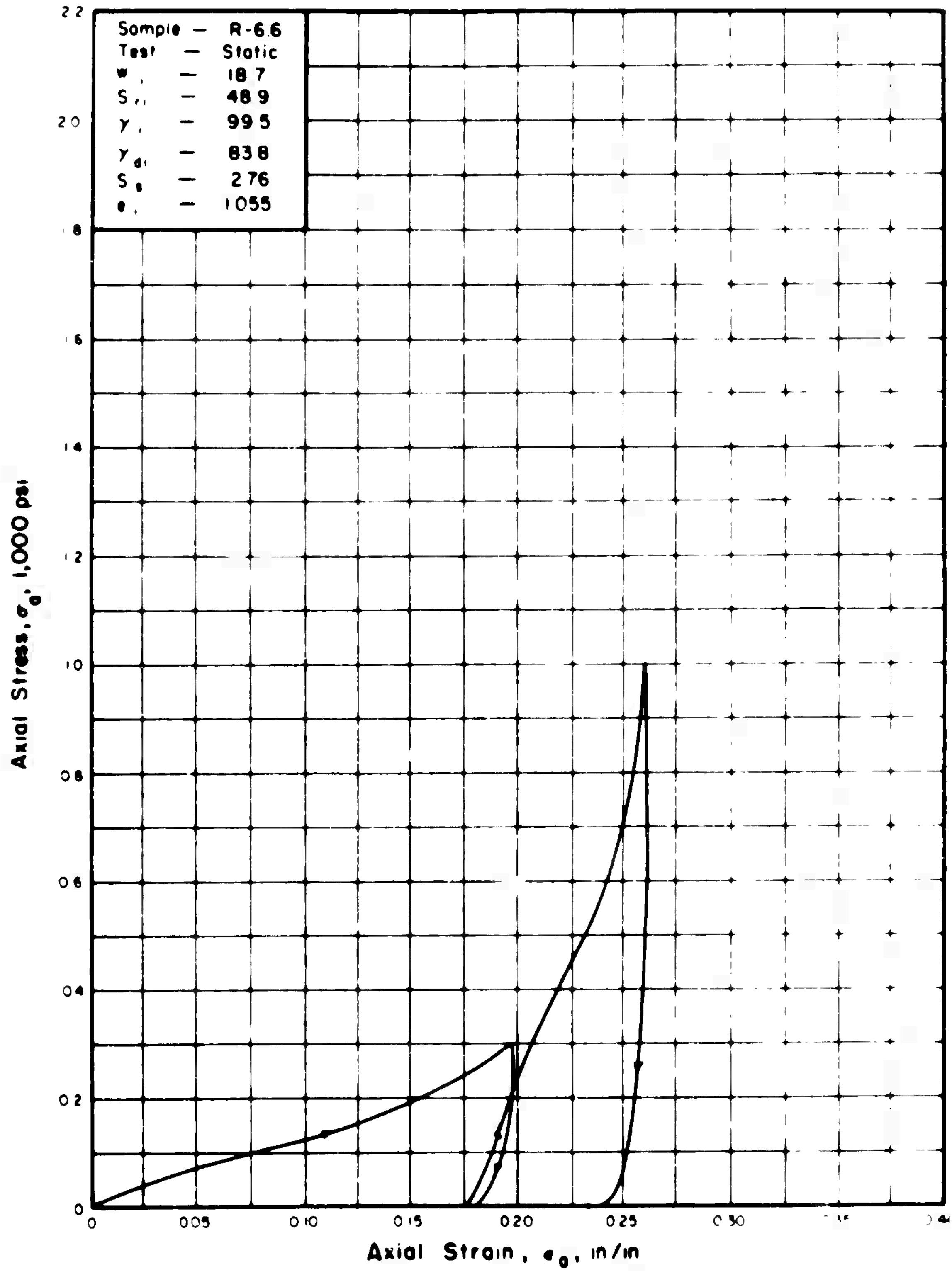

Figure 30. STRESS-STRAIN RELATIONSHIP IN ONE-DIMENSIONAL COMPRESSION.

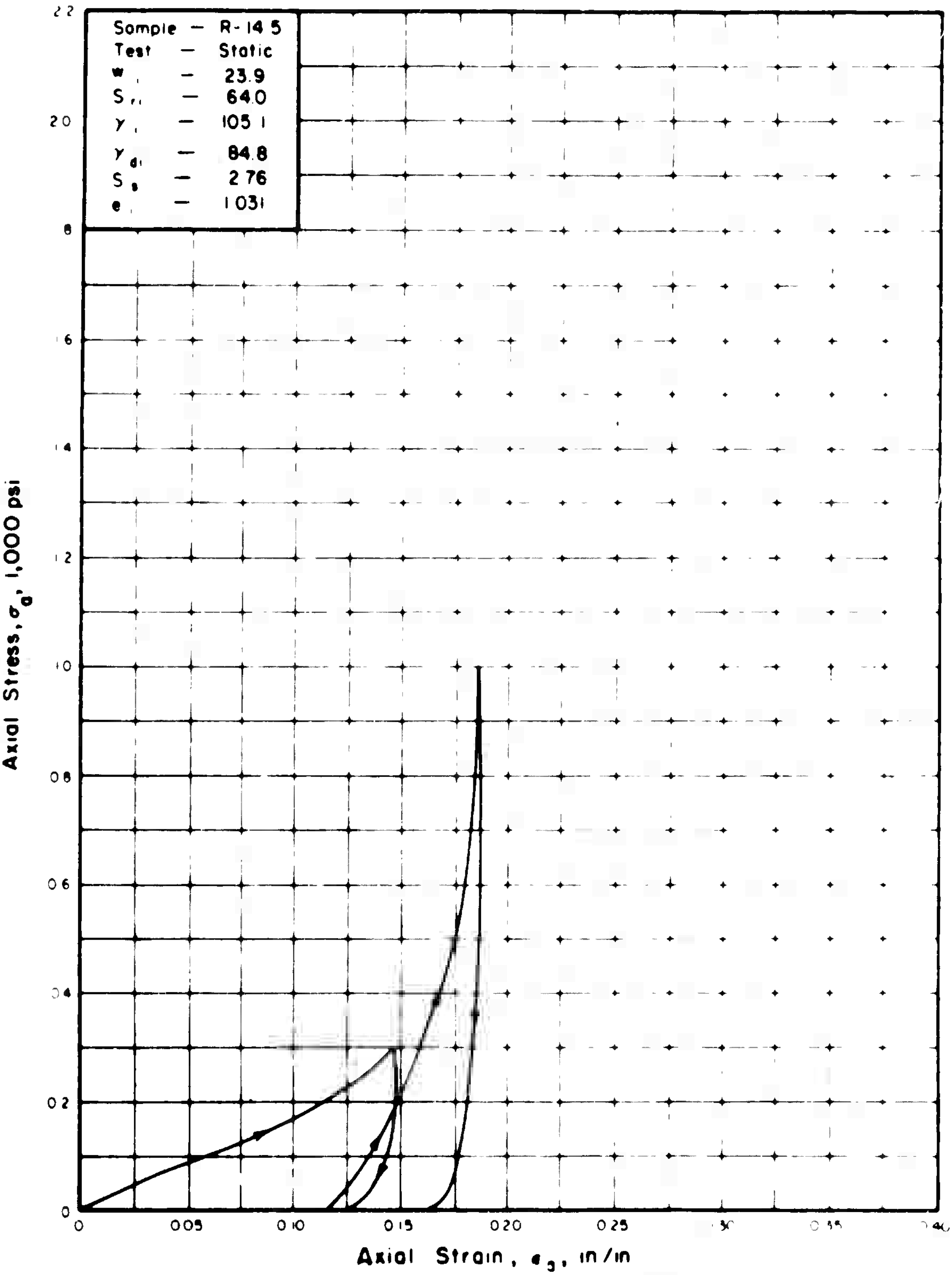

Figure 31. STRESS-STRAIN RELATIONSHIP IN ONE-DIMENSIONAL COMPRESSION.

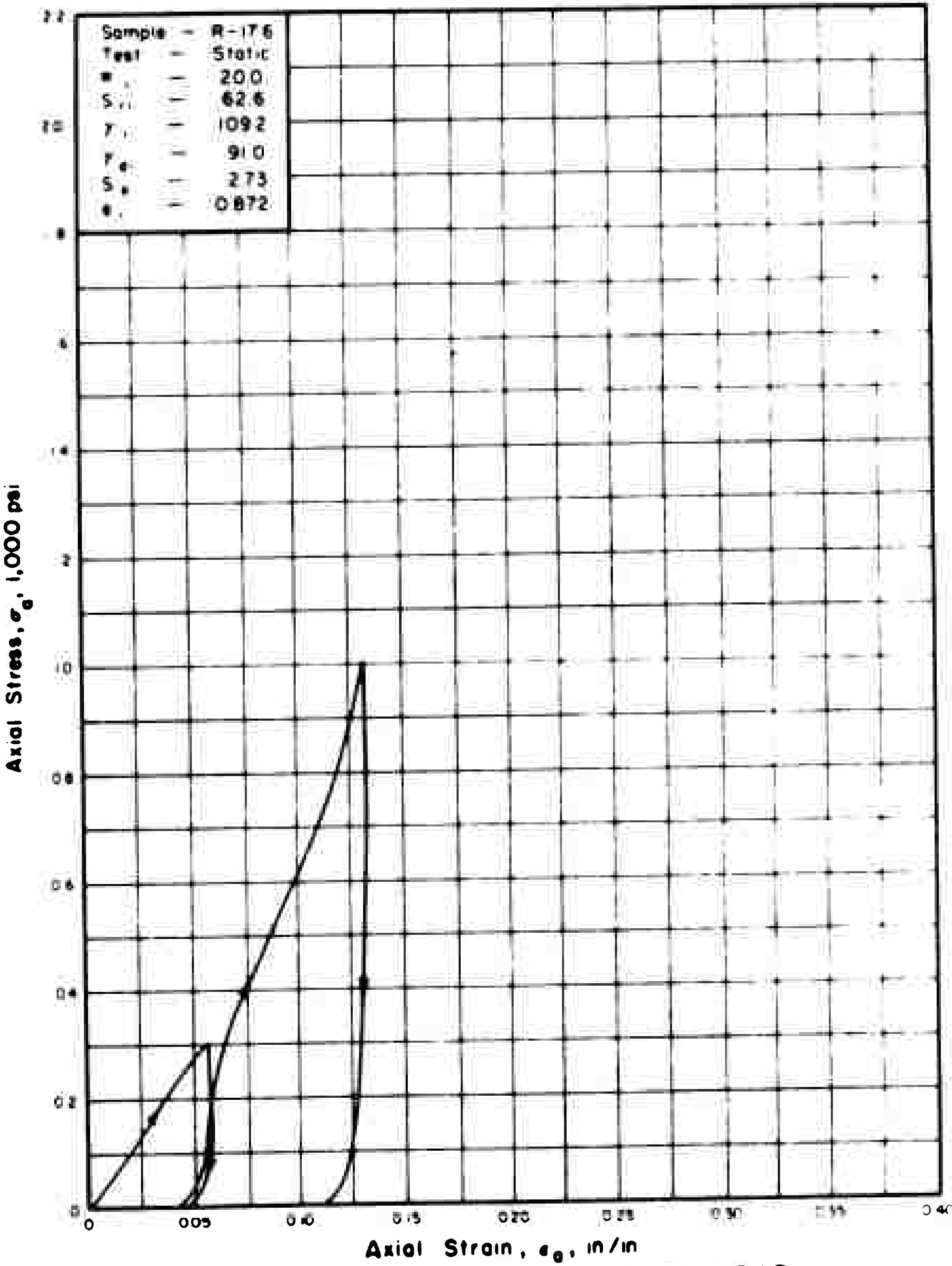

Figure 32. STRESS-STRAIN RELATIONSHIP IN ONE-DIMENSIONAL COMPRESSION.

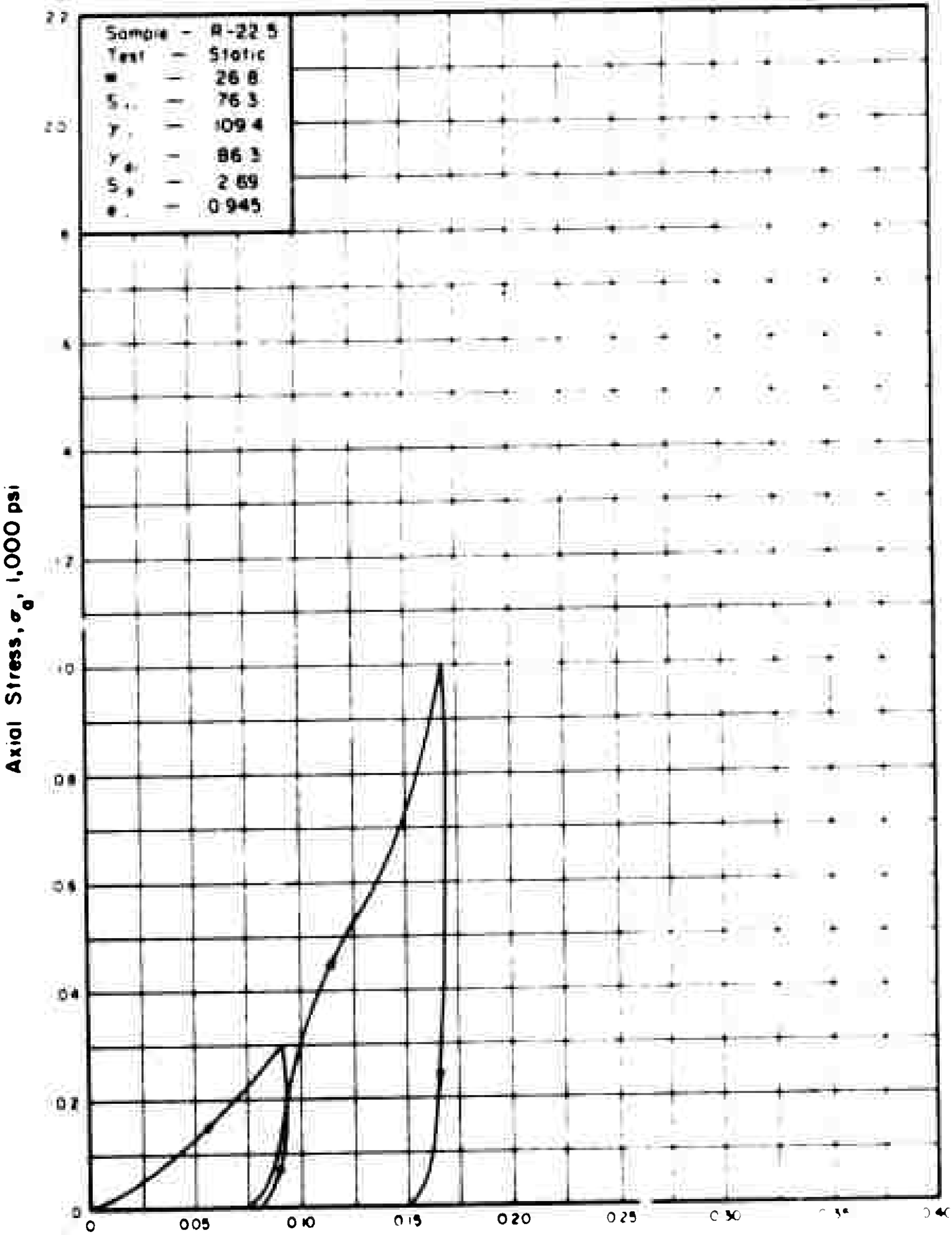

Figure 33. STRESS-STRAIN RELATIONSHIP IN ONE-DIMENSIONAL COMPRESSION.

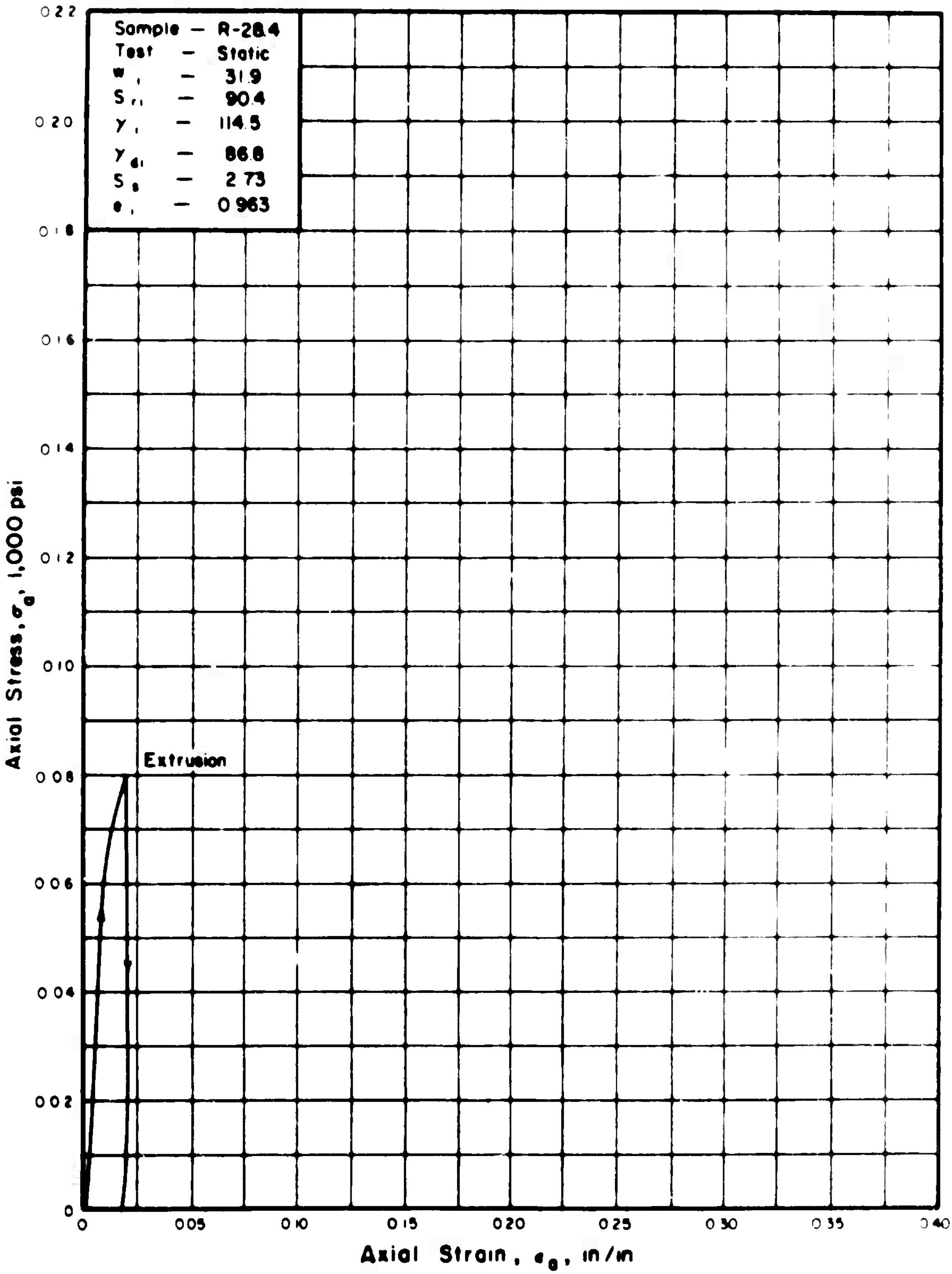

Figure 34. STRESS-STRAIN RELATIONSHIP IN ONE-DIMENSIONAL COMPRESSION.

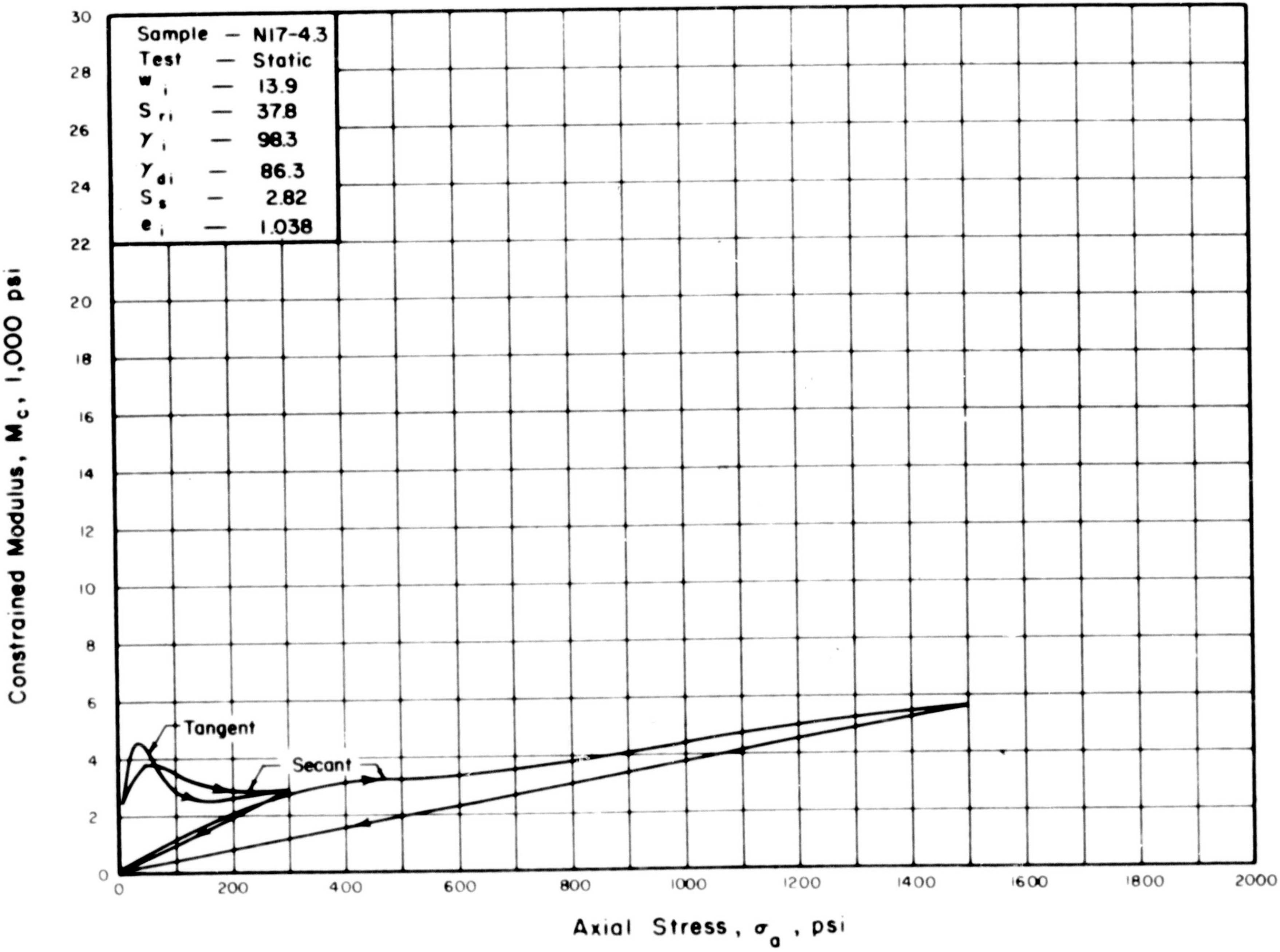

Figure 35. THE RELATIONSHIP BETWEEN CONSTRAINED MODULUS AND AXIAL STRESS.

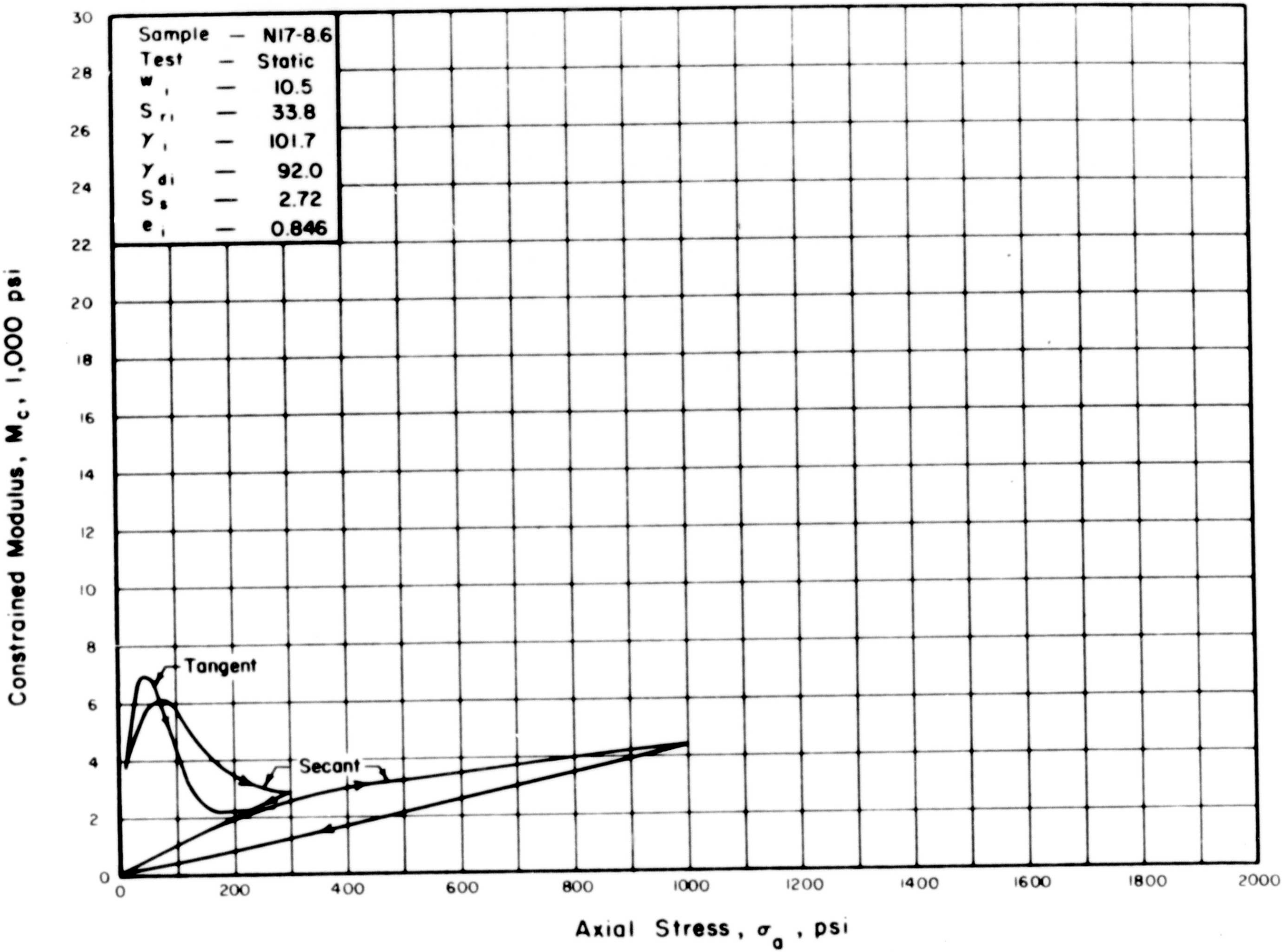

Figure 36. THE RELATIONSHIP BETWEEN CONSTRAINED MODULUS AND AXIAL STRESS.

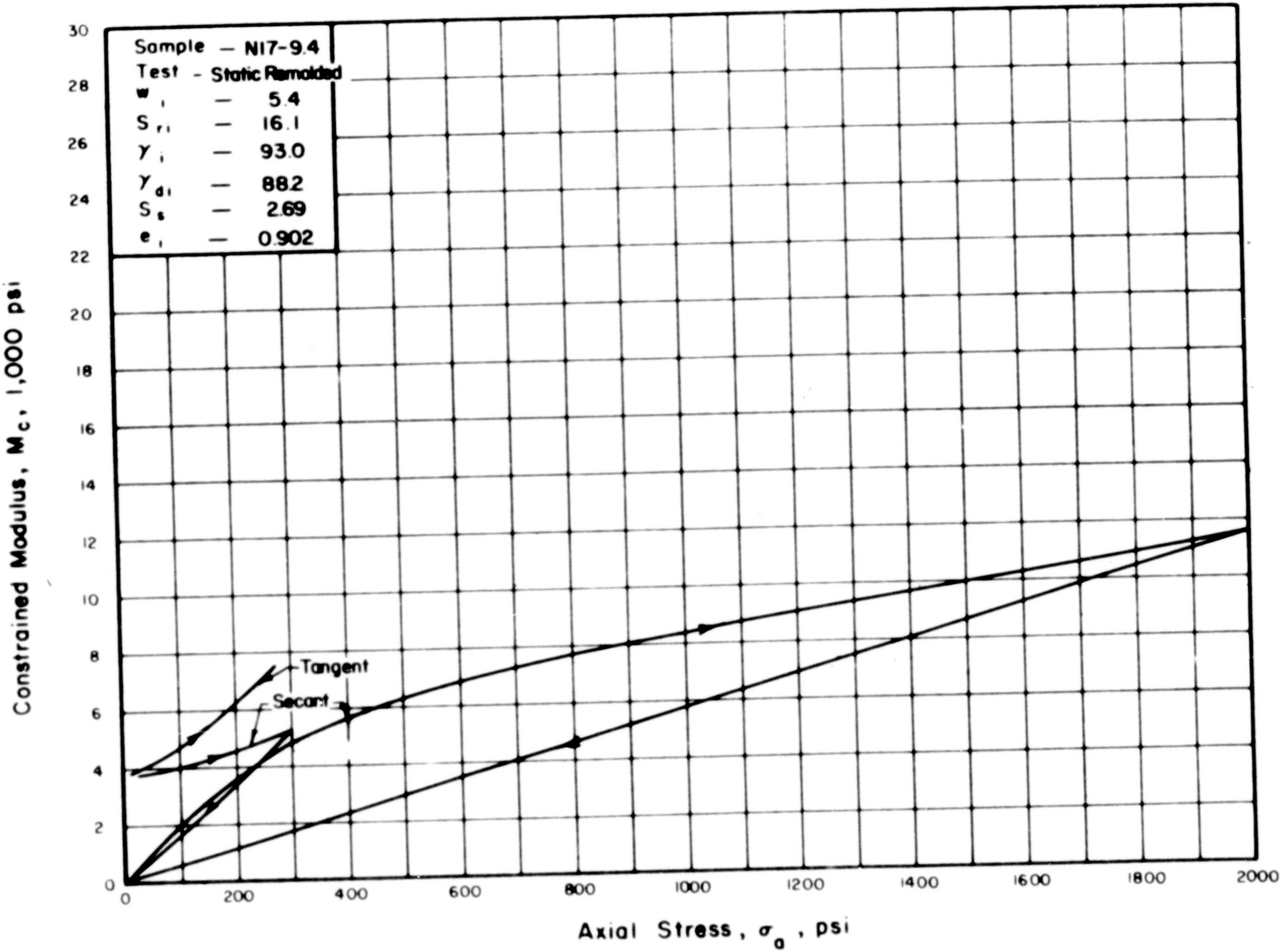

Figure 37. THE RELATIONSHIP BETWEEN CONSTRAINED MODULUS AND AXIAL STRESS.

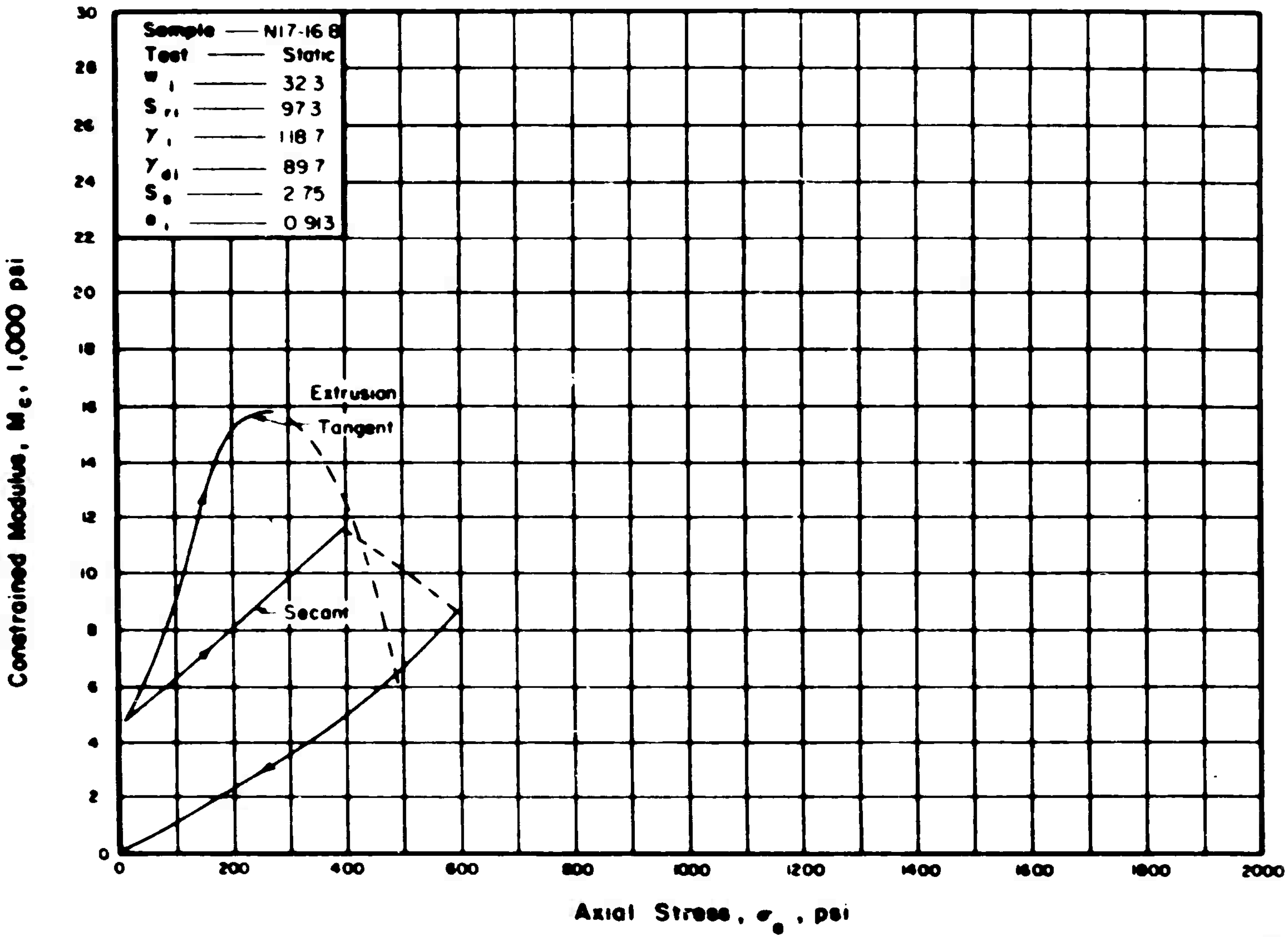

Figure 38. THE RELATIONSHIP BETWEEN CONSTRAINED MODULUS AND AXIAL STRESS.

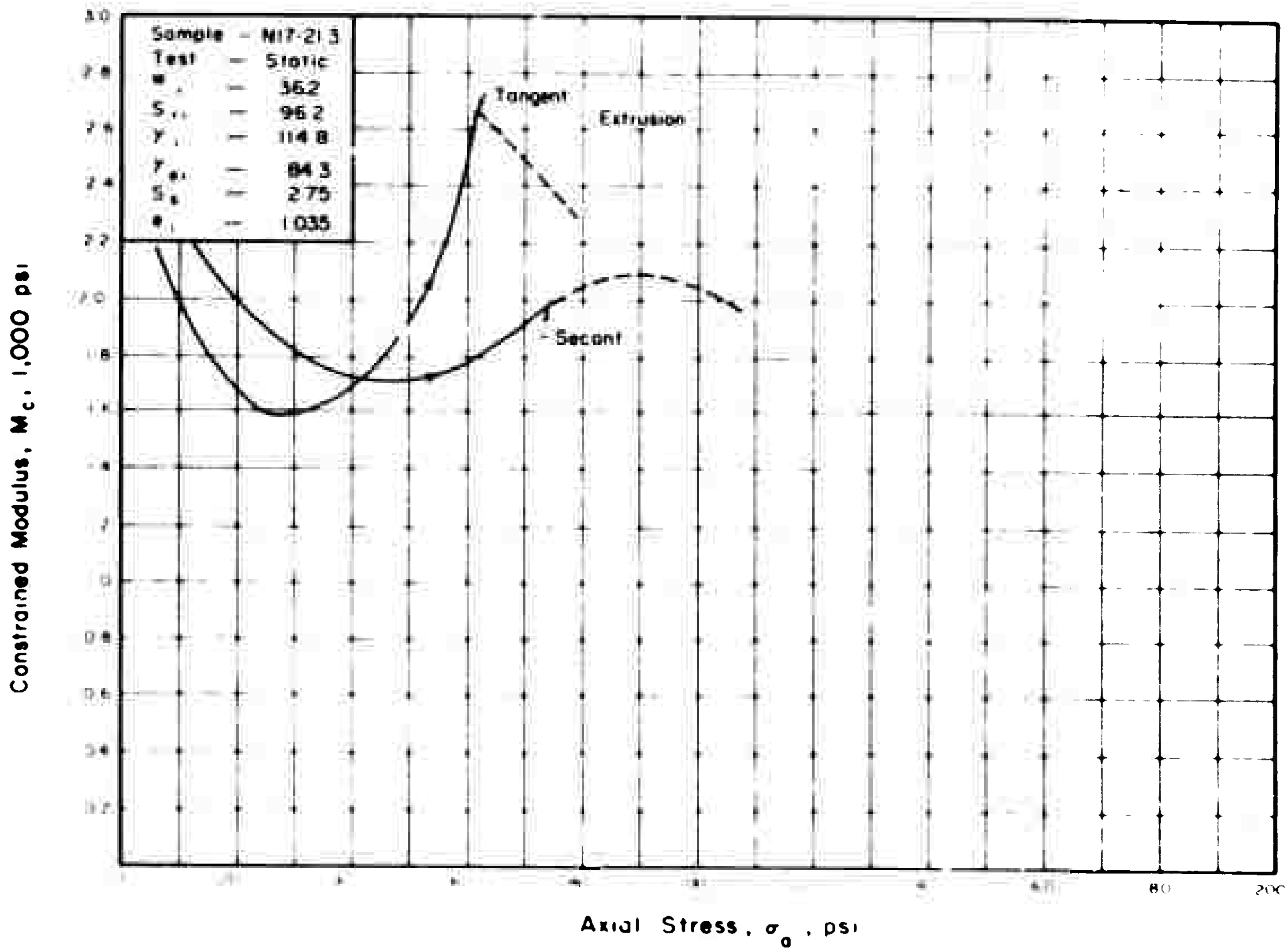

Figure 39. THE RELATIONSHIP BETWEEN CONSTRAINED MODULUS AND AXIAL STRESS.

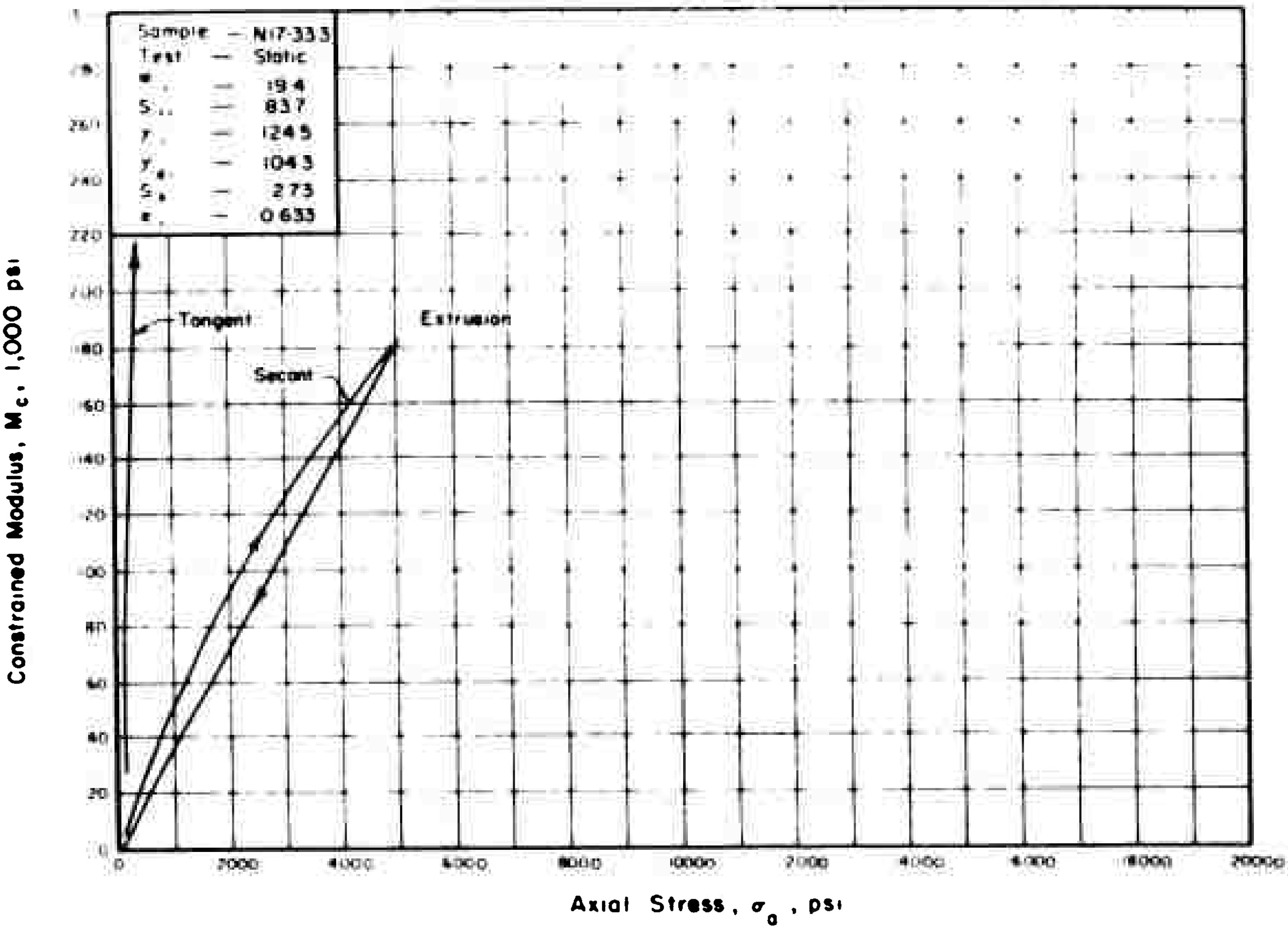

Figure 40. THE RELATIONSHIP BETWEEN CONSTRAINED MODULUS AND AXIAL STRESS.

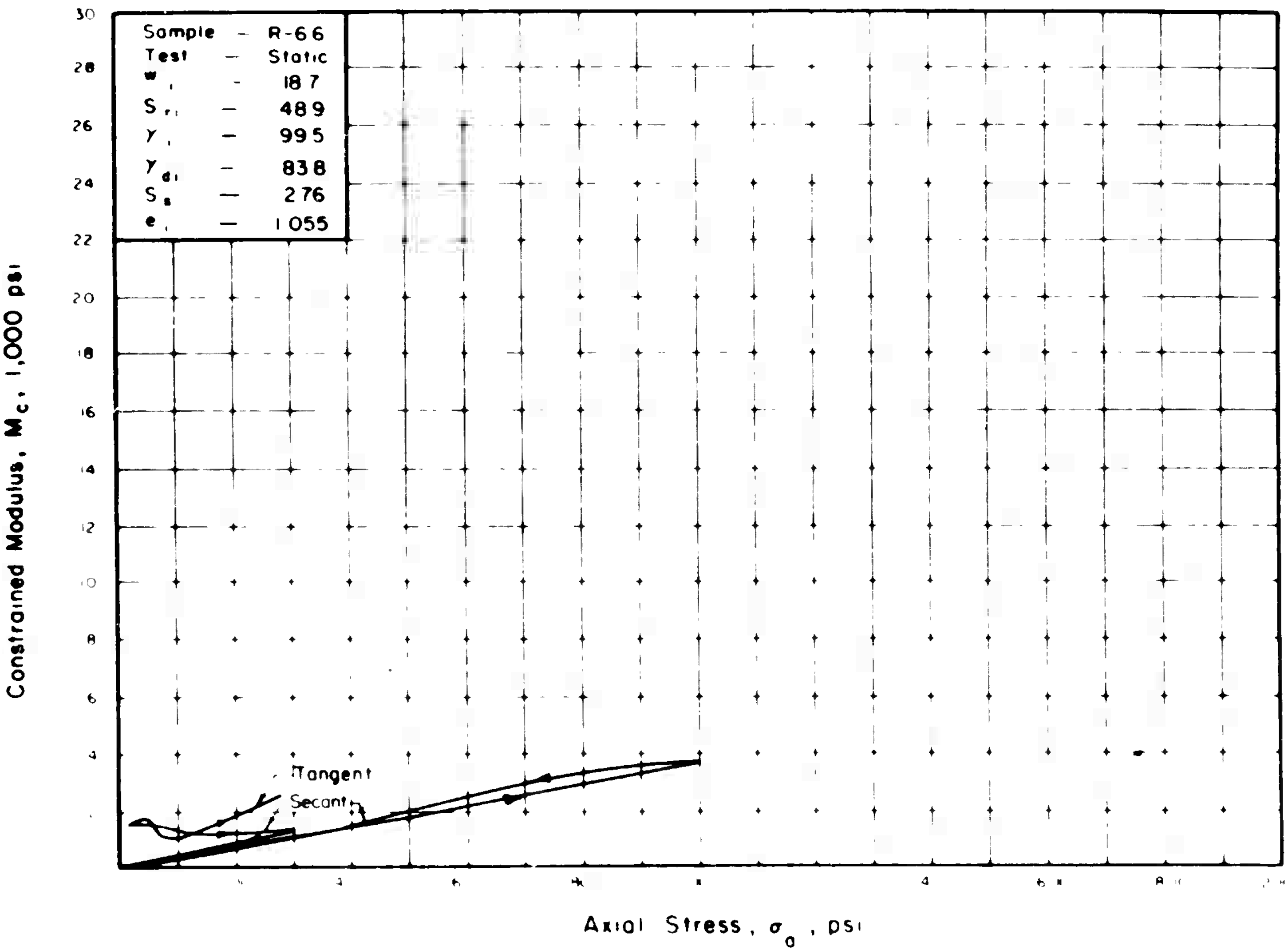

Figure 41 THE RELATIONSHIP BETWEEN CONSTRAINED MODULUS AND AXIAL STRESS

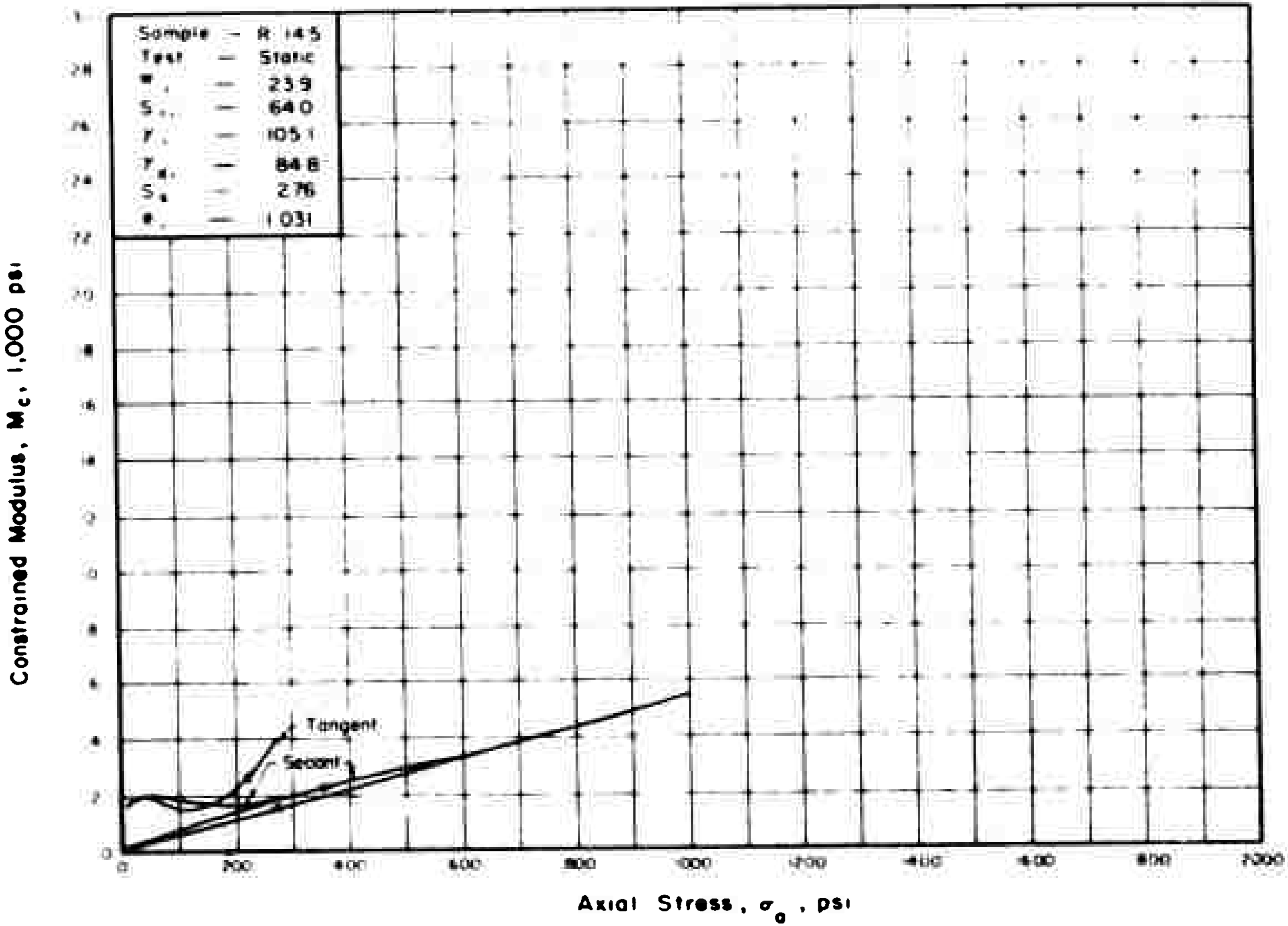

Figure 42. THE RELATIONSHIP BETWEEN CONSTRAINED MODULUS AND AXIAL STRESS.

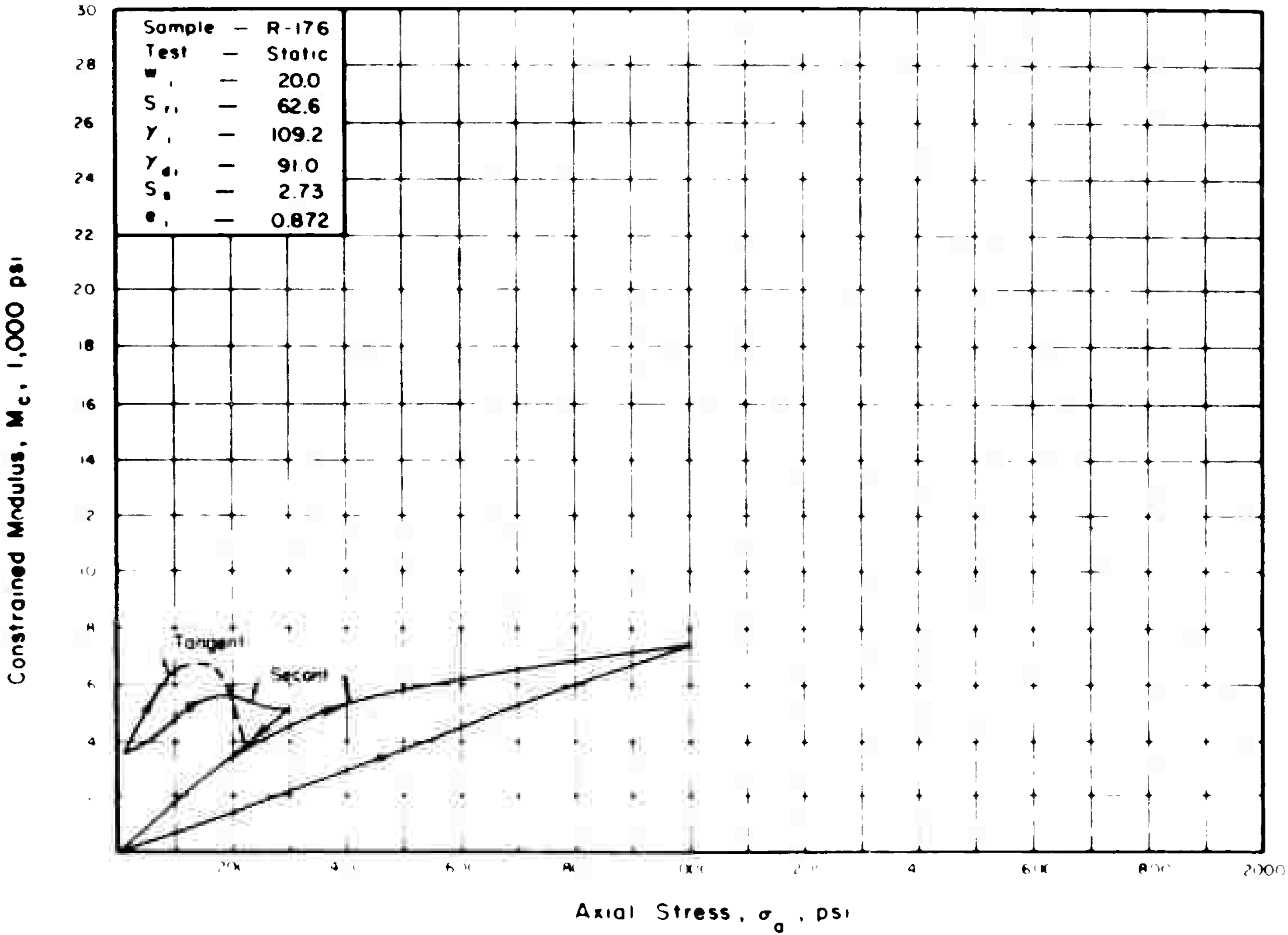

Figure 43. THE RELATIONSHIP BETWEEN CONSTRAINED MODULUS AND AXIAL STRESS.

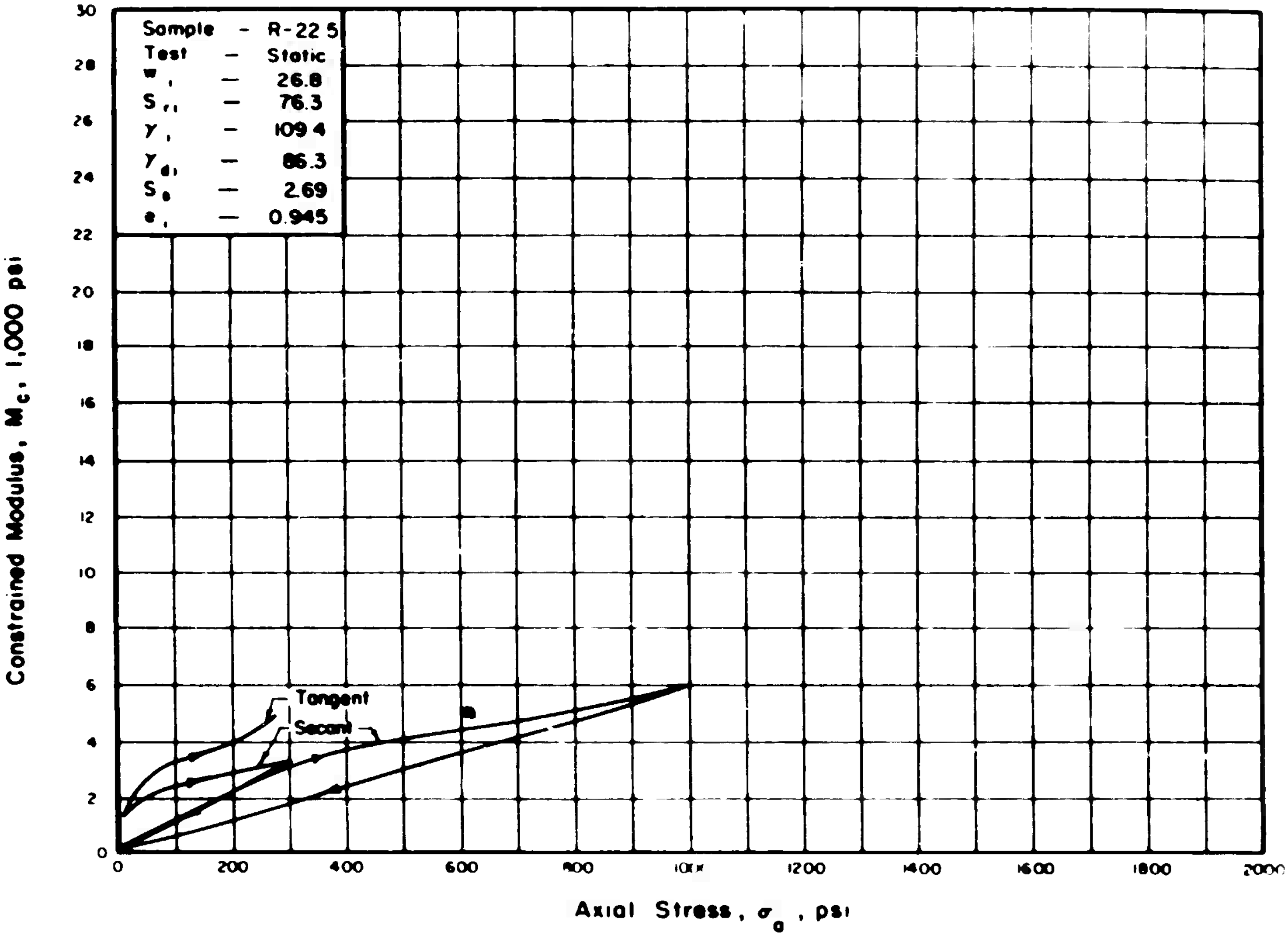

Figure 44. THE RELATIONSHIP BETWEEN CONSTRAINED MODULUS AND AXIAL STRESS.

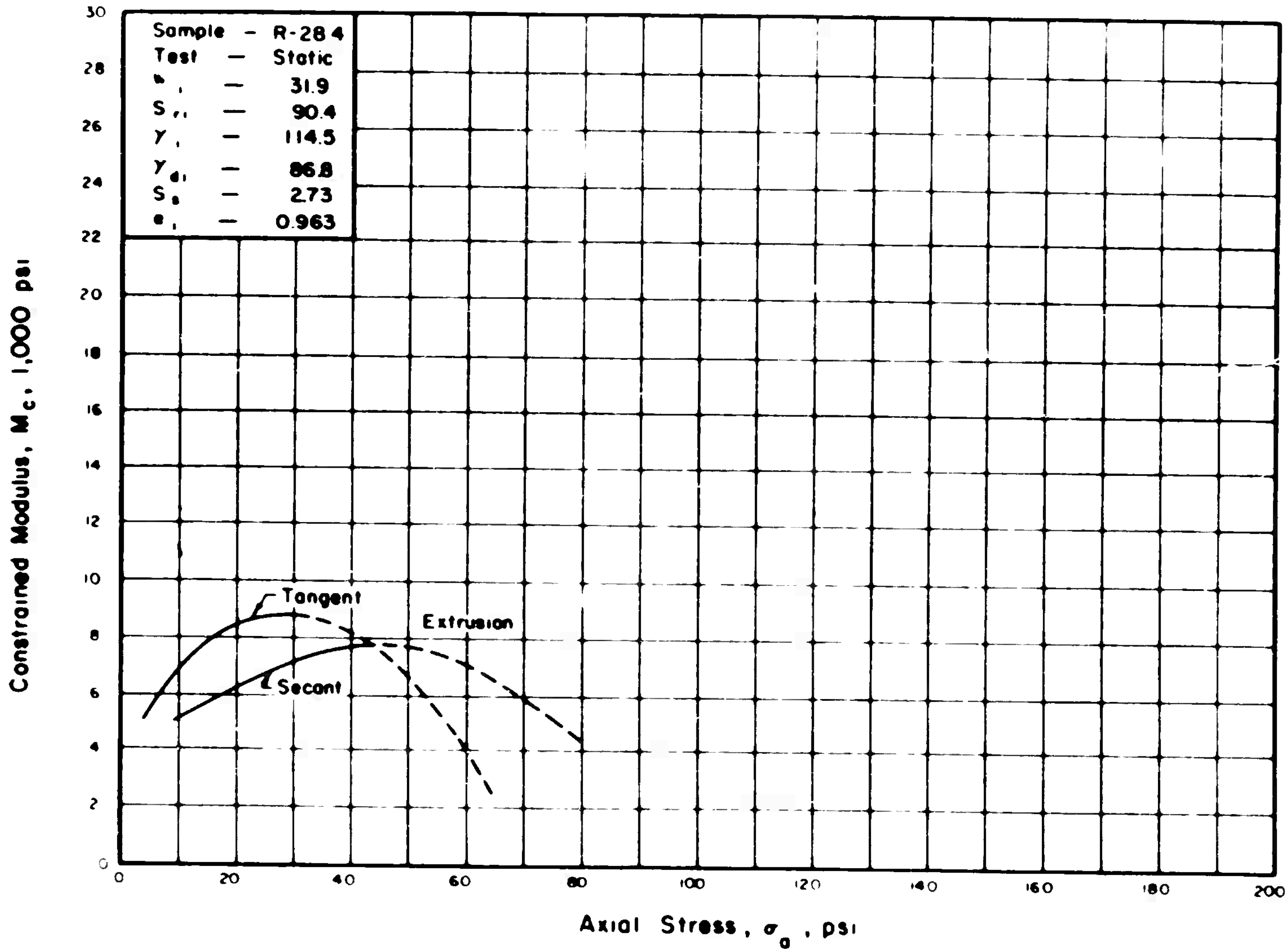

Figure 45. THE RELATIONSHIP BETWEEN CONSTRAINED MODULUS AND AXIAL STRESS.

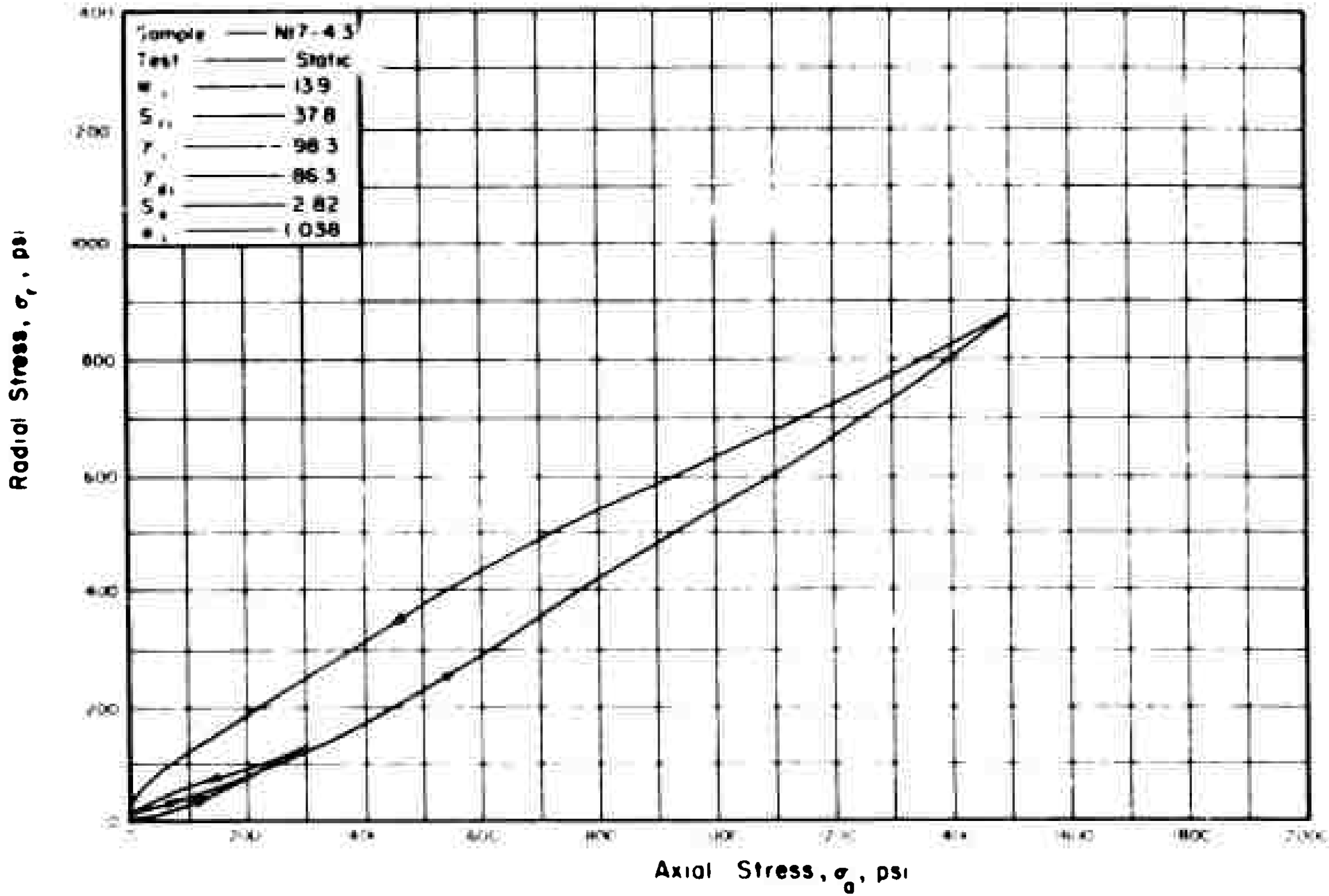

Figure 46. THE RELATIONSHIP BETWEEN RADIAL AND AXIAL STRESS IN ONE-DIMENSIONAL COMPRESSION.

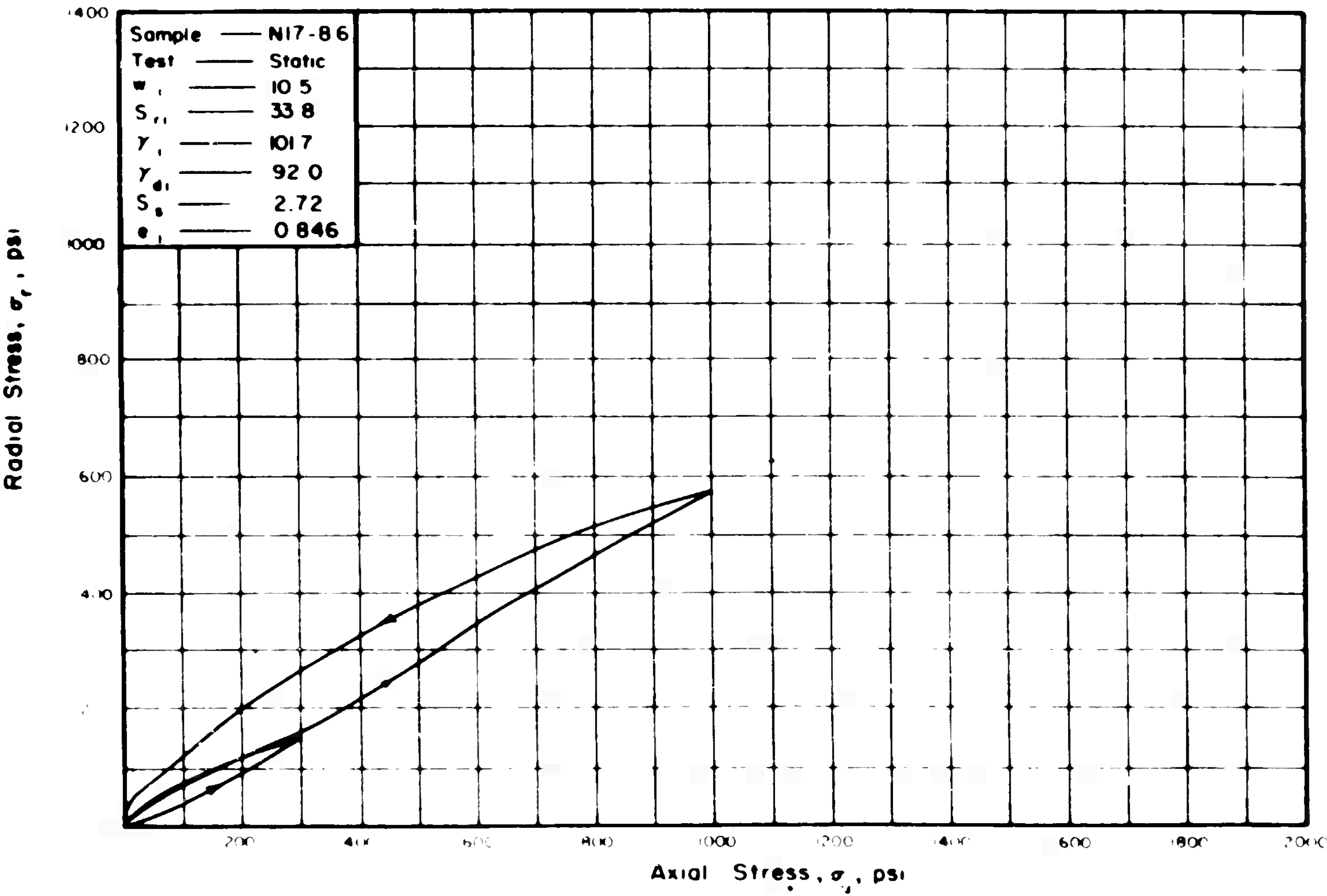

Figure 47. THE RELATIONSHIP BETWEEN RADIAL AND AXIAL STRESS IN ONE-DIMENSIONAL COMPRESSION.

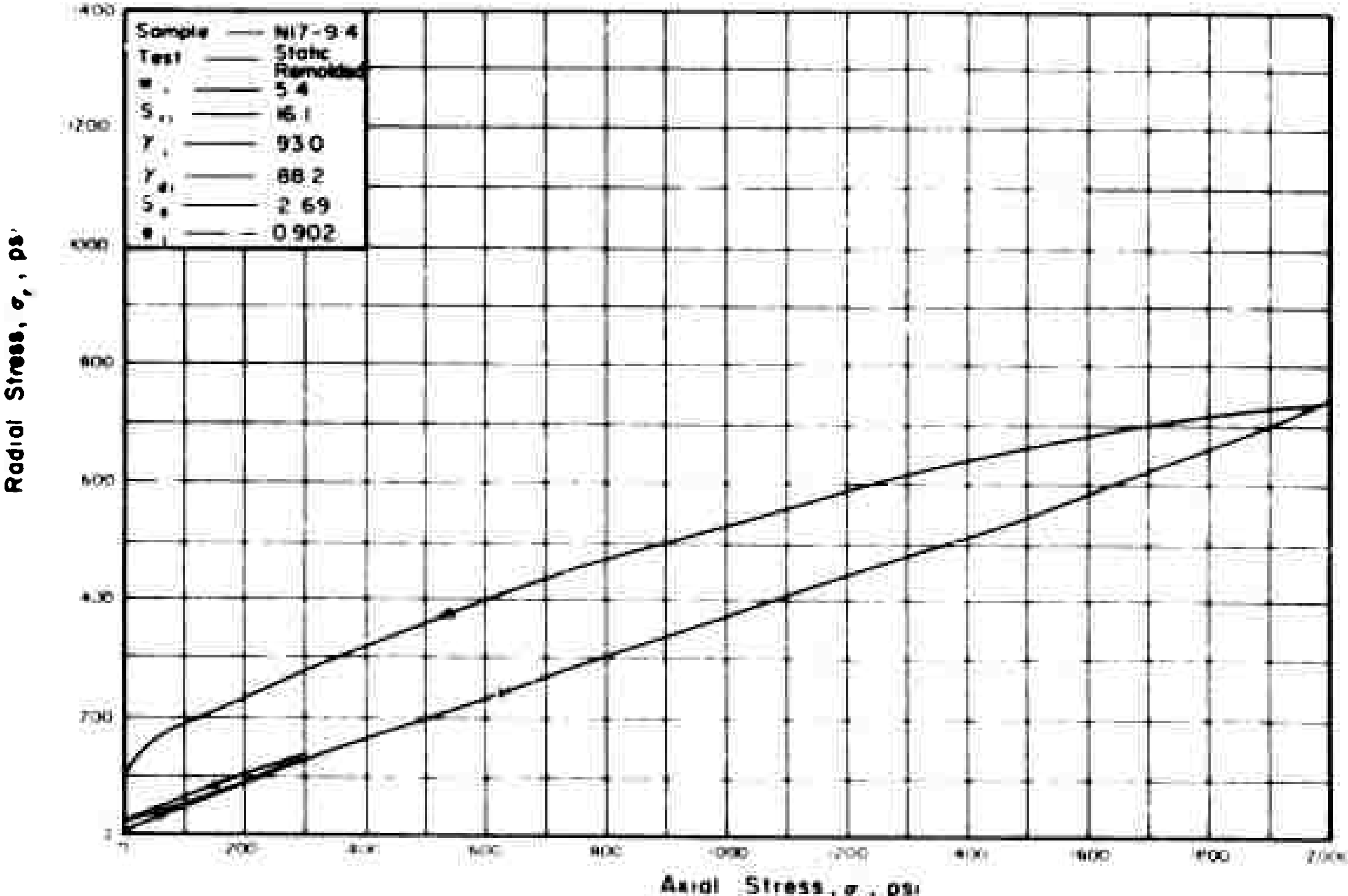

Figure 48. THE RELATIONSHIP BETWEEN RADIAL AND AXIAL STRESS IN ONE-DIMENSIONAL COMPRESSION.

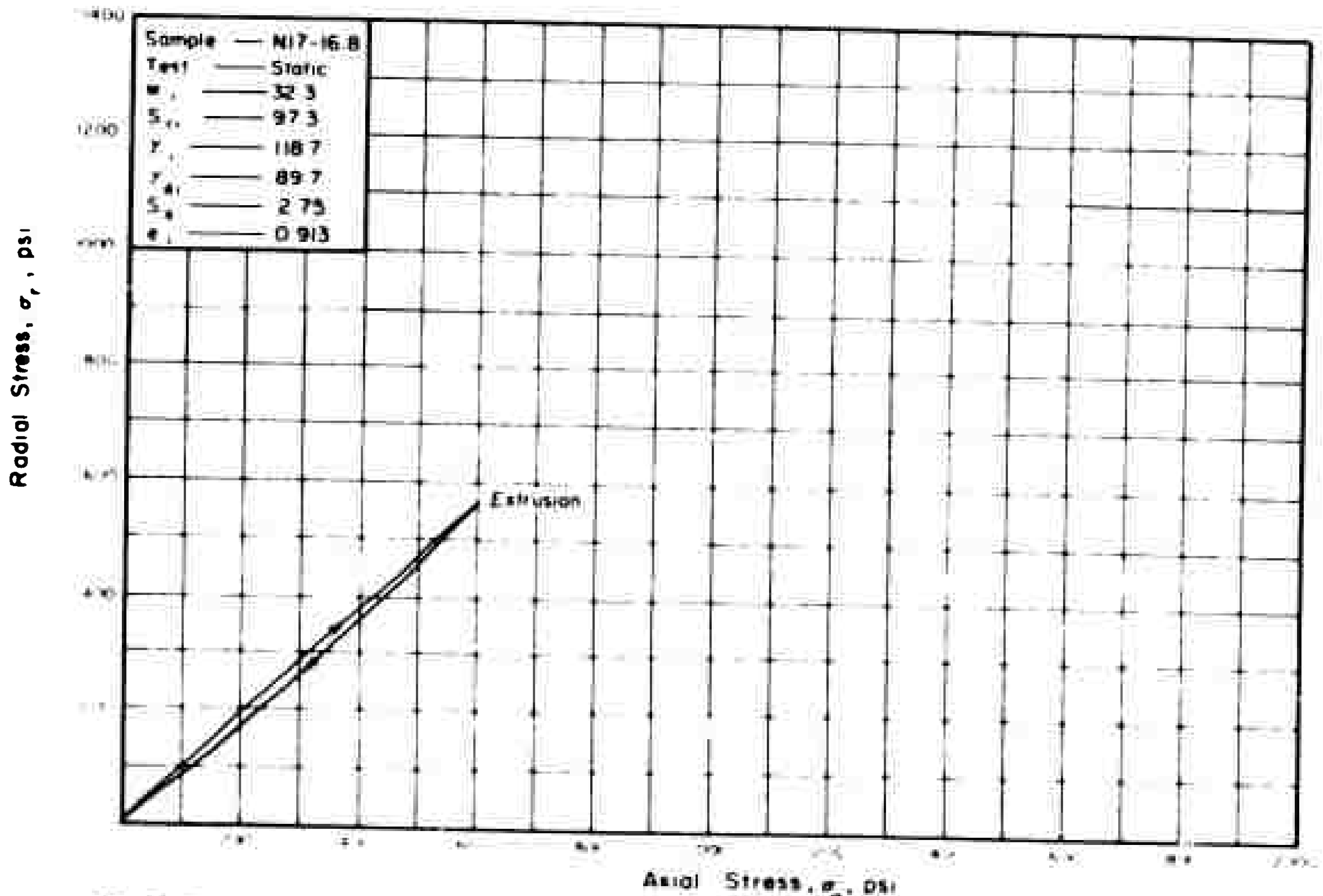

Figure 49. THE RELATIONSHIP BETWEEN RADIAL AND AXIAL STRESS IN ONE-DIMENSIONAL COMPRESSION.

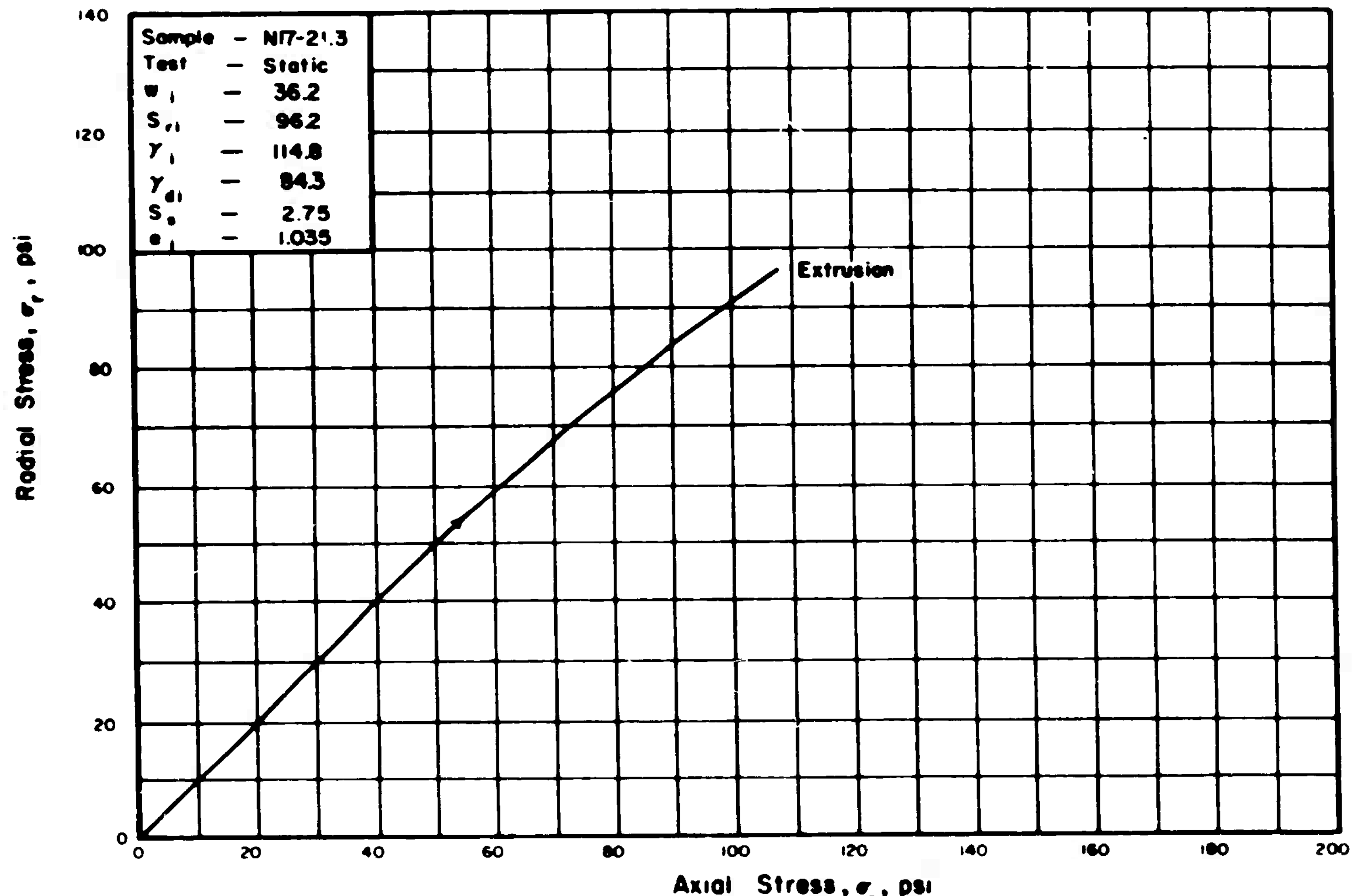

Figure 50. THE RELATIONSHIP BETWEEN RADIAL AND AXIAL STRESS IN ONE-DIMENSIONAL COMPRESSION.

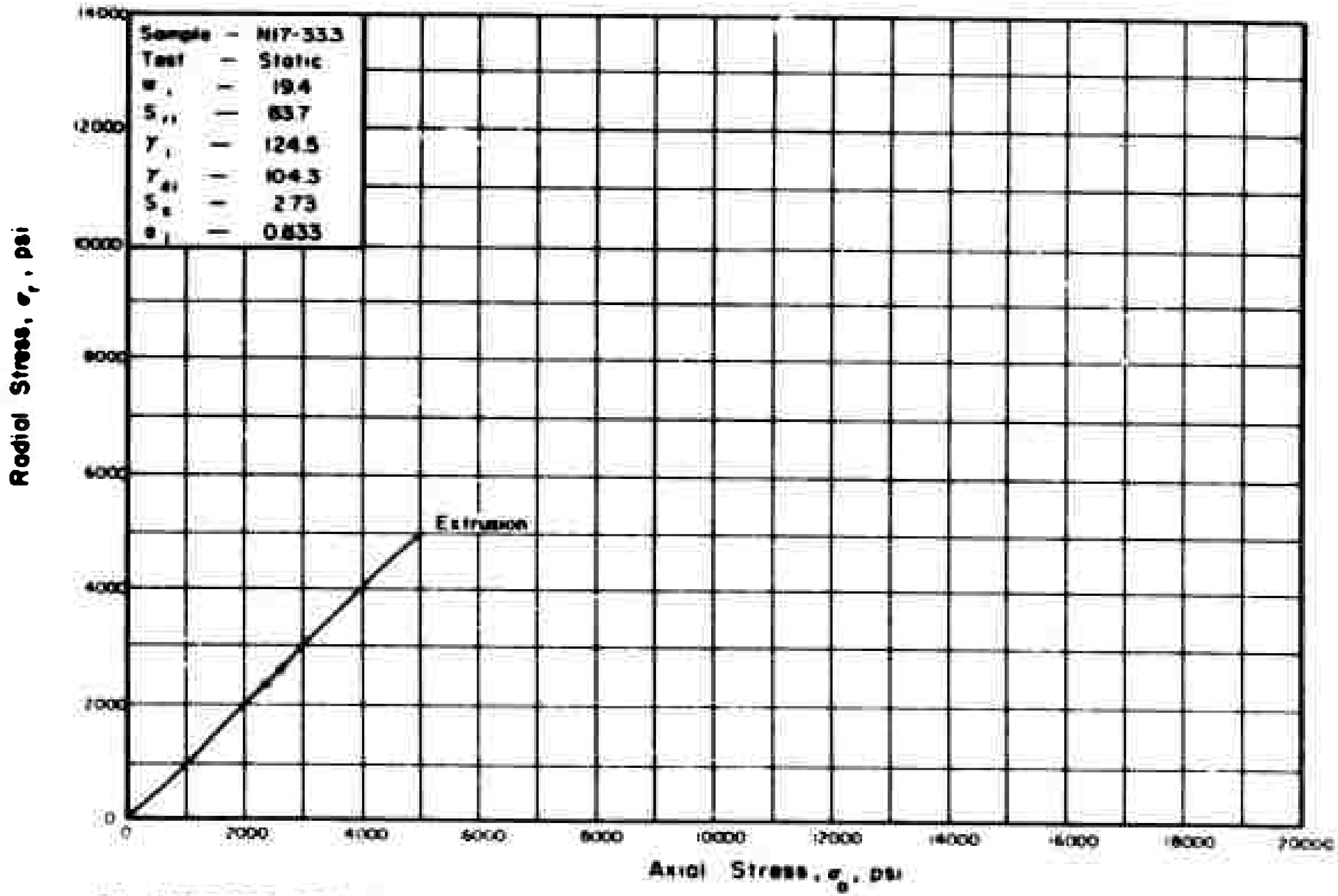

Figure 51. THE RELATIONSHIP BETWEEN RADIAL AND AXIAL STRESS IN ONE-DIMENSIONAL COMPRESSION.

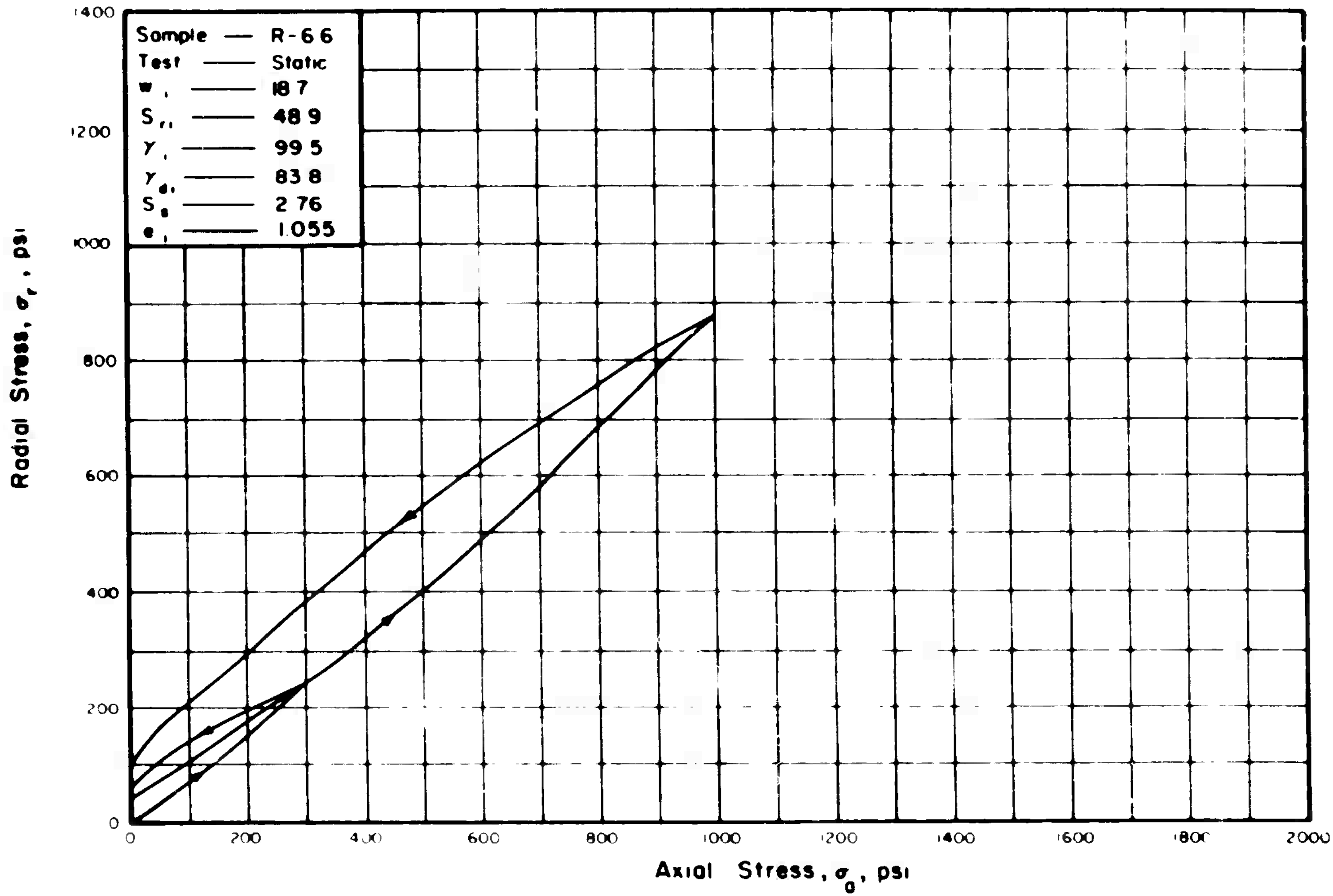

Figure 52. THE RELATIONSHIP BETWEEN RADIAL AND AXIAL STRESS IN ONE-DIMENSIONAL COMPRESSION.

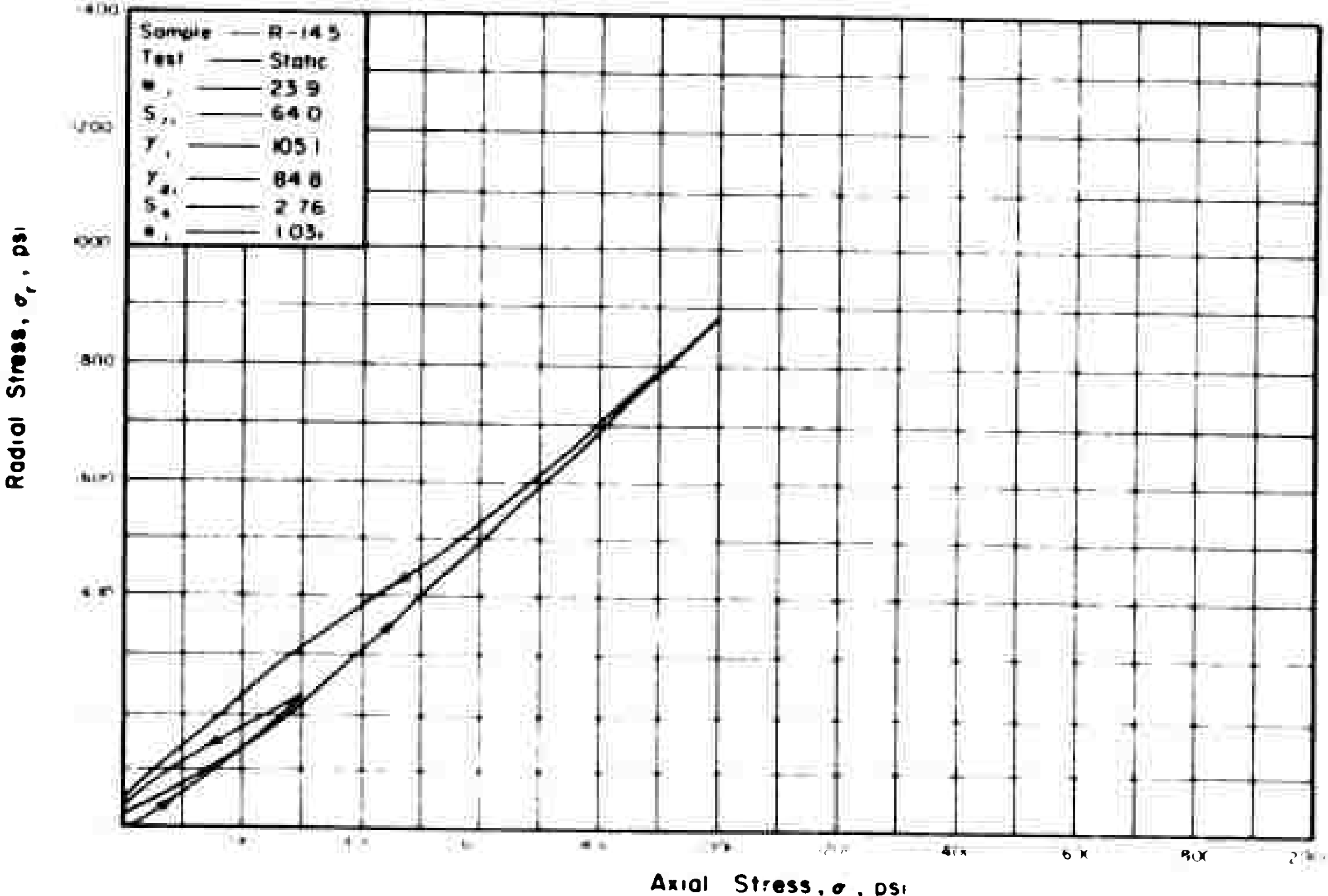

Figure 53. THE RELATIONSHIP BETWEEN RADIAL AND AXIAL STRESS IN ONE-DIMENSIONAL COMPRESSION.

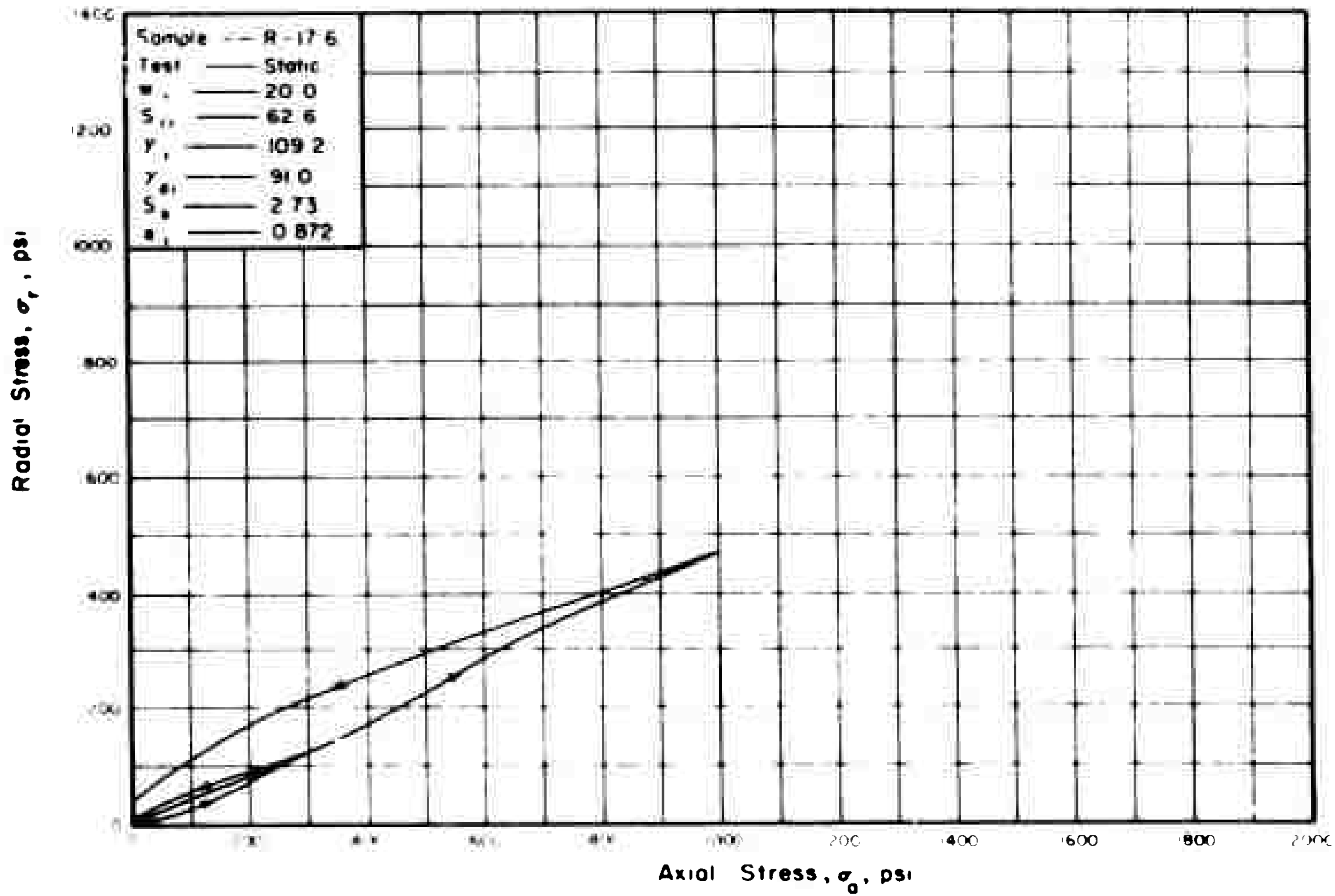

Figure 54. THE RELATIONSHIP BETWEEN RADIAL AND AXIAL STRESS IN ONE-DIMENSIONAL COMPRESSION.

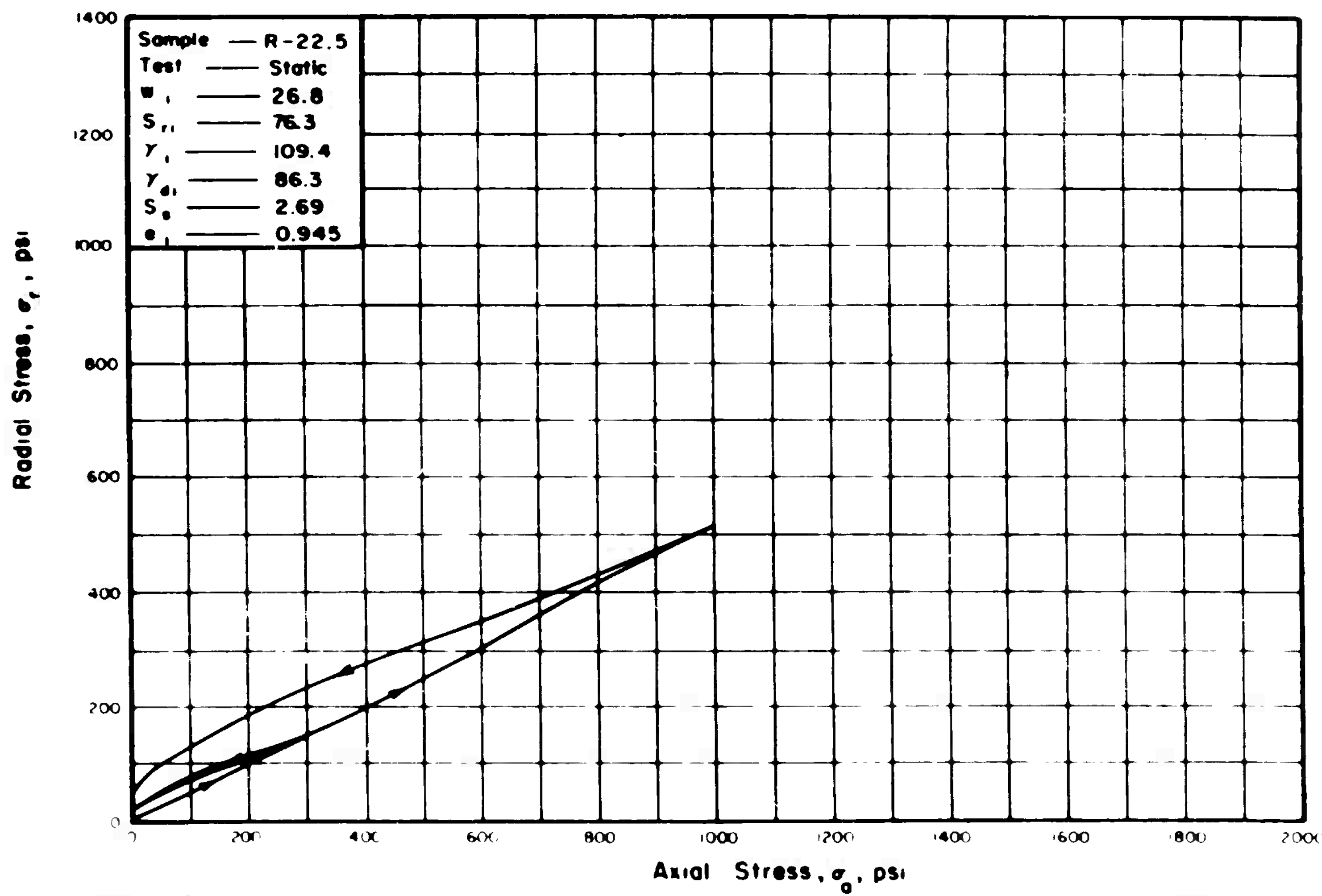

Figure 55. THE RELATIONSHIP BETWEEN RADIAL AND AXIAL STRESS IN ONE-DIMENSIONAL COMPRESSION.

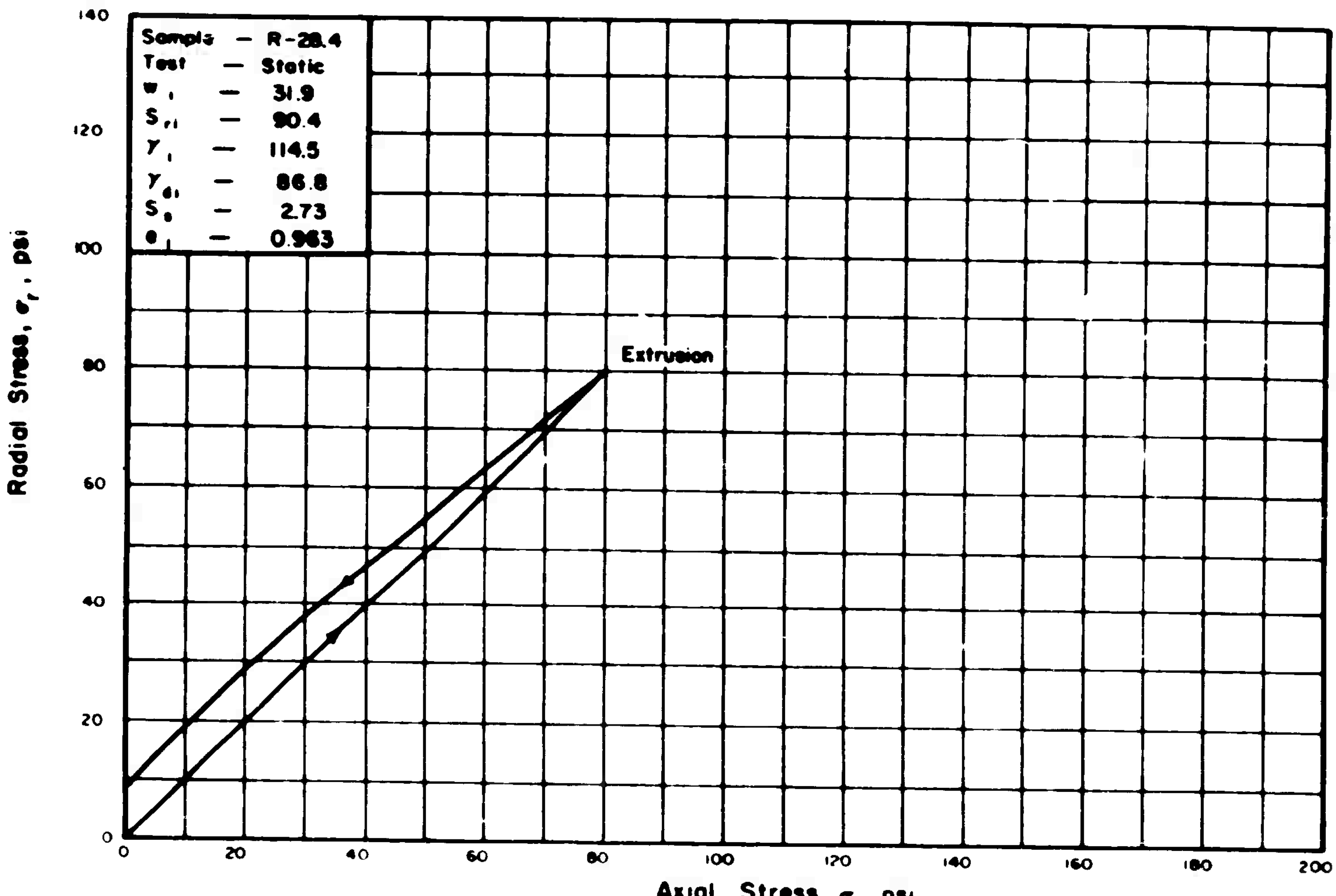

Figure 56. THE RELATIONSHIP BETWEEN RADIAL AND AXIAL STRESS IN ONE-DIMENSIONAL COMPRESSION.

APPENDIX III

DYNAMIC TEST RESULTS

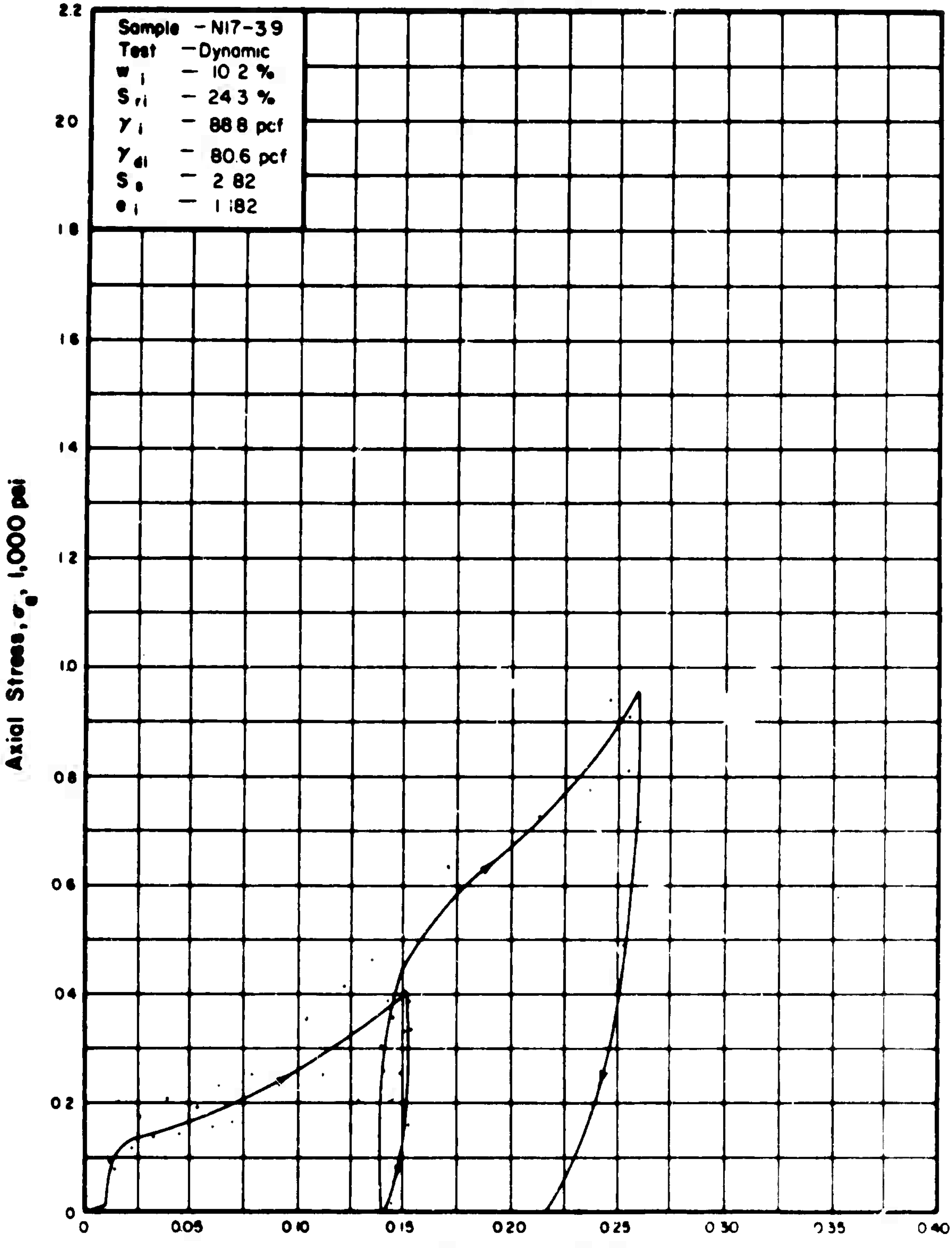

Figure 57. STRESS-STRAIN RELATIONSHIP IN ONE-DIMENSIONAL COMPRESSION.

BLANK PAGE

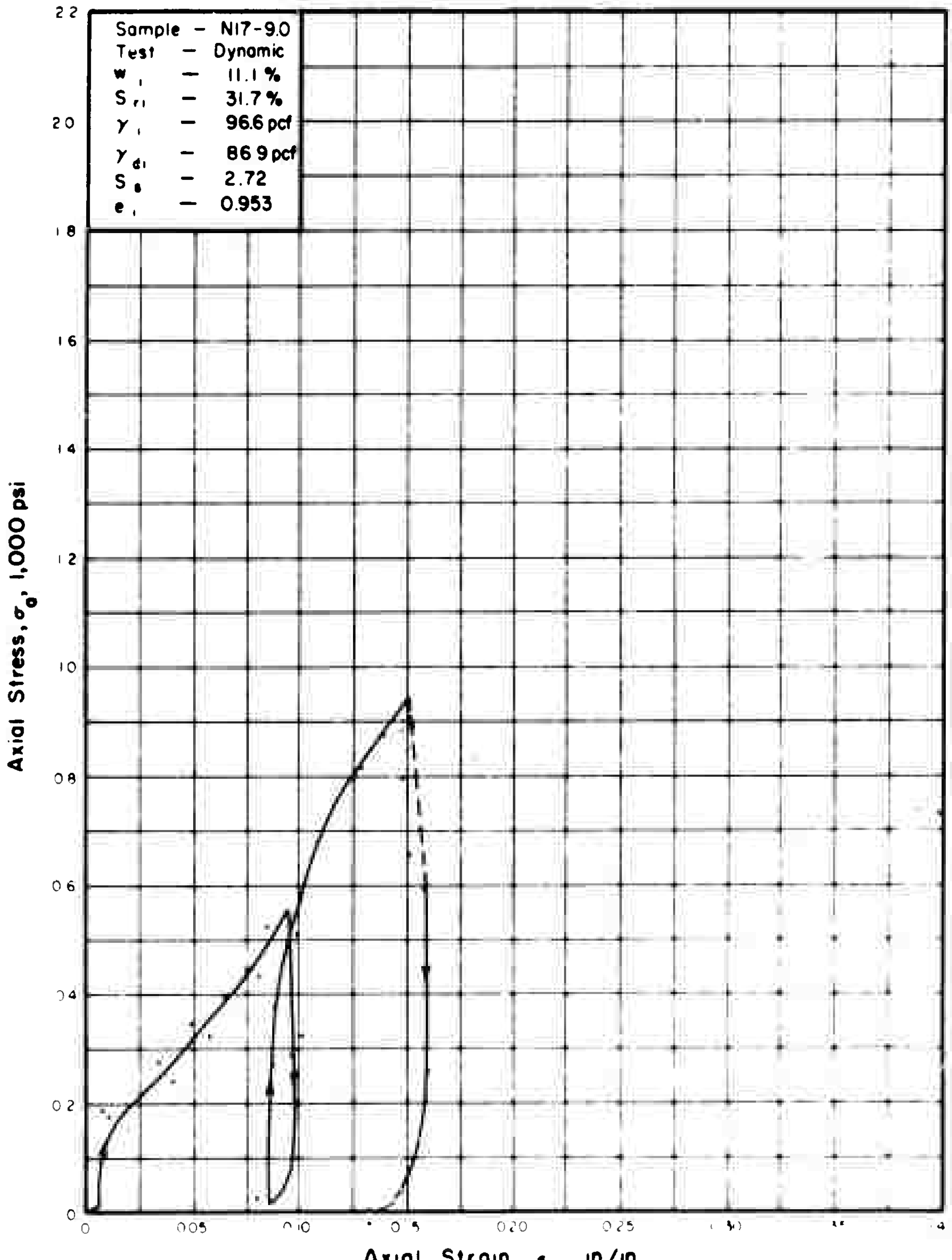

Figure 58. STRESS-STRAIN RELATIONSHIP IN ONE DIMENSIONAL COMPRESSION

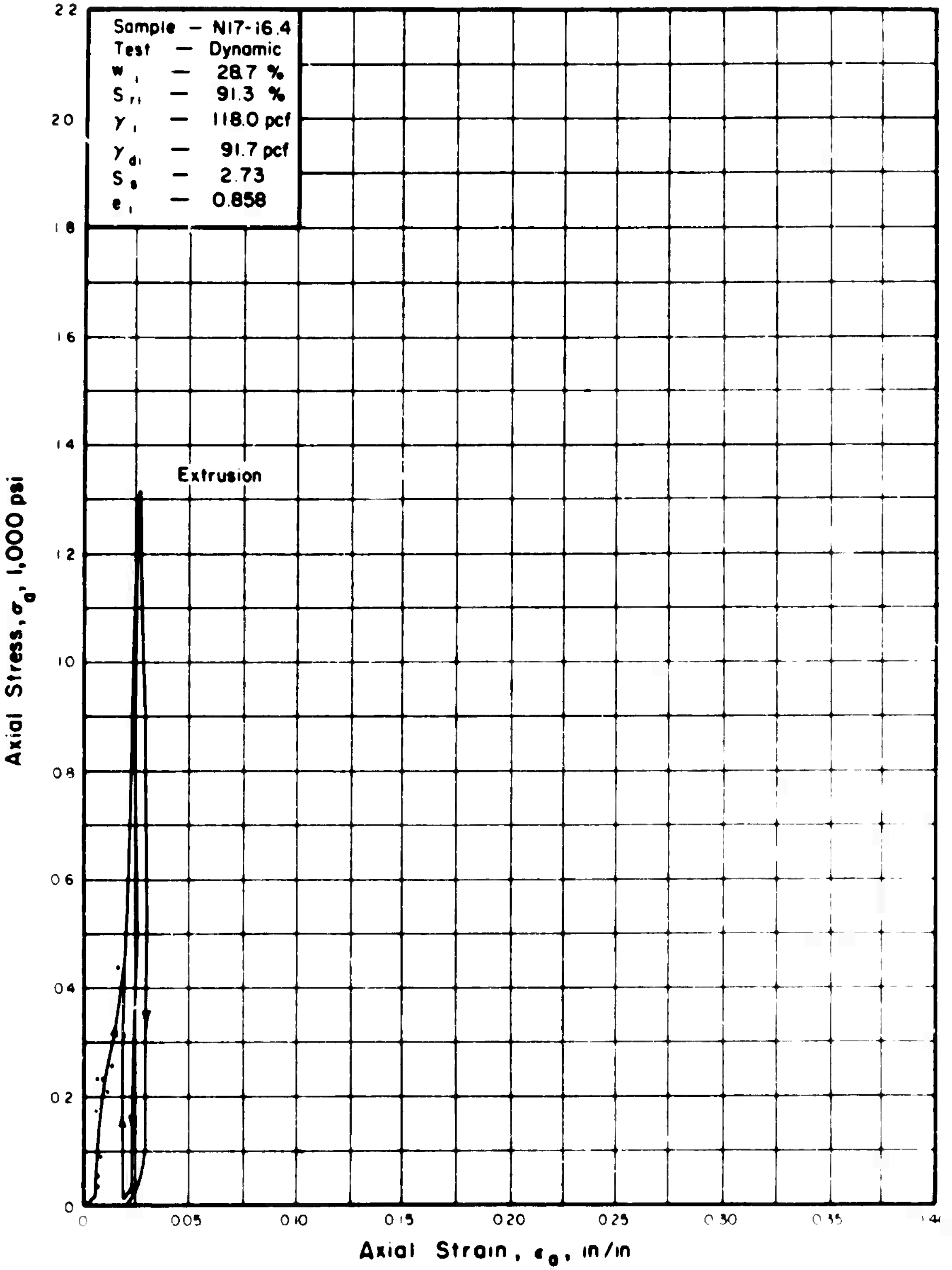

Figure 59. STRESS-STRAIN RELATIONSHIP IN ONE-DIMENSIONAL COMPRESSION

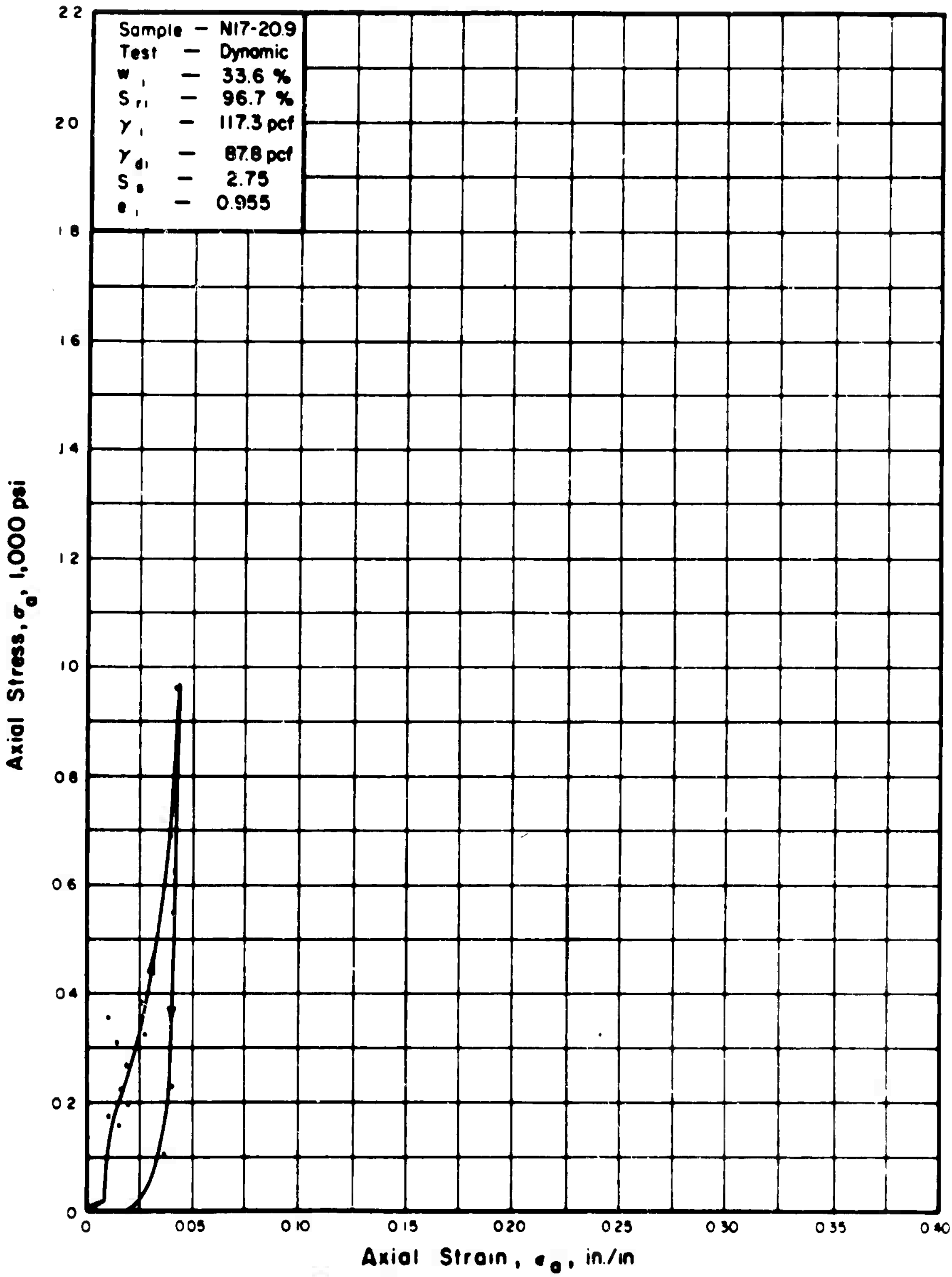

Figure 60. STRESS-STRAIN RELATIONSHIP IN ONE-DIMENSIONAL COMPRESSION.

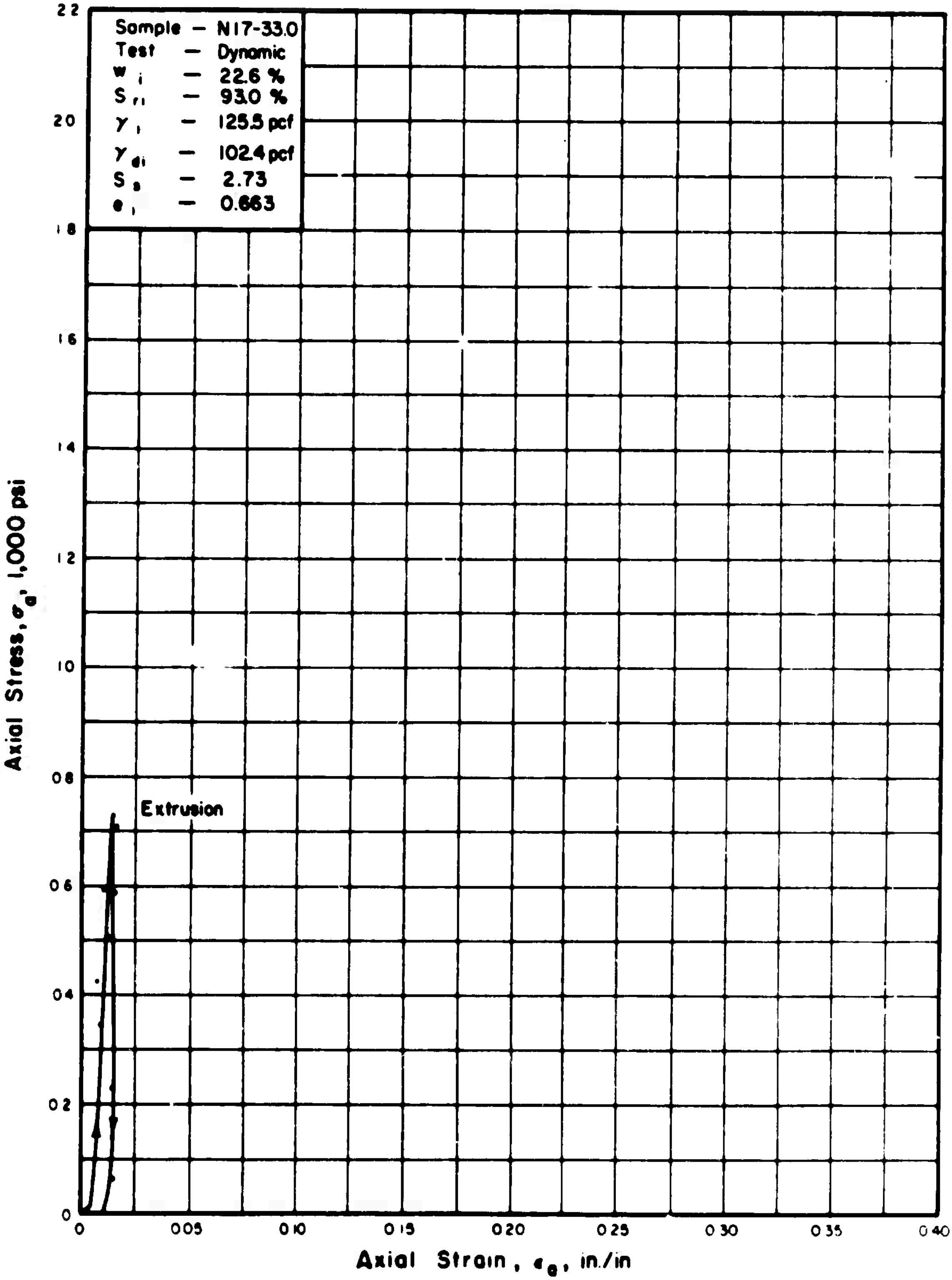

Figure 61. STRESS-STRAIN RELATIONSHIP IN ONE-DIMENSIONAL COMPRESSION

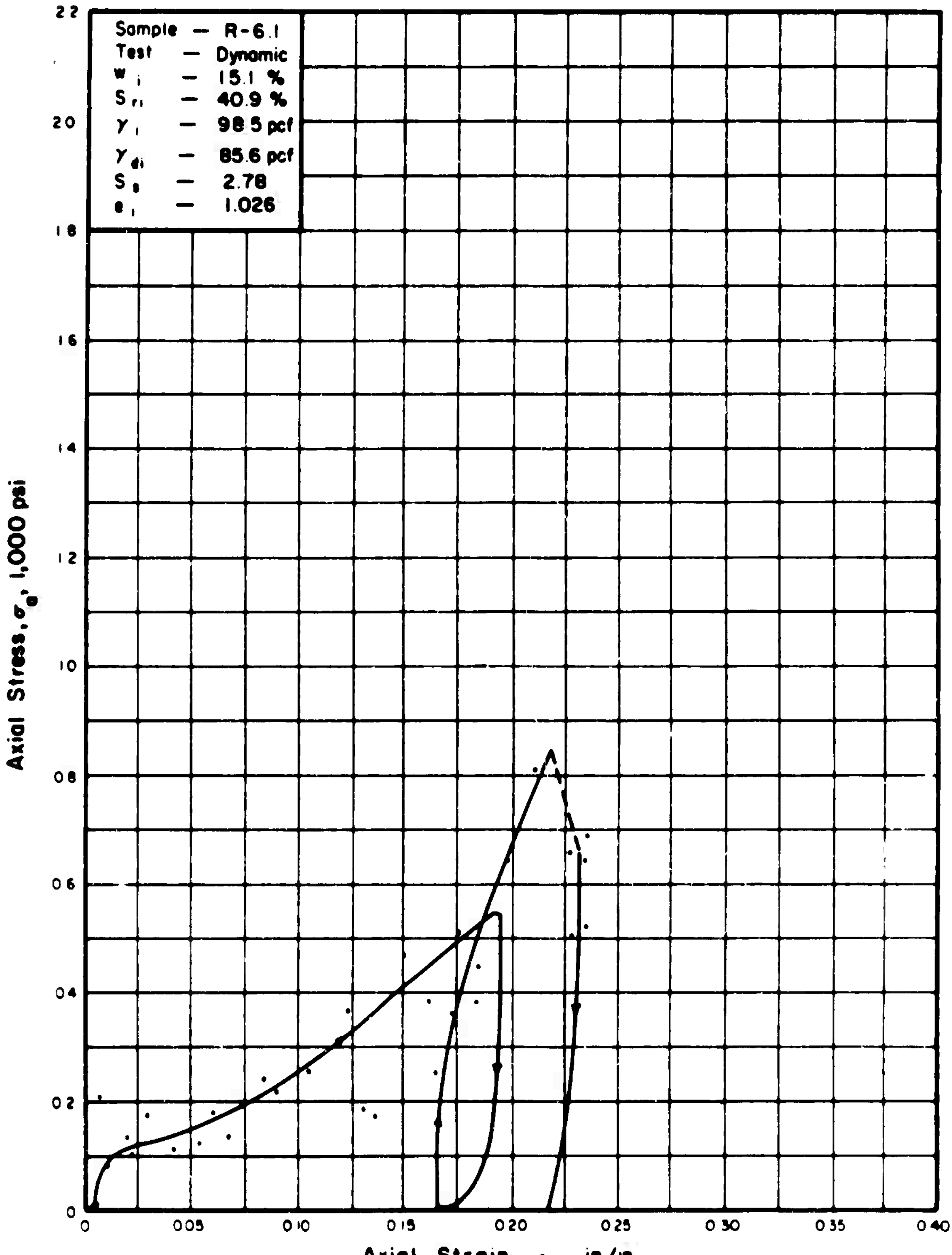

Figure 62. STRESS-STRAIN RELATIONSHIP IN ONE-DIMENSIONAL COMPRESSION

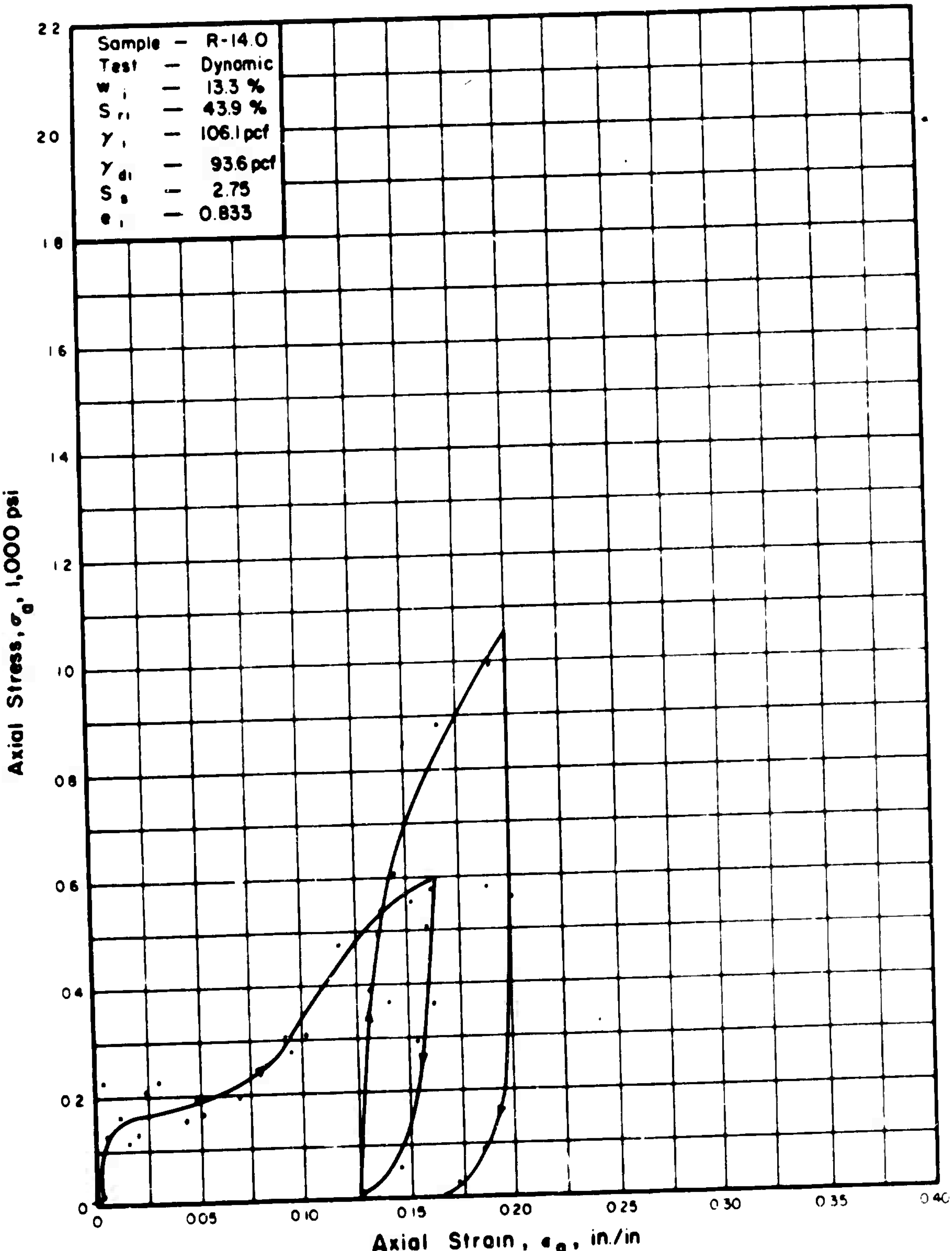

Figure 63. STRESS-STRAIN RELATIONSHIP IN ONE-DIMENSIONAL COMPRESSION.

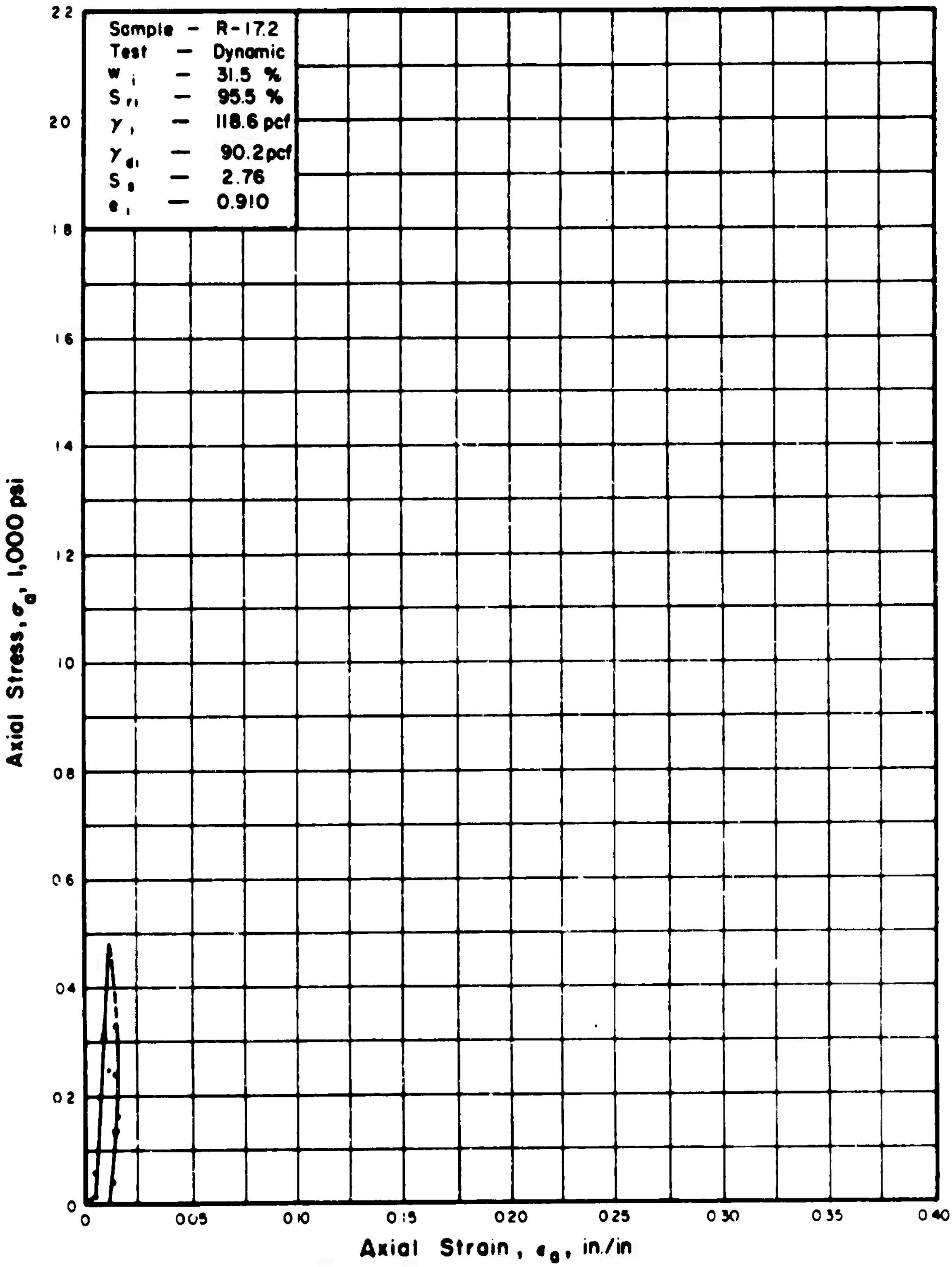

Figure 64. STRESS-STRAIN RELATIONSHIP

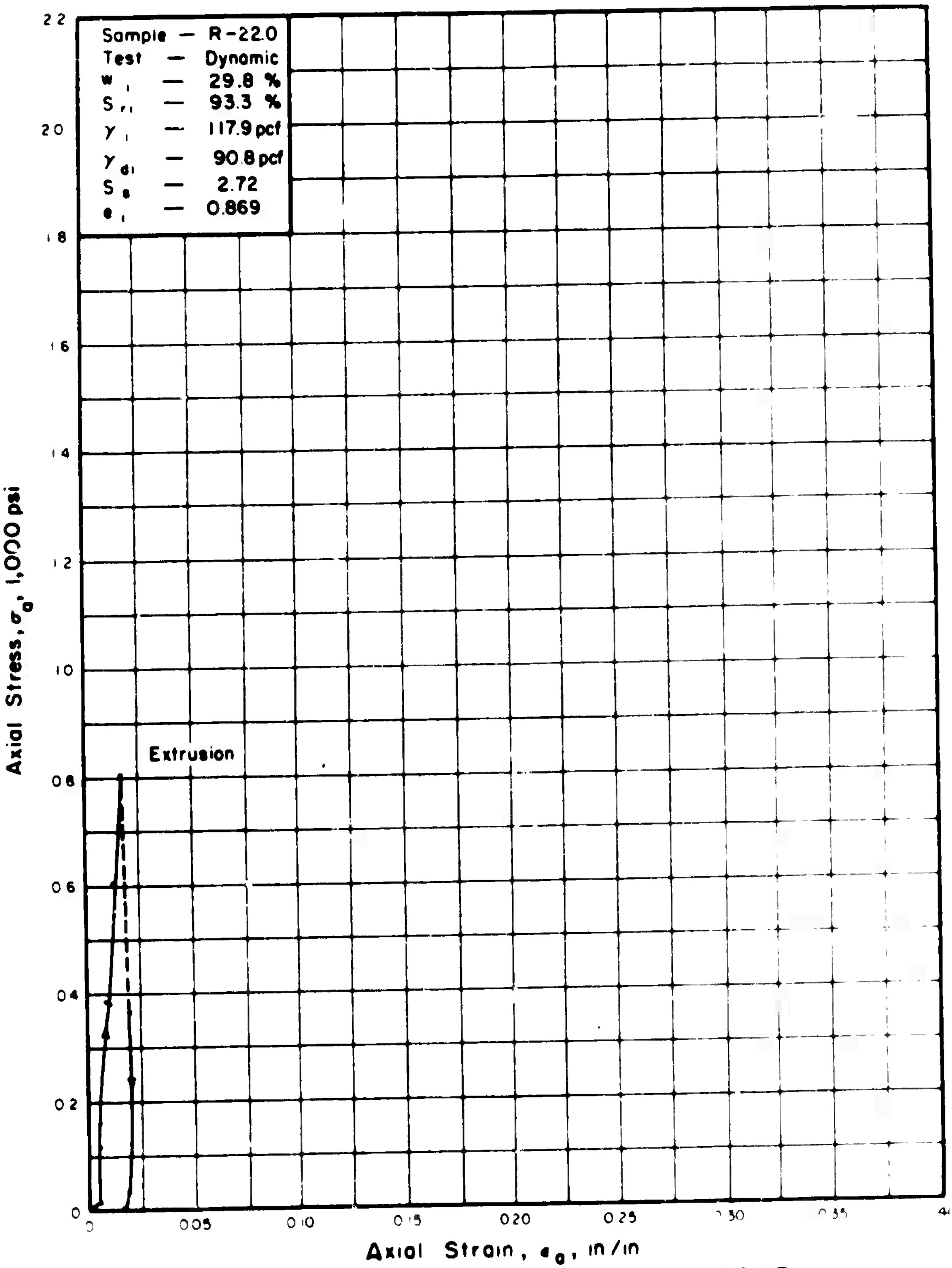

Figure 65. STRESS-STRAIN RELATIONSHIP IN ONE-DIMENSIONAL COMPRESSION.

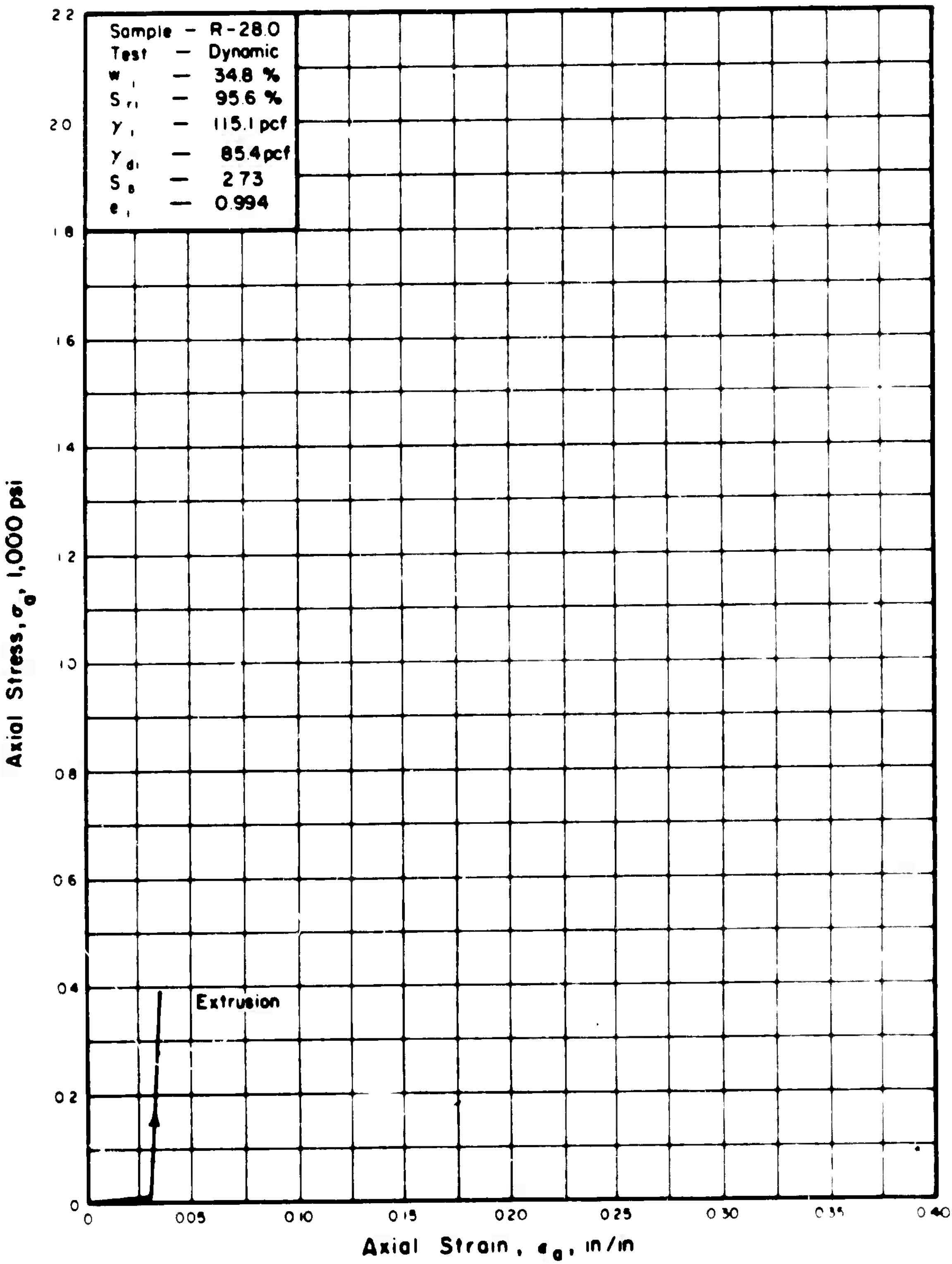

Figure 66. STRESS-STRAIN RELATIONSHIP IN ONE-DIMENSIONAL COMPRESSION.

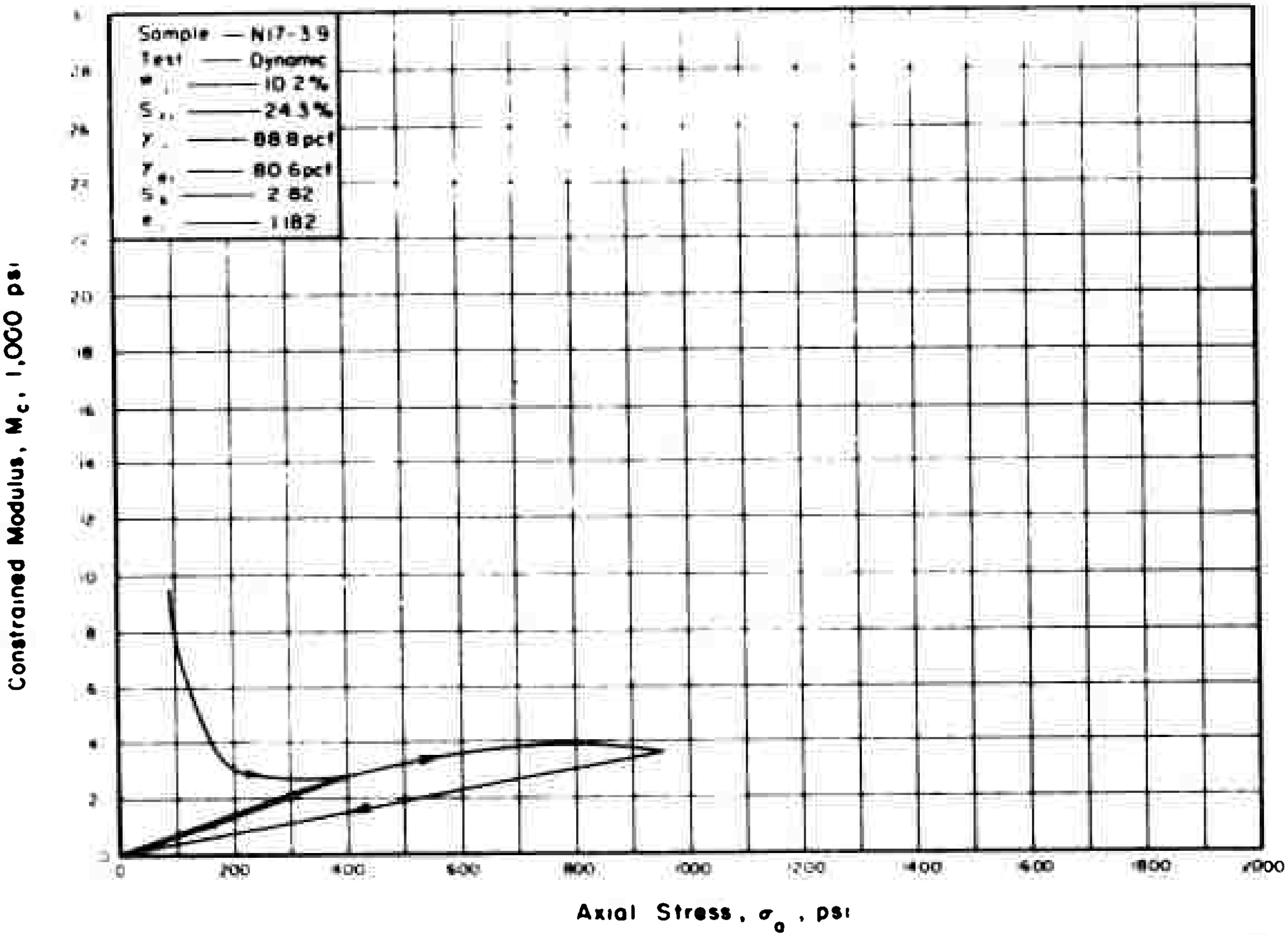

Figure 67. THE RELATIONSHIP BETWEEN CONSTRAINED MODULUS AND AXIAL STRESS.

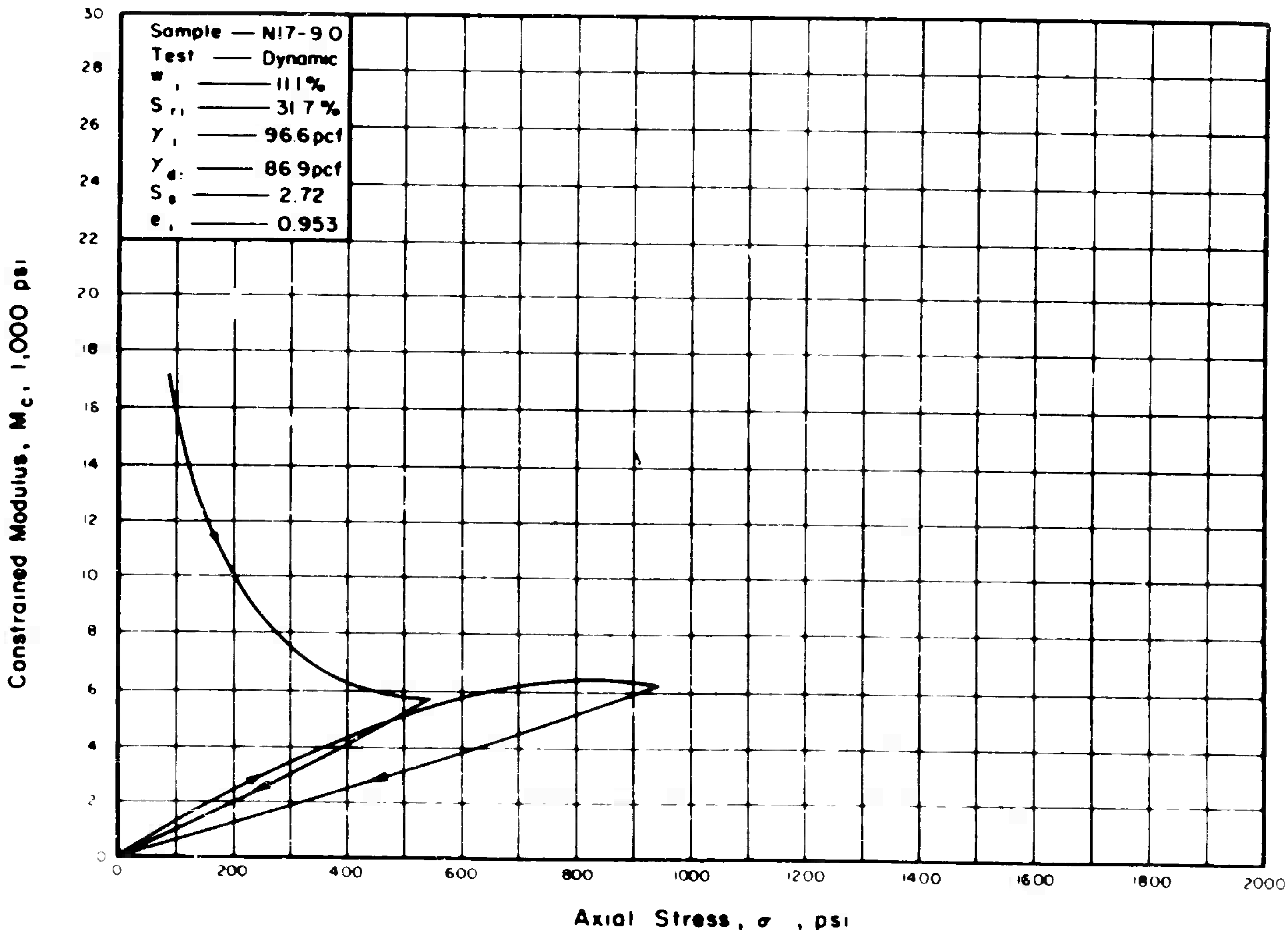

Figure 68. THE RELATIONSHIP BETWEEN CONSTRAINED MODULUS AND AXIAL STRESS.

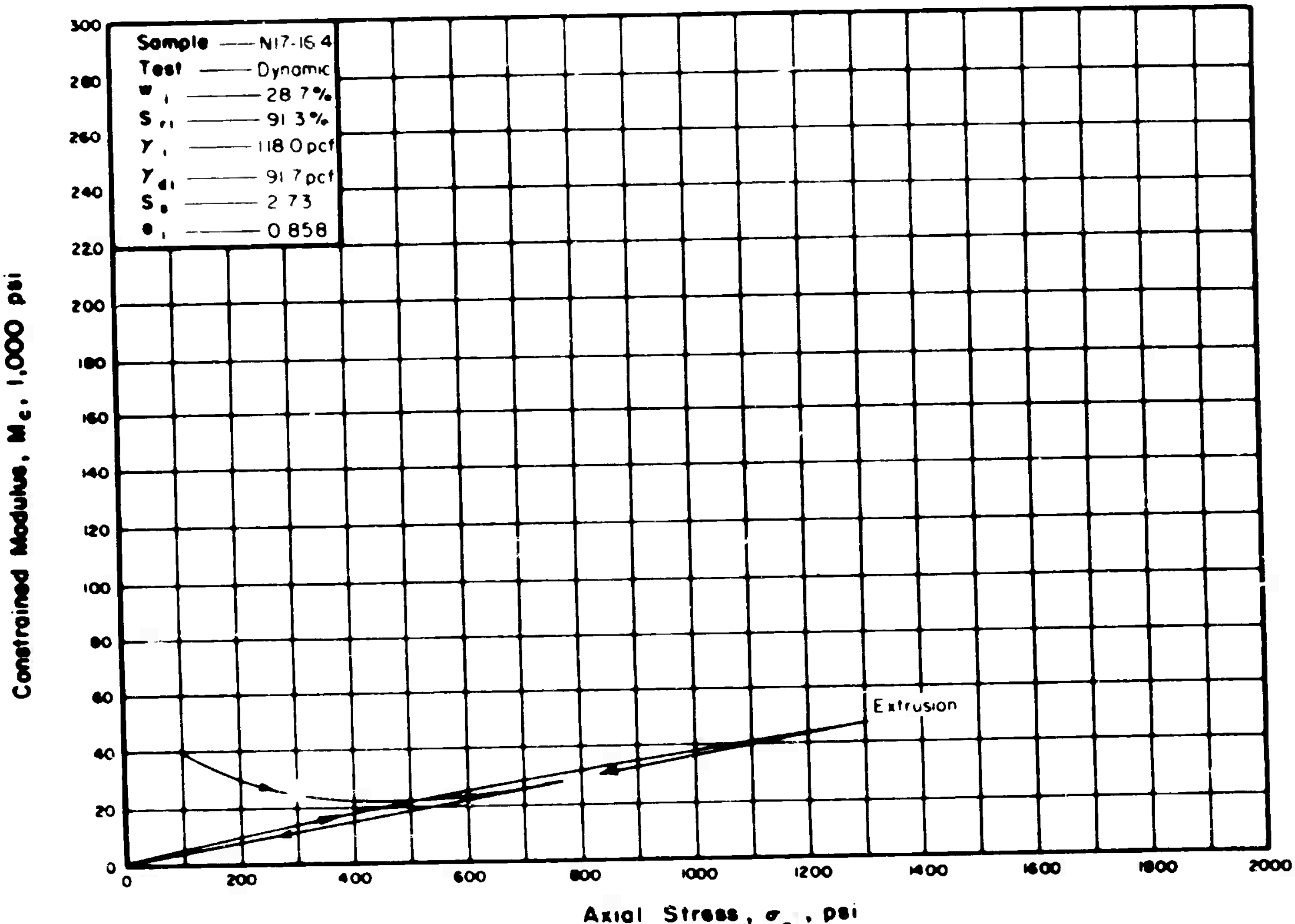

Figure 69 THE RELATIONSHIP BETWEEN CONSTRAINED MODULUS AND AXIAL STRESS.

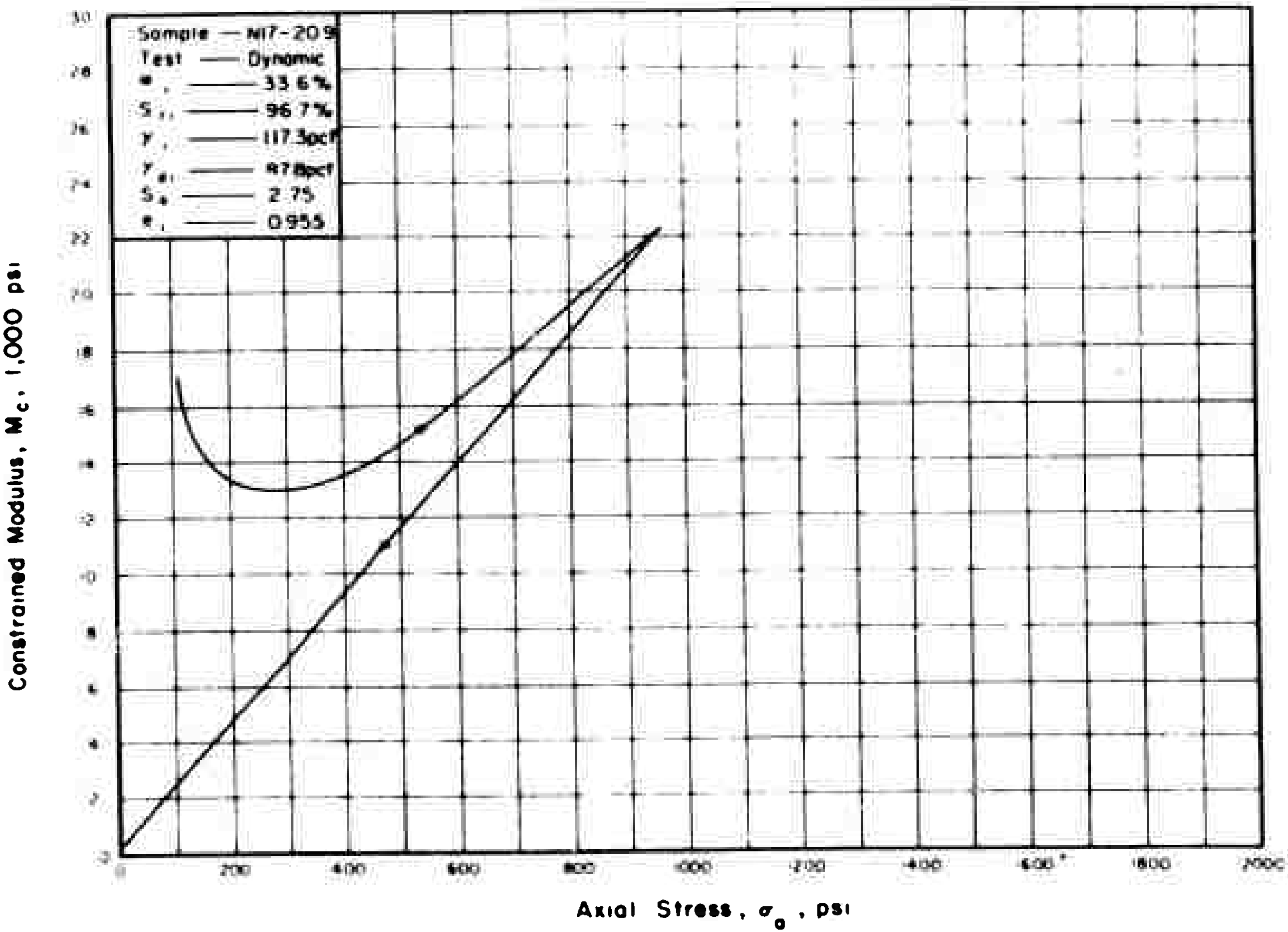

Figure 70. THE RELATIONSHIP BETWEEN CONSTRAINED MODULUS AND AXIAL STRESS.

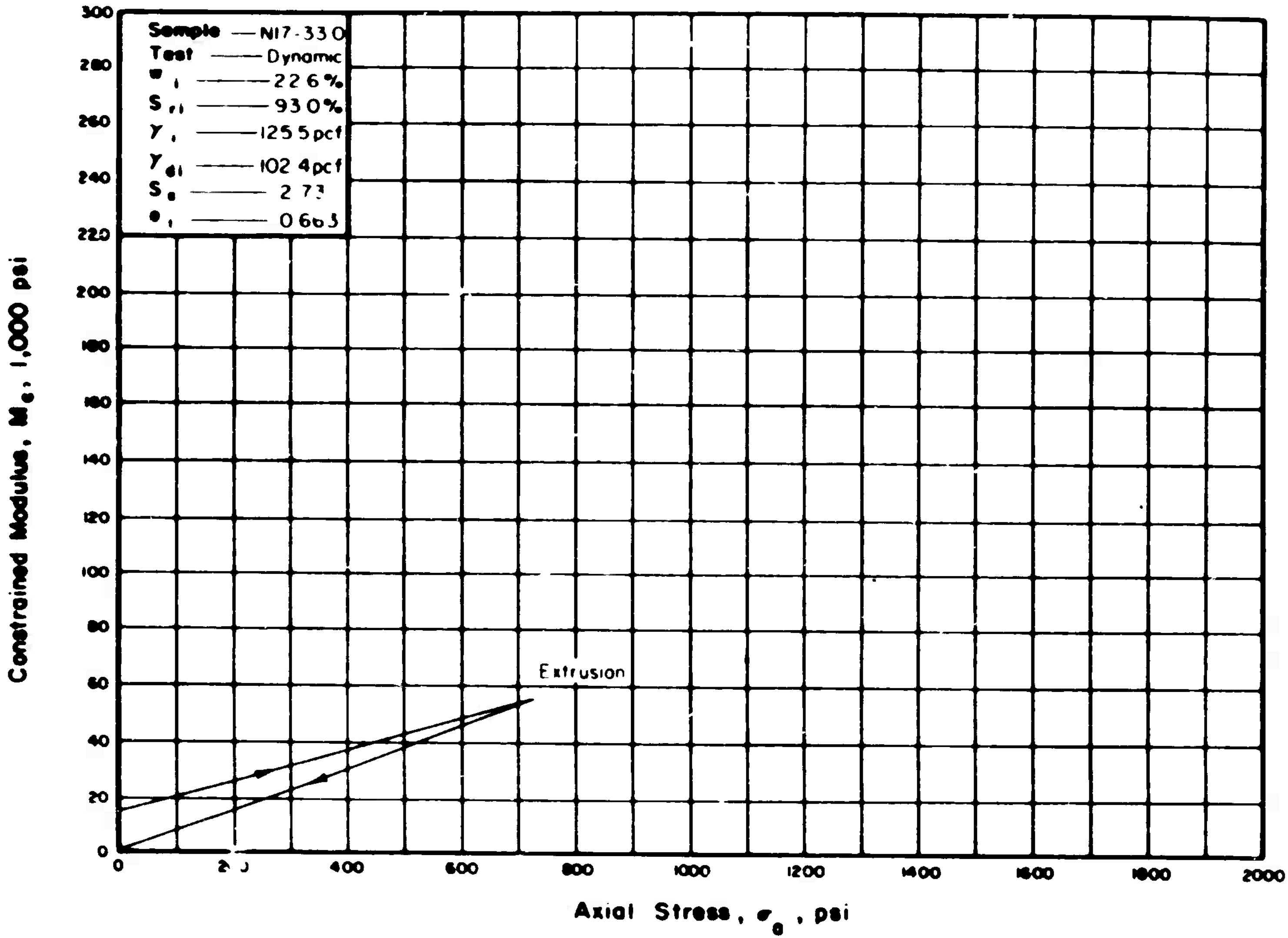

Figure 71. THE RELATIONSHIP BETWEEN CONSTRAINED MODULUS AND AXIAL STRESS.

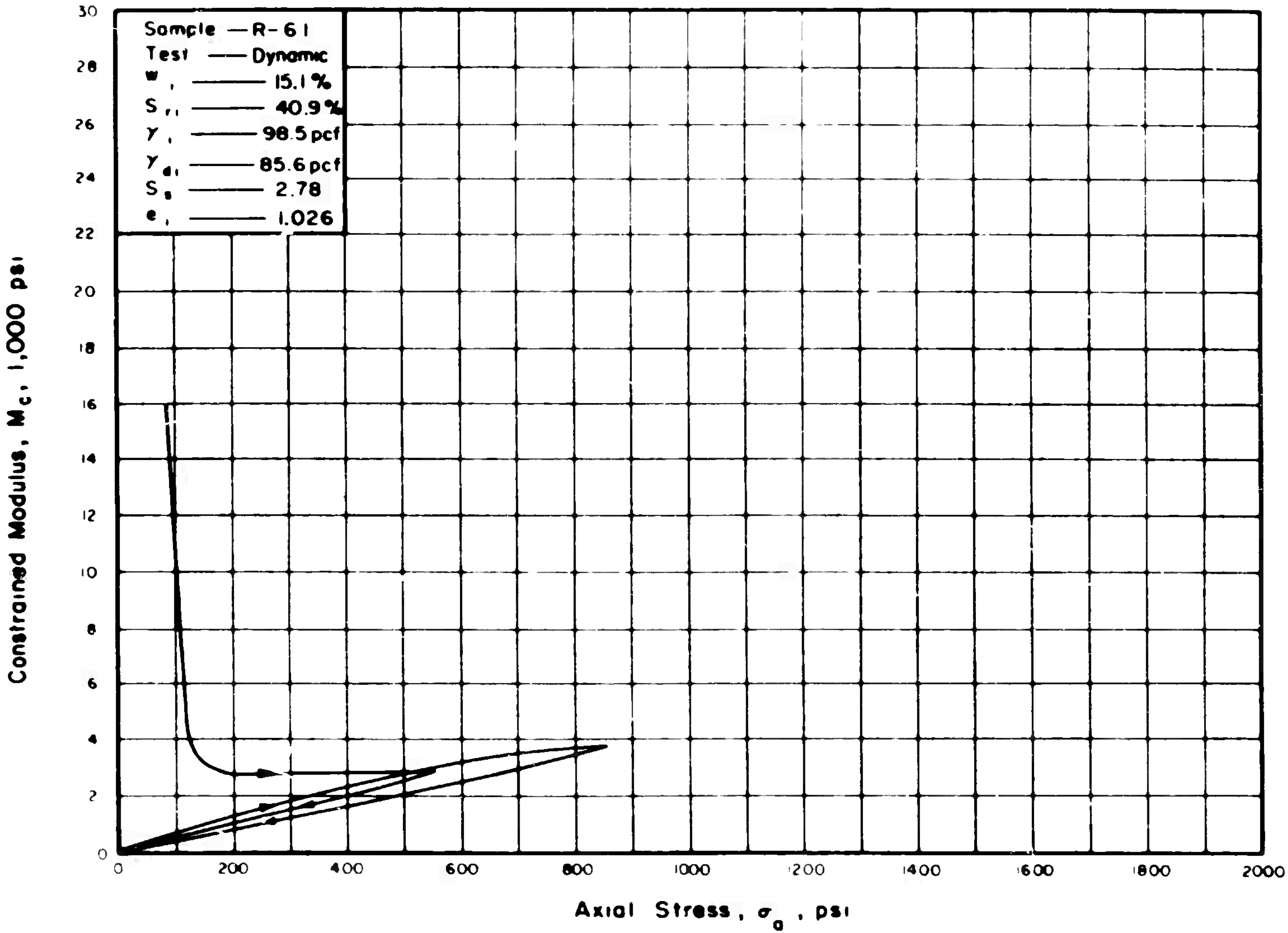

Figure 72. THE RELATIONSHIP BETWEEN CONSTRAINED MODULUS AND AXIAL STRESS.

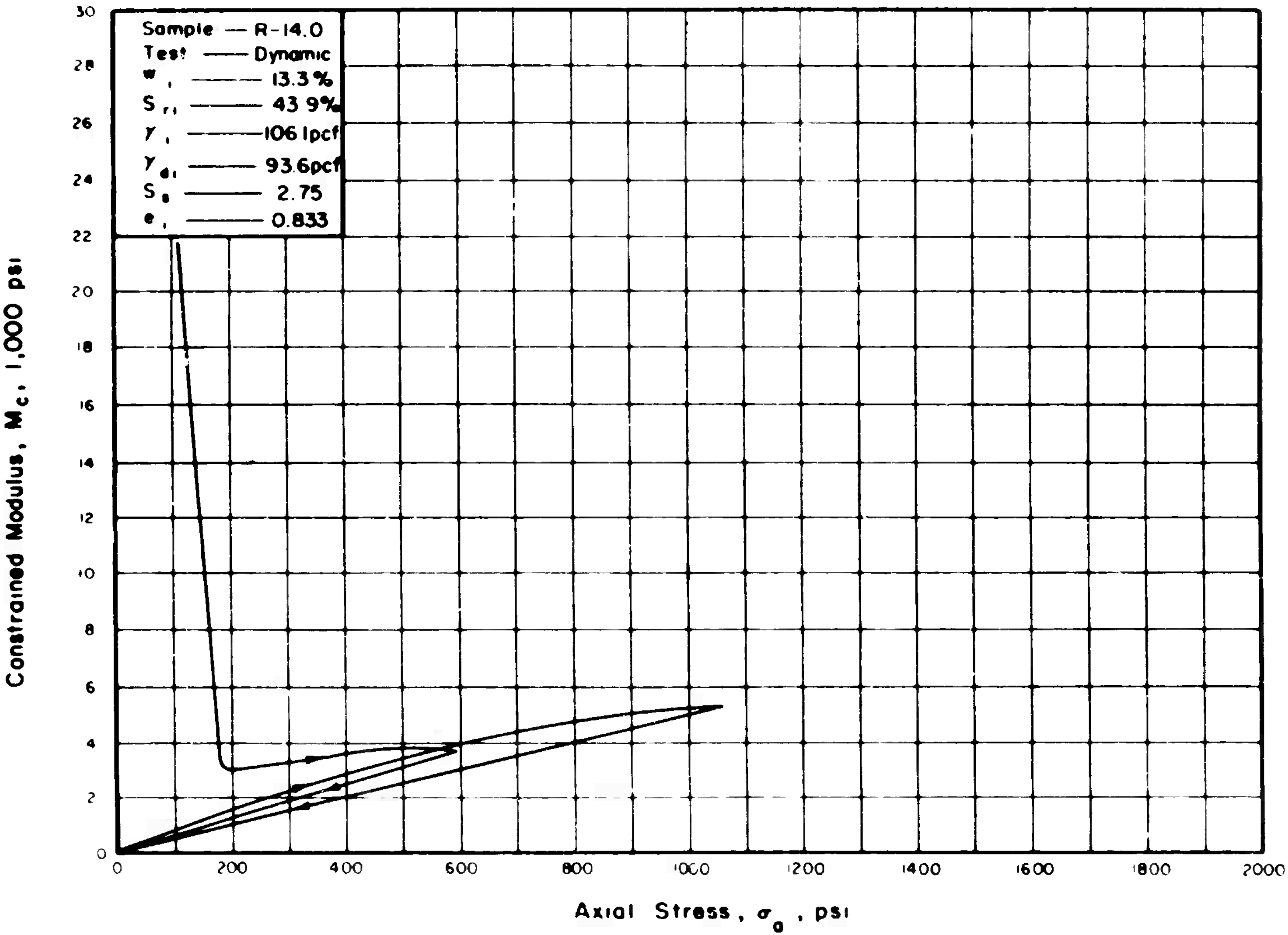

Figure 73. THE RELATIONSHIP BETWEEN CONSTRAINED MODULUS AND AXIAL STRESS.

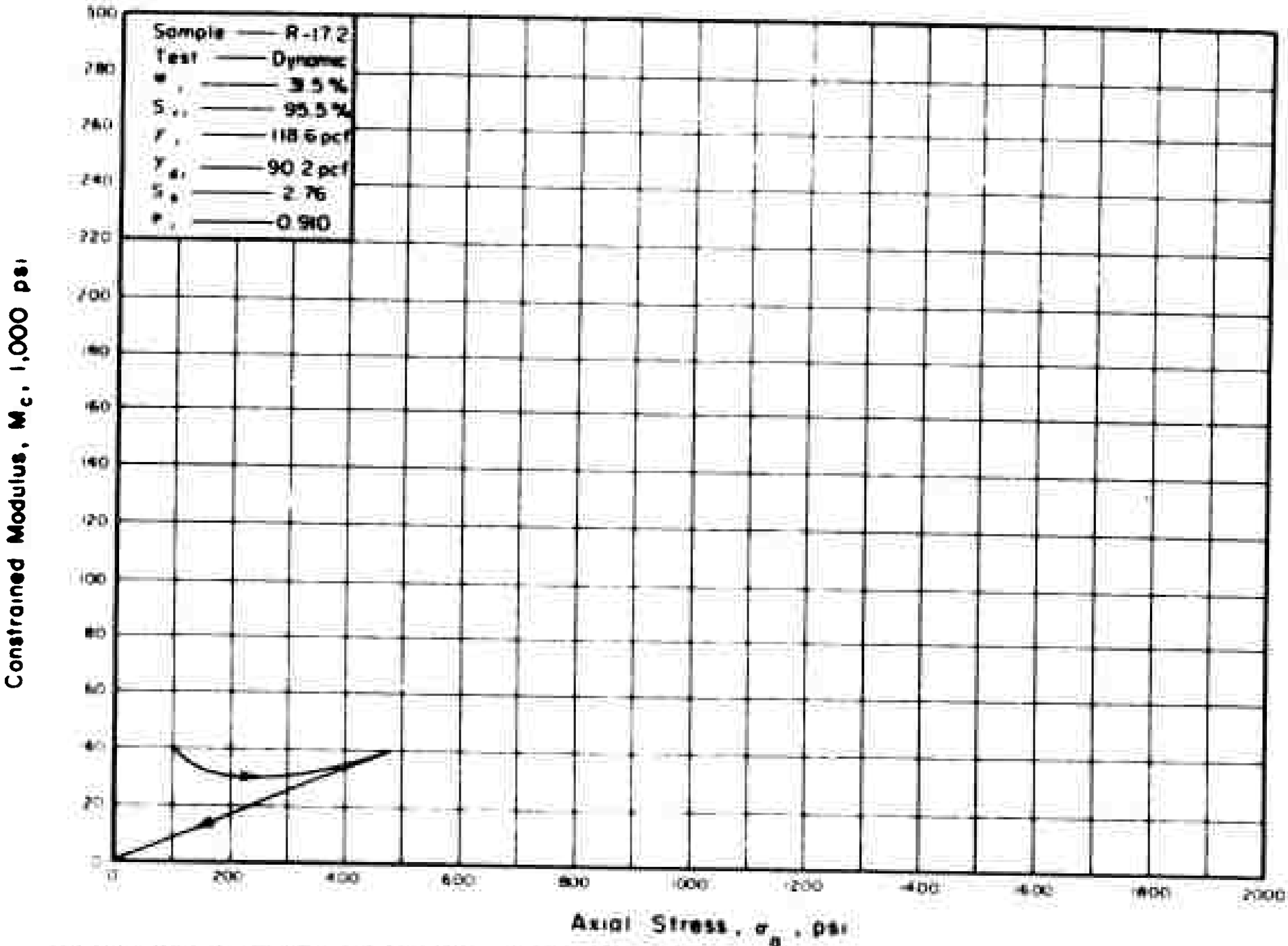

Figure 74 THE RELATIONSHIP BETWEEN CONSTRAINED MODULUS AND AXIAL STRESS.

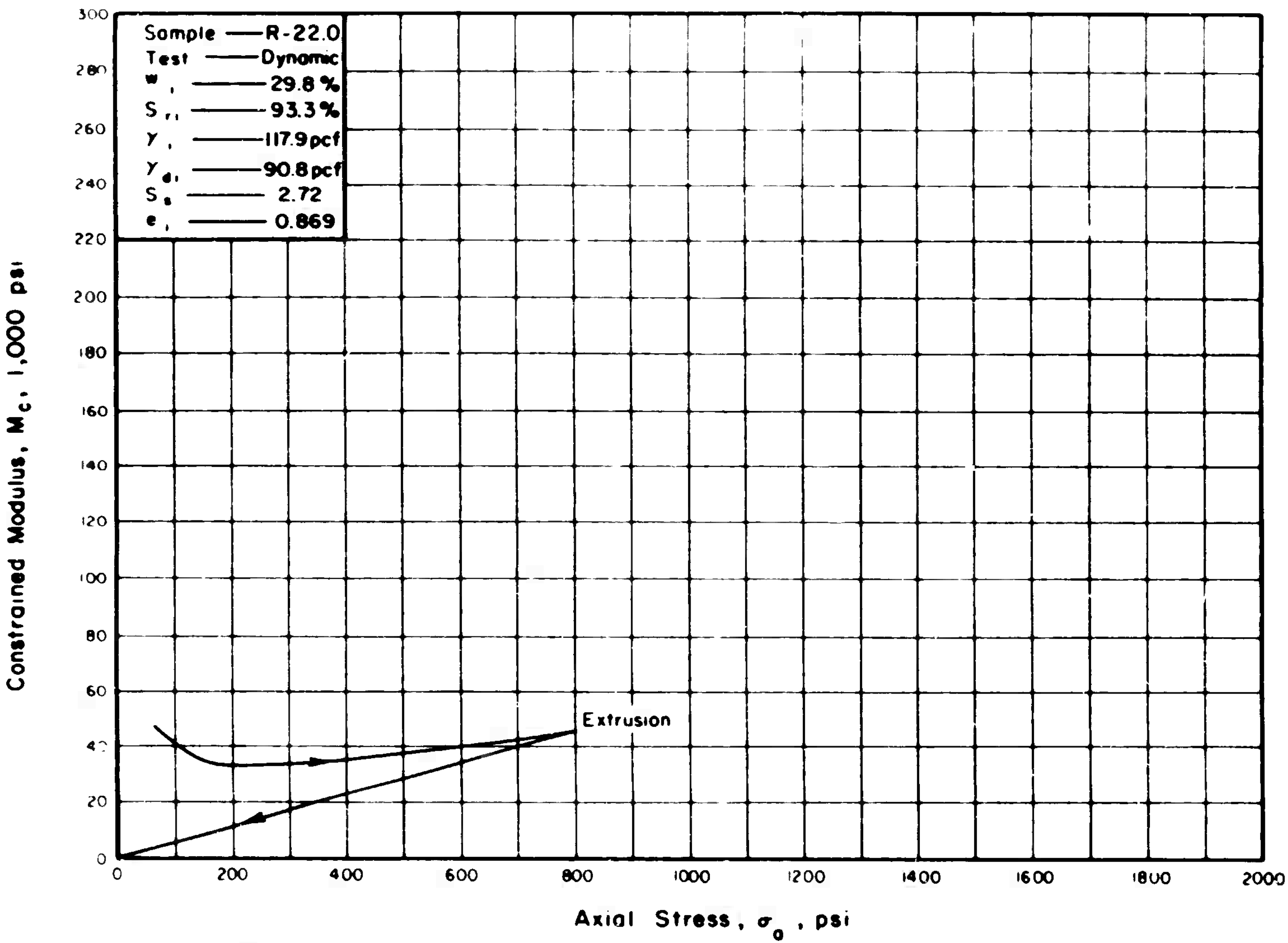

Figure 75. THE RELATIONSHIP BETWEEN CONSTRAINED MODULUS AND AXIAL STRESS.

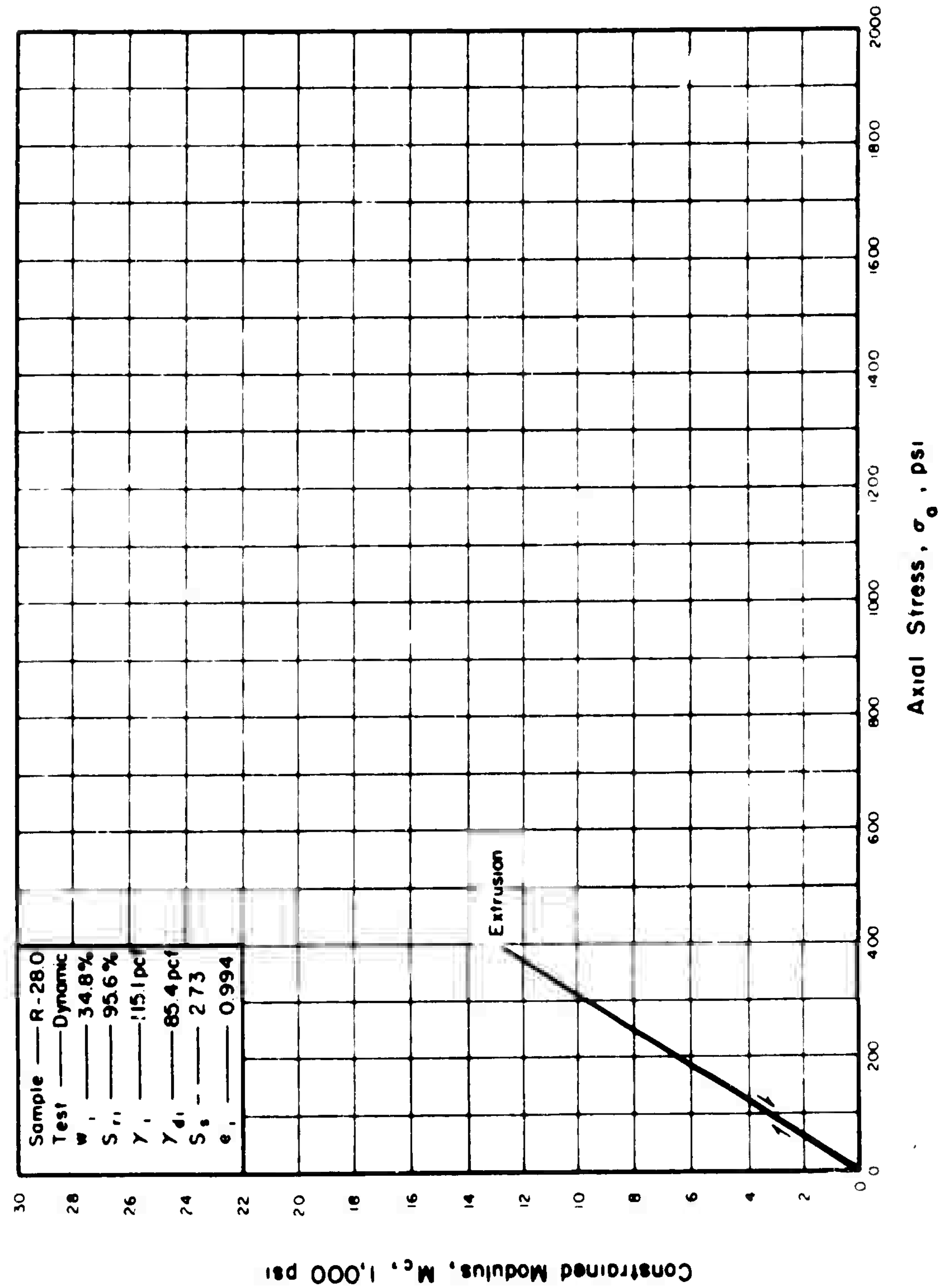

Figure 76. THE RELATIONSHIP BETWEEN CONSTRAINED MODULUS AND AXIAL STRESS.

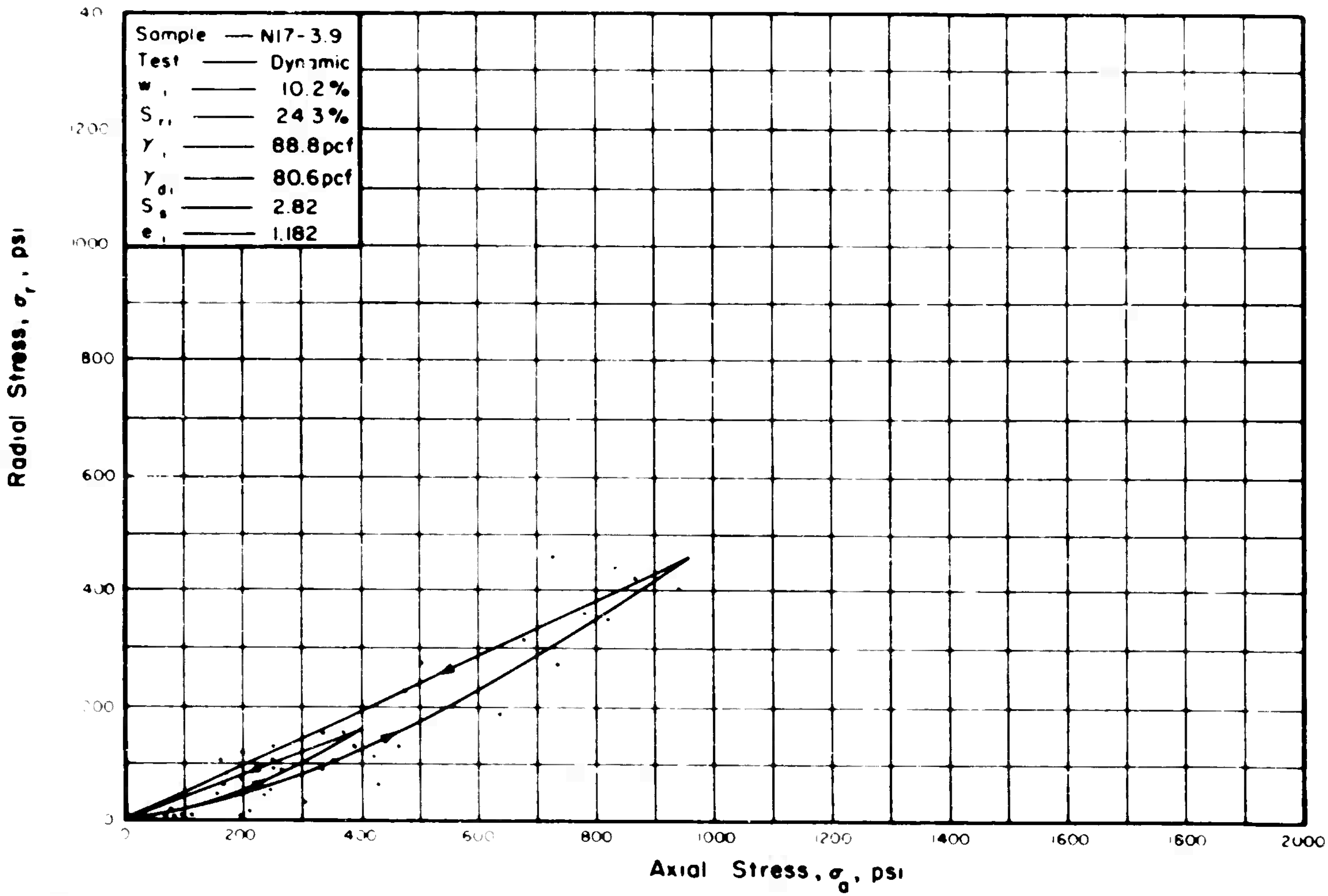

Figure 77. THE RELATIONSHIP BETWEEN RADIAL AND AXIAL STRESS IN ONE-DIMENSIONAL COMPRESSION.

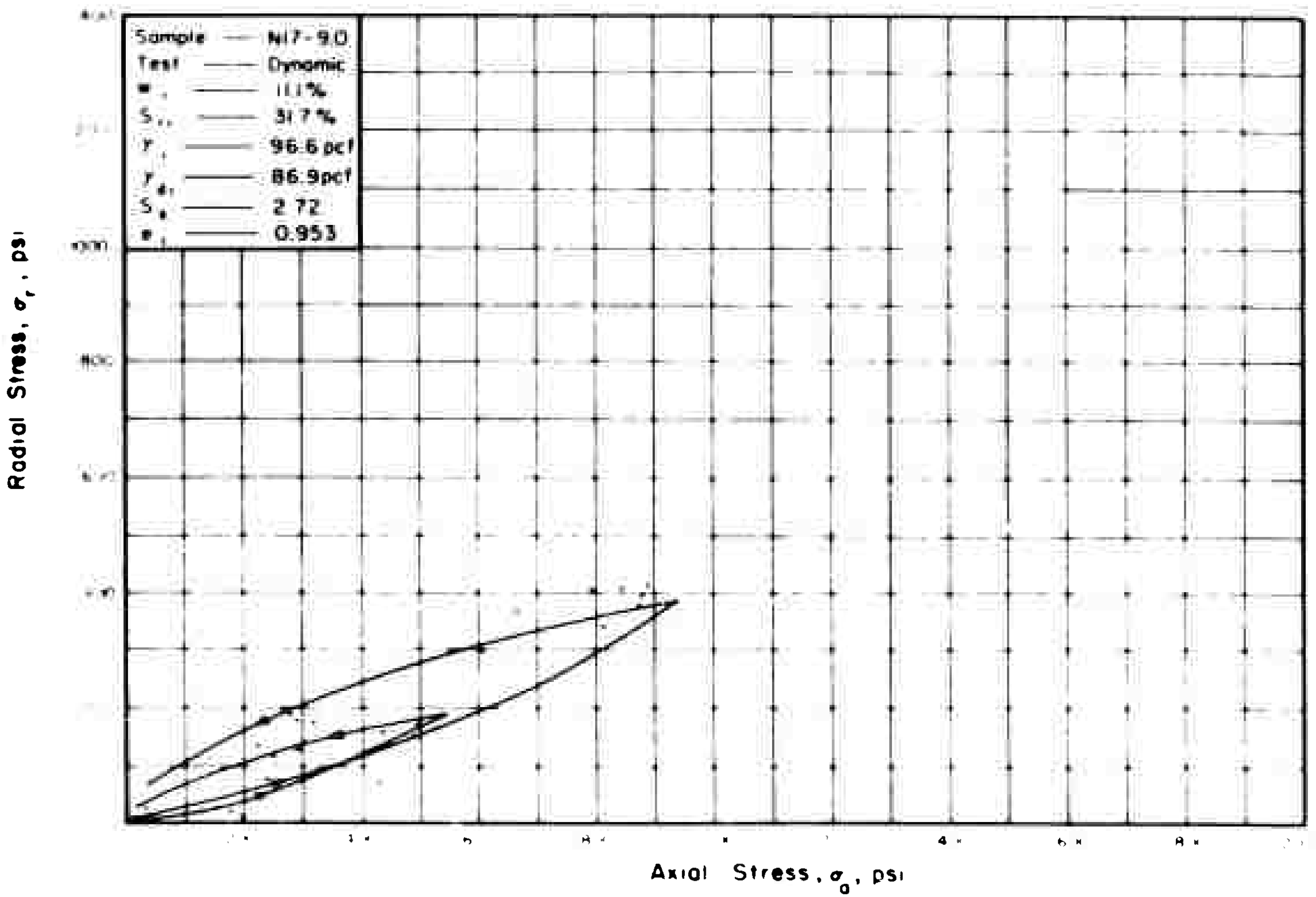

Figure 78. THE RELATIONSHIP BETWEEN RADIAL AND AXIAL STRESS IN ONE-DIMENSIONAL COMPRESSION.

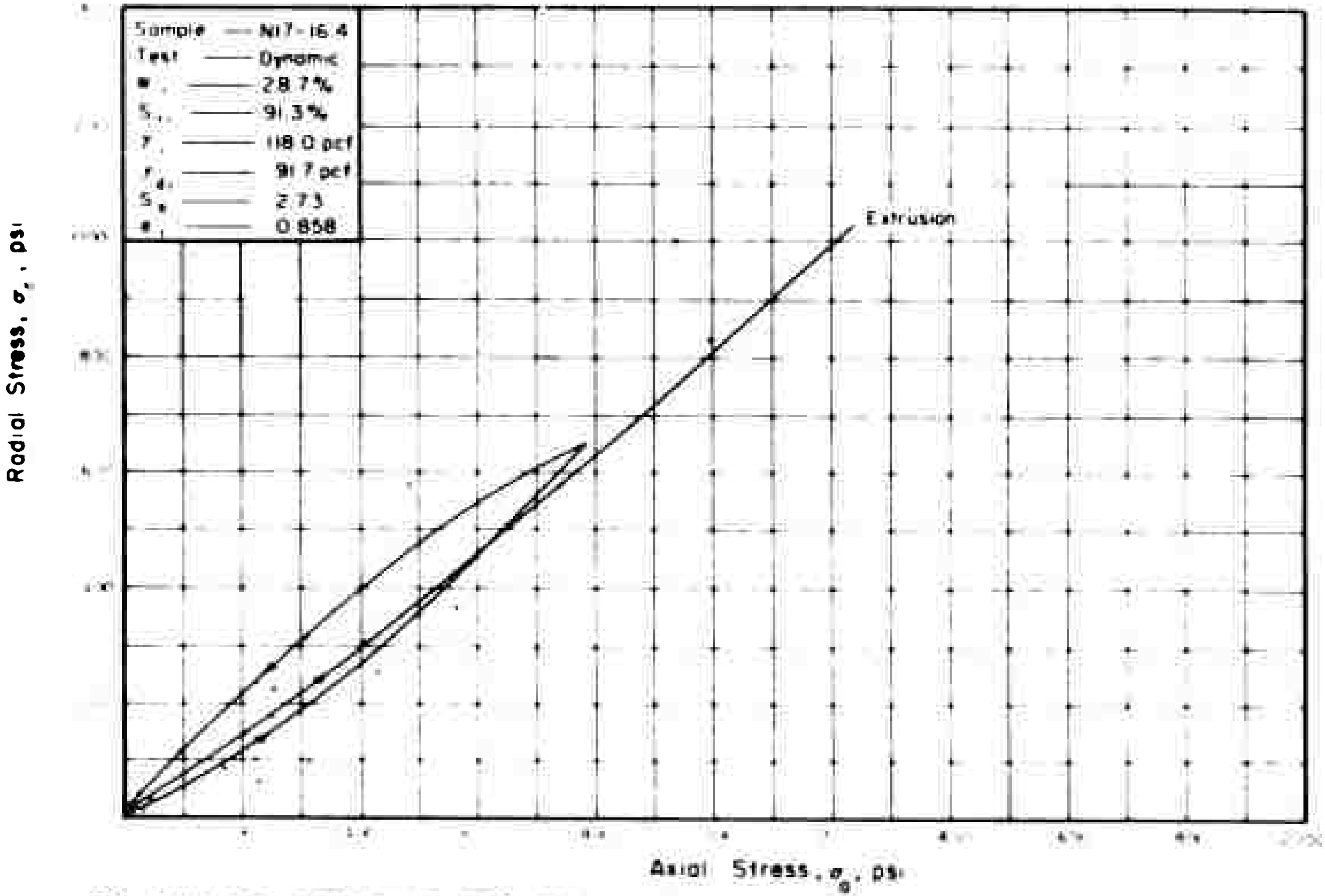

Figure 79 THE RELATIONSHIP BETWEEN RADIAL AND AXIAL STRESS IN ONE-DIMENSIONAL COMPRESSION.

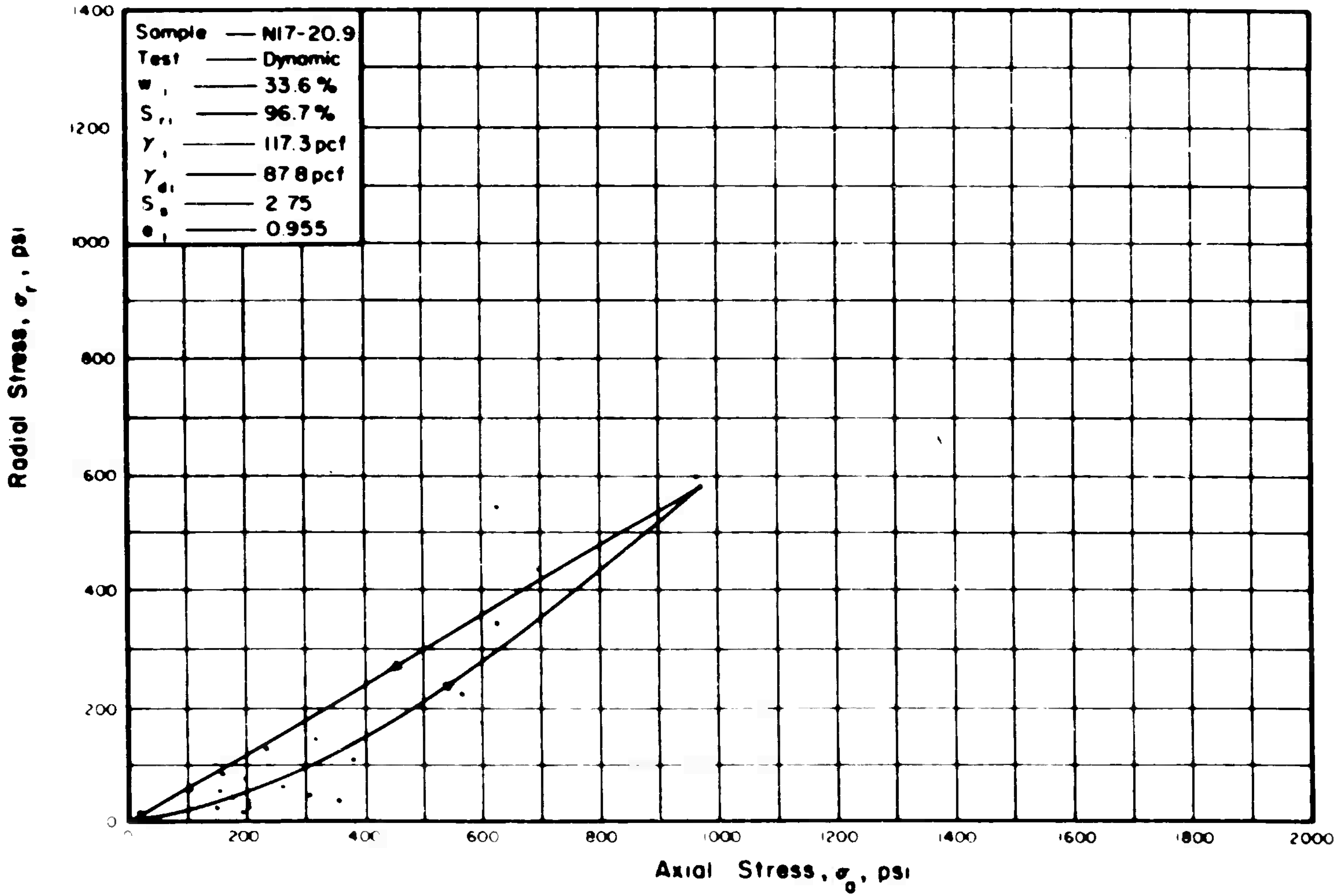

Figure 80. THE RELATIONSHIP BETWEEN RADIAL AND AXIAL STRESS IN ONE-DIMENSIONAL COMPRESSION.

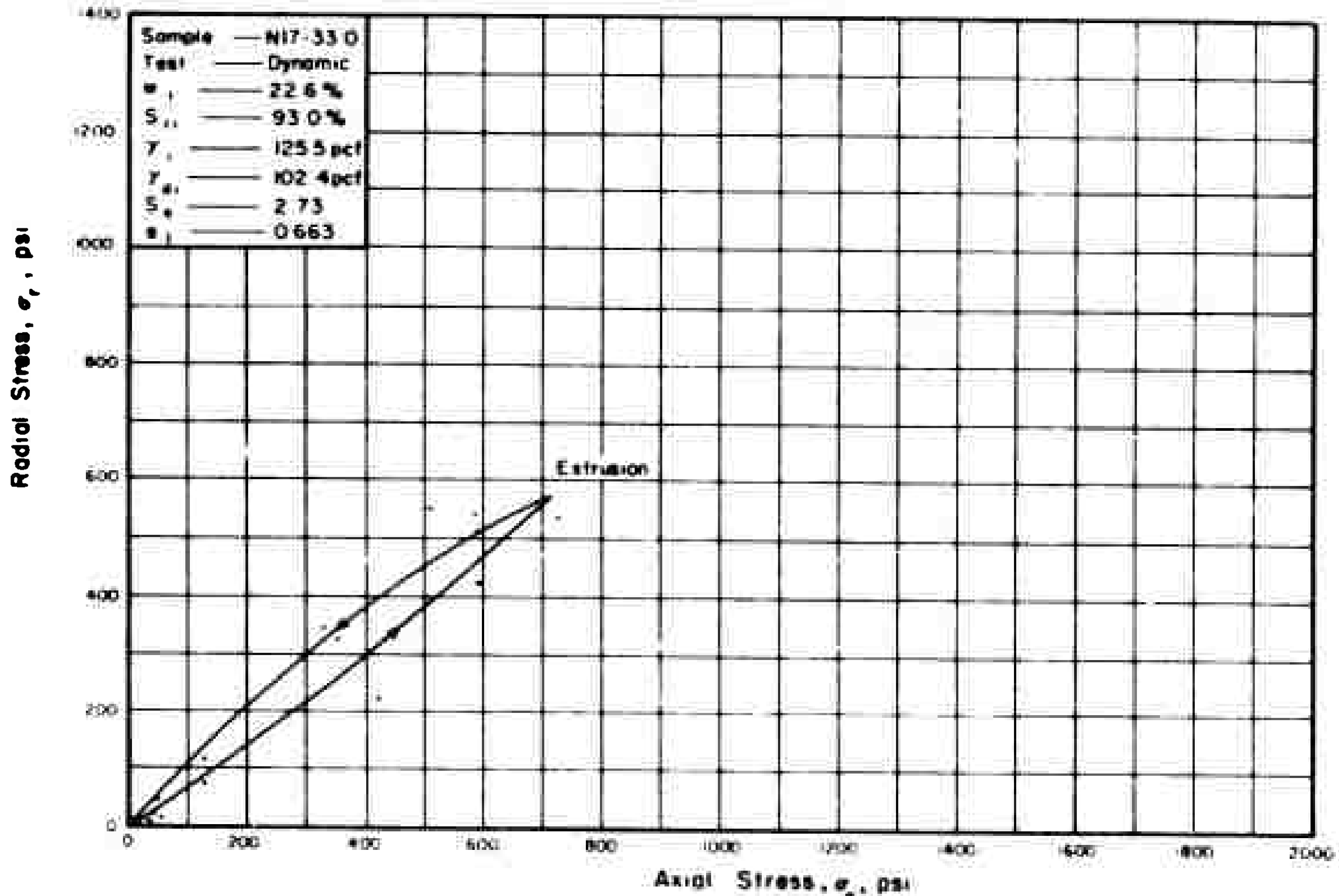

Figure 81. THE RELATIONSHIP BETWEEN RADIAL AND AXIAL STRESS IN ONE-DIMENSIONAL COMPRESSION.

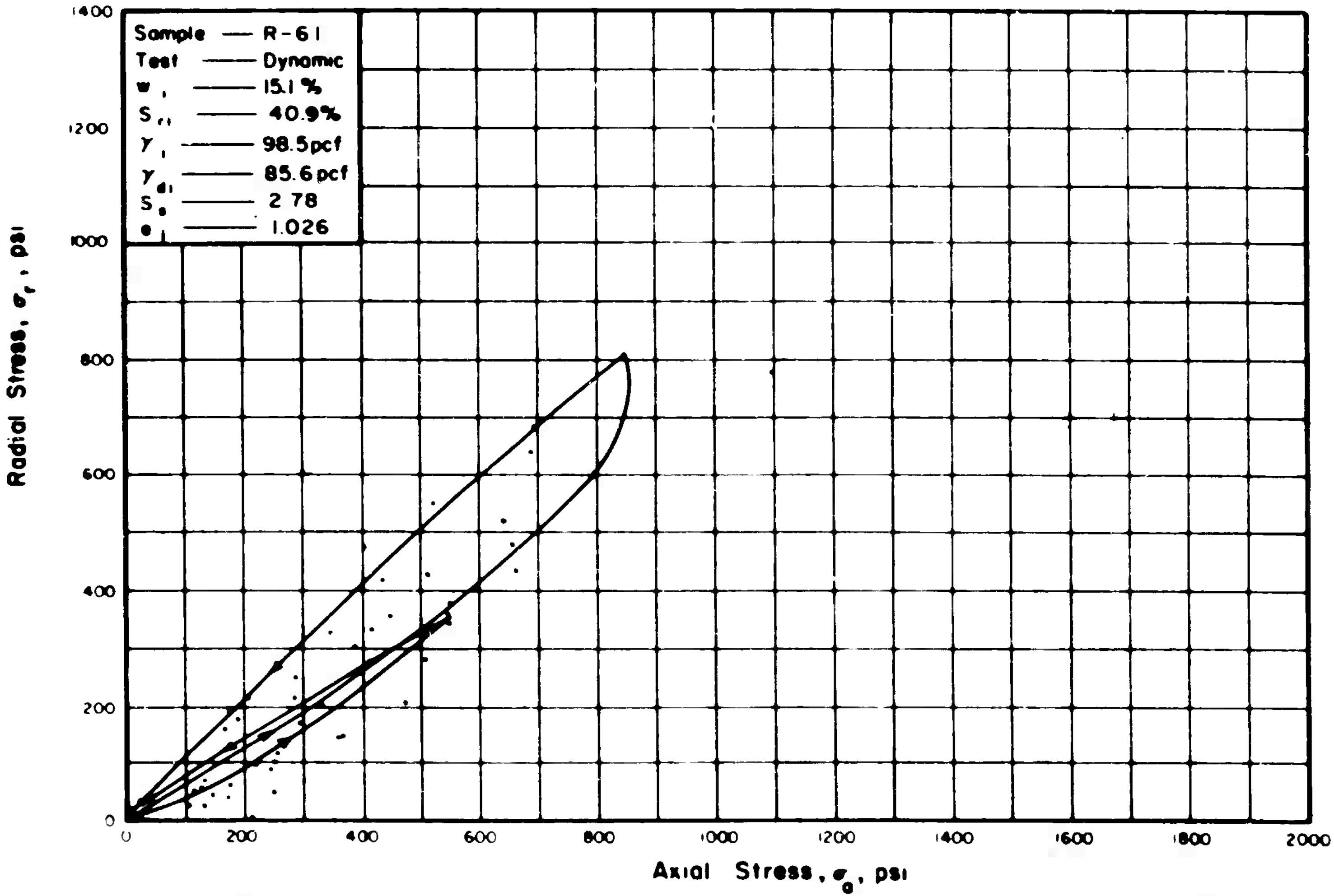

Figure 82. THE RELATIONSHIP BETWEEN RADIAL AND AXIAL STRESS IN ONE-DIMENSIONAL COMPRESSION.

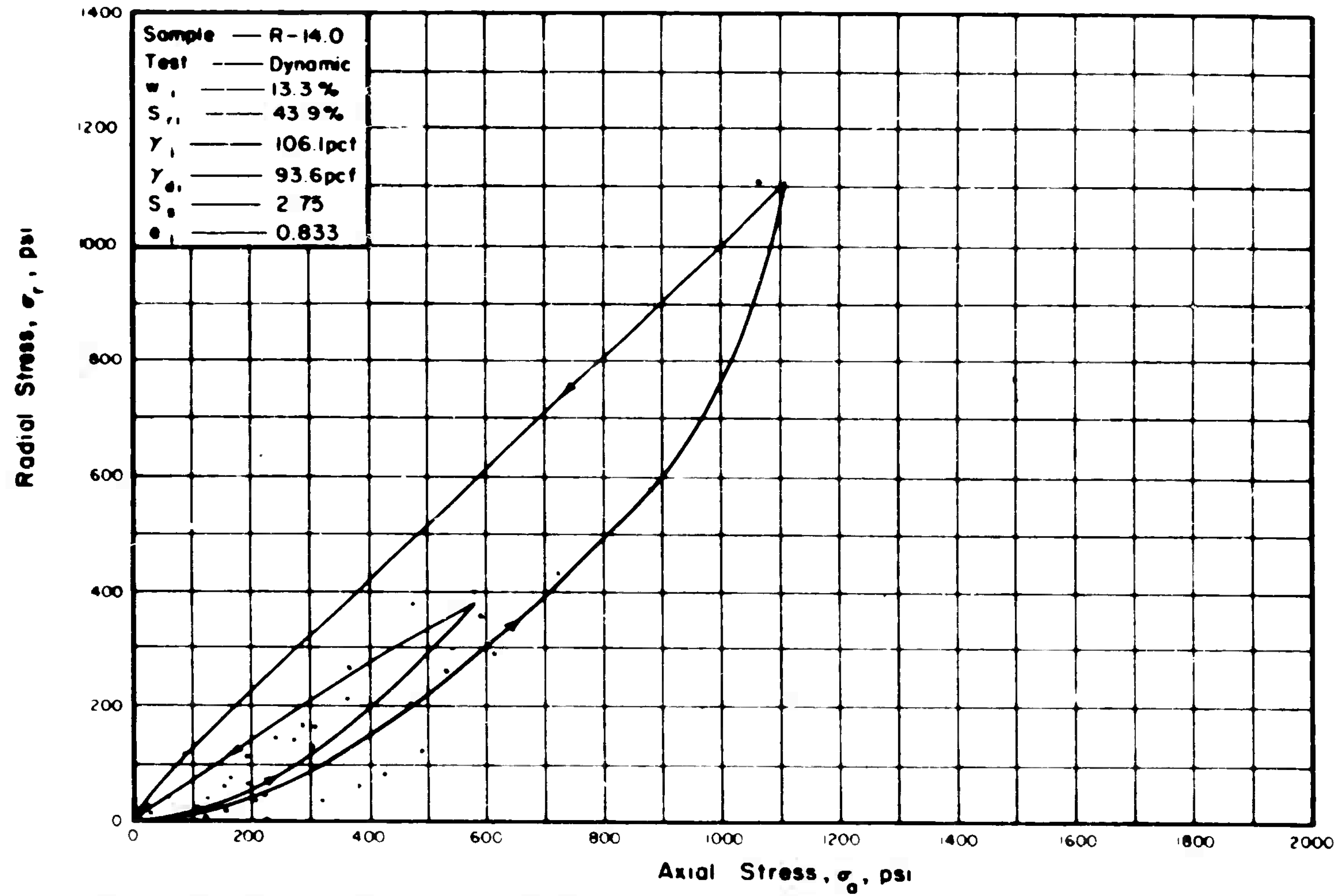

Figure 83. THE RELATIONSHIP BETWEEN RADIAL AND AXIAL STRESS IN ONE-DIMENSIONAL COMPRESSION.

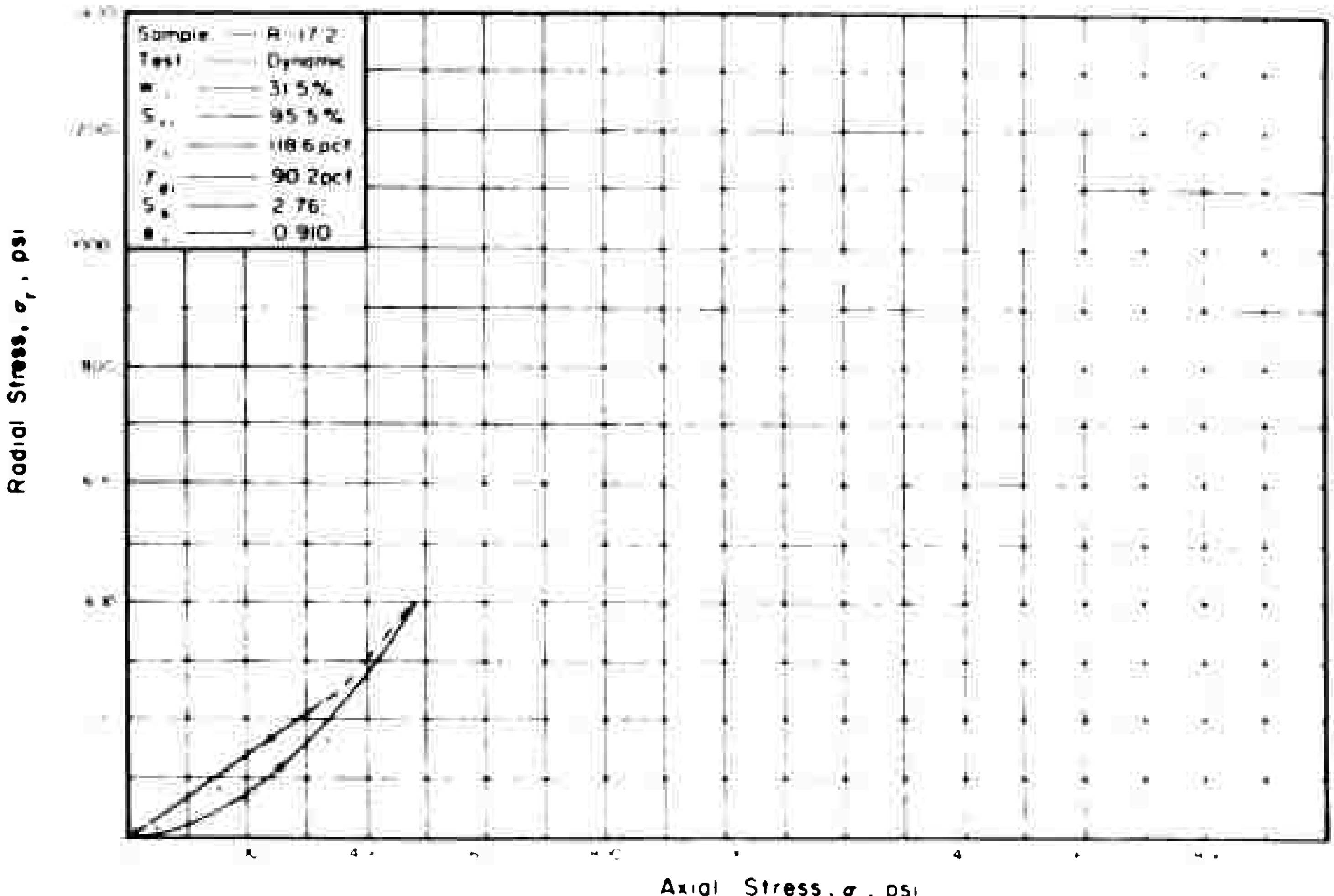

Figure 84 THE RELATIONSHIP BETWEEN RADIAL AND AXIAL STRESS IN ONE-DIMENSIONAL COMPRESSION.

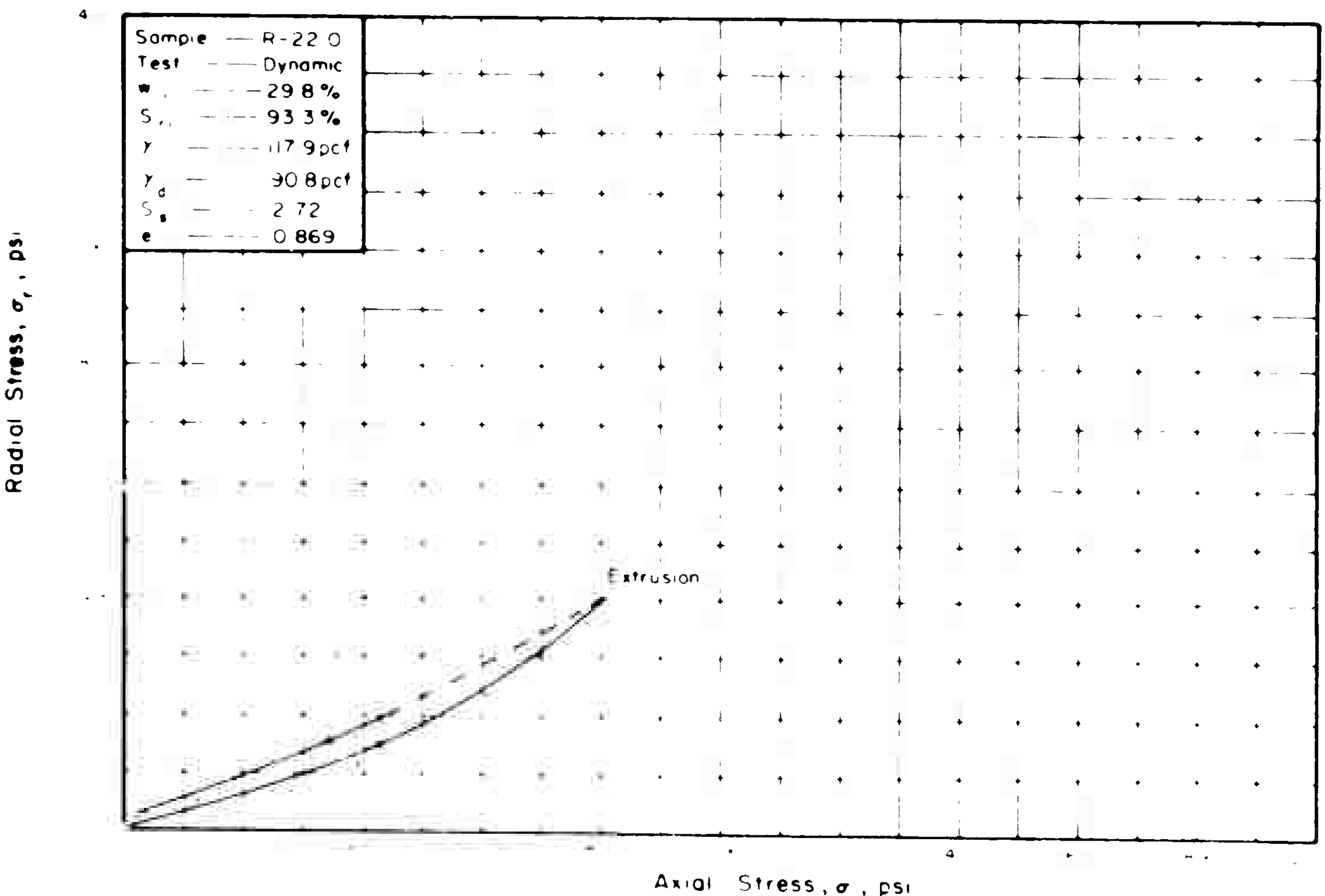

Figure 85 THE RELATIONSHIP BETWEEN RADIAL AND AXIAL STRESS IN ONE-DIMENSIONAL COMPRESSION.

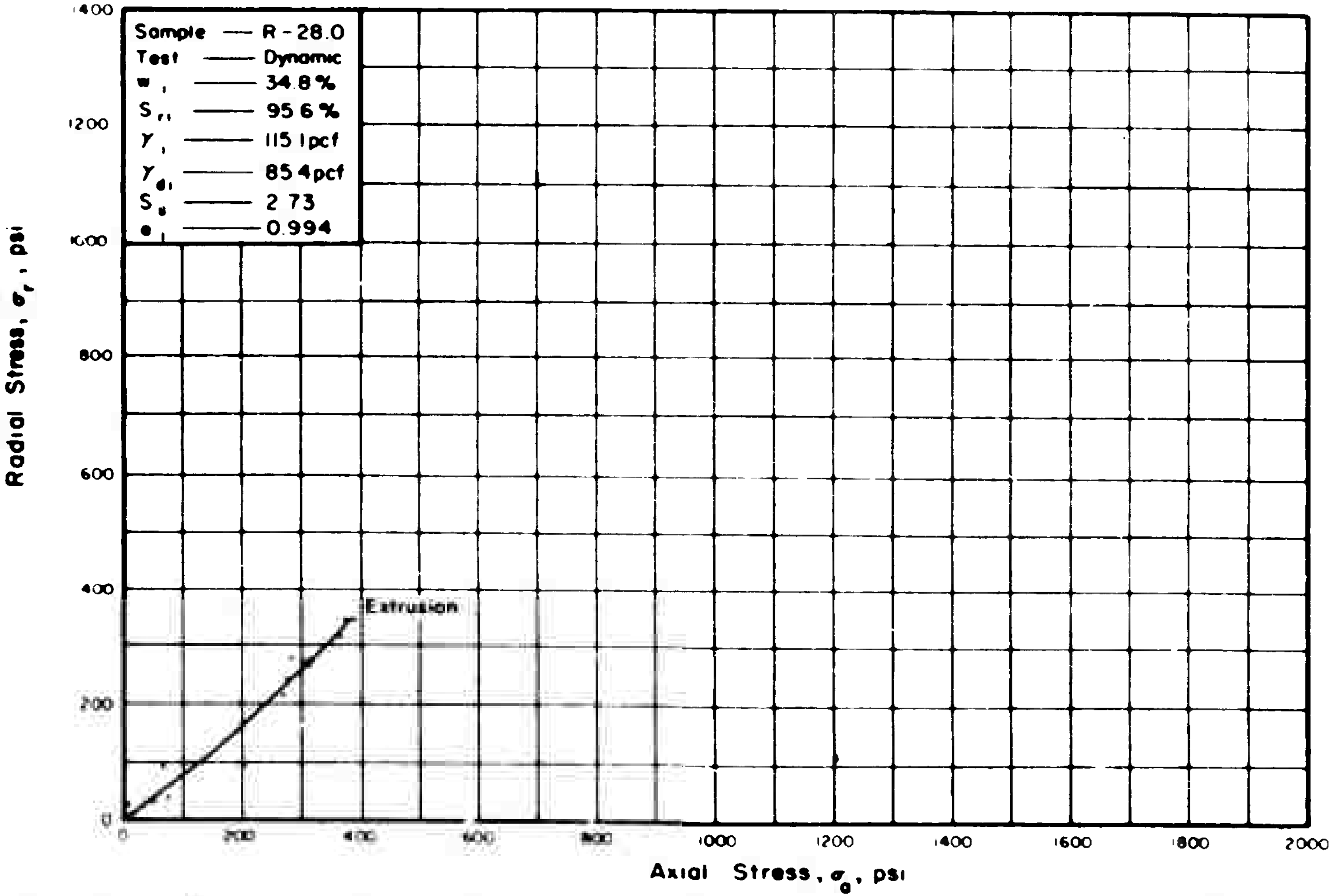

Figure 86. THE RELATIONSHIP BETWEEN RADIAL AND AXIAL STRESS IN ONE-DIMENSIONAL COMPRESSION.